

# **ChemY**

## **Journal for Young Researchers in Chemistry**



**Post Graduate Department of Chemistry**  
**MES Keveeyam College Valanchery**  
Kerala, India  
[www.meskvmcollege.org](http://www.meskvmcollege.org)

Volume 1  
September 2014

**ChemY**

*Journal for Young Researchers in Chemistry*

Volume 01

September 2014

**Printed and Published by**

Principal

MES Keveeyam College Valanchery

Malappuram 676557

Kerala, India

**Editorial Board**

**Lt(Dr). Mohamedali (Chief Editor)**

Principal

MES Keveeyam College Valanchery

Malappuram 676557

Kerala, India

**Prof. E Purushothaman (Executive Editor)**

Department of Chemistry

University of Calicut

Kerala, India

**Prof. Manjula Raman**

Head, Department of Chemistry

MES Keveeyam College Valanchery

Malappuram, Kerala

India

**Dr. A Sujith**

Department of Chemistry

National Institute of Technology Calicut

Kerala, India

**Dr. K Priyadasan**

Material Chemistry Division

School of Advanced Science, Vellore, Tamil Nadu

India

© 2014

## Foreword

Explore within, for, within you is the spring of invaluable thoughts and ideas the elixir of life, always ready to bubble up if you just explore. Chemistry is the proof in print that everything will turnout exceptionally well if you begin a task with a strong, persistent and keen desire to accomplish it successfully. Technology and new teaching, learning practices are trying to find ways of motivating learners and encouraging the development of self efficacy. If we do not change our direction, we are likely to end up where we have headed. Rote learning, drilling and repetition activities have been pushed back by higher order thinking skill and research aptitude. Thinking is the driving skill with which each individual drives his or her intelligence and it comes naturally to scholars but thinking activities need to be planned and scaffolded. Young minds need to realize that they are thinking and the different thinking strategies like synthesizing, analyzing reasoning, comprehending, application and evaluation are required for solving different problems. Any way an unflinching determination and calculated strides are essential for a smooth journey.

Research works in the cutting edge area using state-of-the-art facilities and equipments is the dream of any scholar. The publication of this journal is an important landmark and a source of great pride for the institute. I whole heartedly congratulate the team Chemistry for its untiring hard work in bringing forth such a praiseworthy publication.

I sincerely thank all the authors who have contributed to the first volume of ChemY, Journal for Young Researchers in Chemistry being published by the Department of Chemistry, MES Keveeyam College Valanchery. I also express my thanks to the reviewers of papers and also to the members of the editorial board.

I am eagerly looking forward to more contributions to the forthcoming volumes.

**Lt (Dr.) Mohamedali  
(Chief Editor)**

1. A Novel Method for the Preparation of Core-Shell Silica-12-Tungstophosphoric acid Nanoparticles for *t*-Butylation of phenol  
(Rosilda Selvin, Hsui-Ling Hsu L. Selva Roselin and Prajitha Kumari)
2. Effect of interface modification on the Cure Characteristics and Mechanical Properties of Nylon-6/NBR Composites  
(C.Rajesh)
3. EXAFS studies of Hexanitroferrate of Lead  $K_2Pb[Fe(NO_2)_6]$   
(Padmakumar K)
4. Sol-gel preparation and characterization of nickel and cerium loaded rice husk silica catalyst: Application to the oxidation of cyclohexene  
(Femina K.S , Aswini R , Anjaly Mathew , Sreeja K, Harsha M and Sneha Vijayan)
5. Synthesis of Few Acridine Conjugates and Interaction With Biomolecules  
(Vadakkancheril S. Jisha)
6. Studies on the Effect of Struktol 40 Ms Flakes on the Heavily Filled Vulcanization of EPDM Rubber  
(Ameerali P. K.,Muraleedharan Nair and Divya P )
7. In vivo Analgesic activity of ethanolic extract of medicinal plant Hypericum mysorensense Aerial part  
(Anusha P and Gurusamy R)
8. Pyrrole incorporated Schiff Base Macrocycles  
(Divia P)
9. Sorption Behaviour of Polyethylene/Chitosan Composites in Polar and Non Polar Solvents  
(Mubeena Thaikkadan, Sunil Kumar M and C.Rajesh)
10. Development of LDPE/Low Molecular Weight Chitosan Composite Films for Packaging Applications  
(Rasmi P, Radhakrishnan C. K , Rukkiya KM and Vadakkancheril S. Jisha )

# A Novel Method for the Preparation of Core-Shell Silica-12-Tungstophosphoric acid Nanoparticles for *t*-Butylation of phenol

Rosilda Selvin<sup>1</sup>, Hsui-Ling Hsu, L<sup>1</sup>. Selva Roselin<sup>1</sup> and Prajitha Kumari<sup>2\*</sup>

<sup>1</sup>Lunghwa University of Science and technology, Taiwan

<sup>2</sup>Department of Chemistry, PSMO College, Tirurangadi, Kerala, India

\*prajithakpn@gmail.com

## Abstract

Tert-butylated phenols find many applications in industries. A variety of solid acid catalysts has been reported for the *t*-Butylation of phenol. However, the activity of this catalyst is susceptible to coke formation or poor activity. This paper reports the novelties of steam treated DTP included silica nanoparticle for the liquid phase alkylation of phenol with tert-butanol. The effect of various operating parameters was investigated in terms of conversion and selectivity for the desired product under mild conditions.

**Keywords:** *alkylation; dodecatungstophosphoric acid; nanoparticle; tert-Butylation*

## Introduction

Tert-butylation of phenol is an industrially important reaction and alkylated phenols are widely used for a variety of applications such as antioxidants, herbicides, insecticides, and polymers [1]. They are conventionally prepared by reacting phenol with pure isobutylene gas or C<sub>4</sub> fraction of naphtha using a liquid acid catalyst, which gives wide product distribution. In general, tert-butylation of phenols is carried out in a homogeneous medium using sulphuric acid, phosphoric acid, aluminium chloride–boric acid or boron trifluoride as a catalyst [2]. The use of conventional Friedel–Crafts catalysts gives rise to many problems concerning handling, safety, corrosion, and waste disposal. Therefore, considerable efforts have been made for the development of suitable heterogeneous solid acid catalysts [3]. The current processes use highly polluting and hazardous catalysts. Although many commercial ion exchange resins exhibit high activity for the tert-butylation of phenol and substituted phenols with isobutylene, their lower thermal stability limit their industrial application. Various solid acid catalysts have been reported in the literature for tert-butylation of phenols [4-8]. Most of the solid acid catalysts reported are active and the most important problem is the selectivity for the desired product [9].

Among the solid acid catalysts, heteropoly acids (HPAs) are promising one for Friedel–Crafts reactions. Among Keggin type HPAs, 12-tungstophosphoricacid (TPA) is thermally more stable and acidic than any other HPAs. Supported DTP catalyst is proved to be a highly active solid acid catalyst for various acid catalysed reactions [10]. But, as of now, few works are available on supported heteropoly acid catalyst for the tert-butylation of phenol [11-13]. Herein, we report a highly active catalyst based on 12-Tungstophosphoricacid (DTP) included into a silica nanoparticle for the t-Butylation of phenol.

## Experimental

### *A. Preparation of DTP included silica nanoparticle*

The modified version of DTP included silica nanoparticle was prepared by sol–gel technique followed by steaming. In a typical procedure, 30wt % DTP/SiO<sub>2</sub> was prepared by dissolving dodecatungstophosphoric acid (3 g) in DI (10ml) water. Tetraethoxysilane mixed with ethanol (24.3 g TEOS in 10 g EtOH) was dropped into the above solution under vigorous stirring. The solution turned into a transparent viscous gum-like liquid. The gel was subjected to vacuum evaporation at 70°C. Upon vacuum evaporation, the solution turned into a transparent sticky solid, which finally turned into transparent sugar-like cubes. The solid was dried in an air oven at 120°C for 6 hrs. The dried solid was steamed in an autoclave at 150°C for 6 hrs.

### *B. Characterization*

Powder X-ray diffraction patterns were recorded using a Rigaku 2000 diffractometer equipped with a Cu-K $\alpha$  radiation ( $\lambda = 1.5418 \text{ \AA}$ ) from  $2\theta = 2.5$  to  $60^\circ$  at a scan rate of  $2^\circ/\text{min}$  using a step size of  $0.04^\circ$ . Morphology and particle size examinations of the samples were carried out using TEM (JEM-2010, 200kV). Nitrogen adsorption measurements were carried out at 77.4 K on a Micromeritics ASAP 2010 instrument. The nature of the acid sites of the catalyst sample was determined by Fourier transform infrared (FTIR) spectroscopy with chemisorbed pyridine. The vapor phase adsorption of pyridine as probe molecule was adopted to find out the acidity of catalyst samples [14]. The nature of acid sites was characterized on the basis of IR spectral data of pyridine adsorbed catalyst samples. The strength of acidic sites were determined by differential scanning calorimetric studies.

### C. Catalytic activity studies

All experiments were carried out in a 100 ml round bottom flask. Phenol (150 mmol), tert-butyl alcohol (10 mmol) and 0.15 g catalyst was added and heated in oil bath to a given temperature. The products formed were analyzed by GC and are confirmed by GC-MS.

## Results and Discussion

### *Surface area measurements*

The surface area of the unsteamed 30 wt % DTP/SiO<sub>2</sub> is only 27 m<sup>2</sup>/g whereas after steaming, it increases drastically up to 10 times, i.e. 30 wt % DTP/SiO<sub>2</sub> is 277 m<sup>2</sup>/g. During the steaming process, the solubility of polymeric silicate species increases due to the presence of steam at high pressure under acidic heteropoly anion condition. The local concentration domains of silicate ions increases, which deprives their growth. Thus, a steamed sample will have a large number of small particles. Similar observation was also noticed in the vapour phase transport method for the zeolite synthesis [15]. During this process, it is possible that the DTP dissolved and distributed more uniformly on the silica nanoparticles.

### *Determination of Acidity*

The XRD patterns of 30 wt % DTP/SiO<sub>2</sub> sample before and after steaming are shown in Fig. 1.

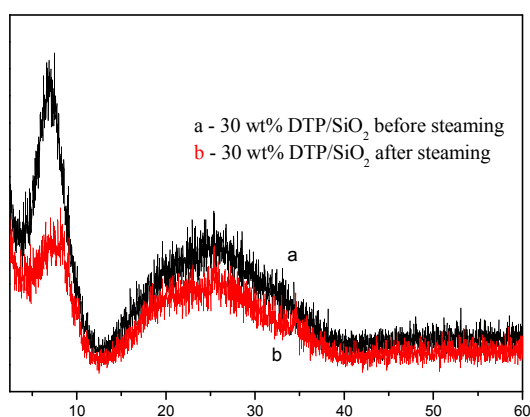


**Fig 1.** XRD patterns of 30 wt % DTP/SiO<sub>2</sub> (a) before steaming (b) after steaming

The XRD pattern of the sample is similar to that of silica except a broad peak located at 2θ between 3 - 8°. It is more likely that this low angle very broad peak is due to the

scattering of small particles. The XRD result confirms that no free DTP particles before and after steaming can be observed.

### **TEM analysis**

TEM micrographs of 30 wt % DTP/SiO<sub>2</sub> sample prepared before and after steaming are reported in Fig. 2. As seen in the micrograph, steaming clearly leads to a decrease of the size of silica particles and an increase of the DTP particles sizes. This means and confirms that after steaming the DTP particles are coated uniformly on the surface of the much smaller silica particles, thus forming SiO<sub>2</sub>/DTP core-shell nanoparticles.

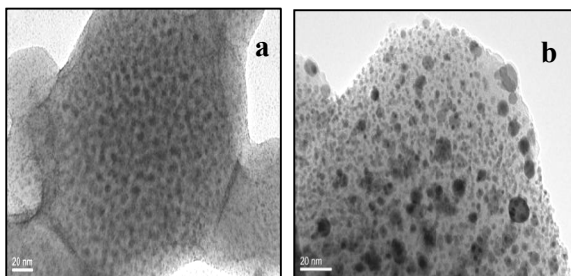


**Fig 2.** TEM image of 30 wt % DTP/SiO<sub>2</sub>: (a) before steaming (b) after steaming

### **Determination of Acidity**

The IR bands recorded for pyridine adsorbed on the catalyst samples are shown in Fig. 3.

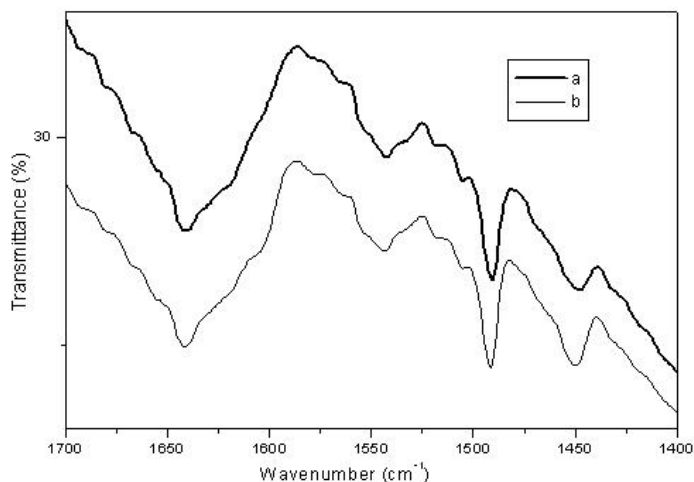


**Fig 3.** FTIR spectra of 30 wt % DTP/SiO<sub>2</sub> exposed with pyridine (a) before steaming and (b) after steaming

The absorption bands of  $1630\text{ cm}^{-1}$  indicate the presence of Bronsted acid sites. The intensity of the absorption bands at  $1630\text{ cm}^{-1}$  increased after steaming. Differential scanning calorimetric thermograms of pyridine desorption from the catalyst shows that steaming of silica included heteropoly acid enhanced the strength of Bronsted acid sites as included by the increase in heat of desorption of pyridine from 300 to 720 J.

### *Alkylation of phenol with tert-butyl alcohol*

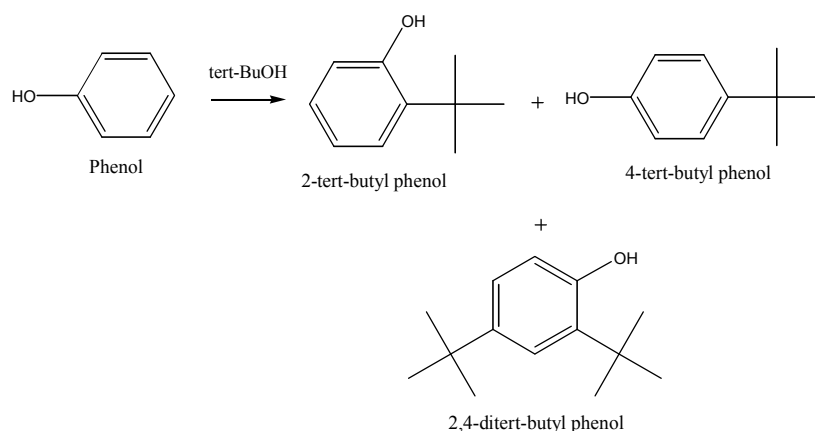


**Fig. 6.** Tert-butylation of phenol

Alkylation of phenol with tert-butyl alcohol was carried out using the supported DTP catalysts. This reaction leads to the formation of 4-tert-butyl phenol (4-TBP) as the major product along with significant amount of 2-tert-butyl phenol (2-TBP). Under specific conditions negligible amount of 2,4-di-tert-butyl phenol (2,4-DTBP) was obtained. The reaction scheme is represented as follows (Scheme 1). Preliminary studies were performed to optimize reaction parameters such as, reaction temperature; phenol/ tert-butyl alcohol molar ratio and catalyst quantity using the steamed 30 wt % DTP/SiO<sub>2</sub> catalyst.

### *Effect of catalyst quantity*

The effect of catalyst quantity was studied over a range of 0.05–0.2 g for alkylation of phenol with tert-butyl alcohol at 80 °C (Table. 1).

**Table 1.** Effect of catalyst amount on the conversion of tert-butyl alcohol

Catalyst Weight (g)	Conversion of tert-butyl alcohol (%)	Selectivity (%)		
		4-TBP	2-TBP	2,4-DTBP
0.05	67	95	4.5	0.5
0.10	84.0	95.8	3.7	0.5
0.15	95.6	98.5	0.1	0.4
0.20	97.8	98	1.6	0.4

Conditions: catalyst, steamed DTP/silica; molar ratio of phenol: tert-butyl alcohol, 15 : 1; reaction temperature, 80 °C.

The conversion of tert-butyl alcohol was found to increase with increase in catalyst amount, which is due to the proportional increase in the number of active sites and the increase becomes less significant beyond 0.15 g. This indicates that beyond 0.15 g, the additional active sites do not increase the adsorption of reactants at a given concentration and so the conversion of tert-butyl alcohol does not increase much

### *Effect of Temperature*

The fresh 12-tungstophosphoricacid included on silica nanoparticles was found to be less active (44 % conversion). The steam treatment tremendously increased the catalytic activity of 30 wt % DTP/SiO<sub>2</sub> catalyst sample and is due to the drastic increase of the surface area and Bronstead acid strength. Also, the conversion was increased with increasing temperature till 80 °C and thereafter remained constant.

**Table 2.** Effect of Temperature on the conversion of tert-butyl alcohol

Temperature (°C)	Conversion of tert-butyl alcohol (%)	Selectivity (%)		
		4-TBP	2-TBP	2,4-DTBP
40	54.8	97.9	1.7	0.4
60	86.5	99.0	0.5	0.5
80	95.6	98.5	0.1	0.4
100	95.8	97.2	2.2	0.6

Conditions: *catalyst, 0.15 g of steamed 30 wt % DTP/SiO<sub>2</sub>; molar ratio of phenol: tert-butyl alcohol, 15: 1.*

#### *Reusability of the catalyst*

To investigate the efficiency of the newly developed steamed 30 wt % DTP/SiO<sub>2</sub> catalyst, it was reused three times. The used catalyst was centrifuged, washed with CH<sub>2</sub>Cl<sub>2</sub> and subsequently dried at 120°C for 6 hrs before being reused in subsequent batches. It was found that there was no loss of the catalytic activity up to three runs. Thus it is concluded that DTP was chemically adsorbed on the catalyst surface, hence, the catalyst was reusable.

#### **Conclusions**

The present work deals with the alkylation of phenol by tert-butyl alcohol using steamed DTP/silica nanoparticle catalysts as a potential replacement for conventional Lewis acid or mineral acid catalysts. The reaction parameters, such as reaction temperature and catalyst quantity were optimized. Under the optimum reaction conditions. conditions (80°C, a phenol by tert-butyl alcohol mole ratio of 1:5, and reaction time for 6 h), the steamed DTP/ Silica nanoparticles gave 95.6 % conversion of tert-butyl alcohol. We believe that the present approach of preparing this catalyst may be extended to the fabrication of monolithic stirrer reactor which was proven to be a versatile system for fine chemicals production in batch mode.

#### **Acknowledgement**

Financial support from the Ministry of Higher Education via the Taiwan-India collaboration research program, in addition to the basic funding provided by the Lunghwa University of Science and Technology is gratefully acknowledged.

#### **References**

1. Voges H.-W, in: B. Elvers, S. Hawkins, and G. Schulz (Eds.), Ullmann's Encyclopedia of Industrial Chemistry, Weinheim, Germany, vol. A19, VHC, 328-328 (1991).
2. Patinuin S.H and Friedman B.S., in: G.A. Olah (Ed.), Alkylation of Aromatics with Alkenes and Alkanes in Friedel-Crafts and Related Reactions, vol. 3, Interscience, New York, 75-81 (1964).
3. Mathew T., Rao B.S and Gopinath C.S., Tertiary butylation of phenol on Cu<sub>1-x</sub>Co<sub>x</sub>Fe<sub>2</sub>O<sub>4</sub>: catalysis and structure-activity correlatio , *J. Catal.* **222**, 107 - 116(2004).

4. Kamalakar G., Komura K and Sugi Y., tert-Butylation of Phenol over Ordered Solid Acid Catalysts in Supercritical Carbon Dioxide: Efficient Synthesis of 2,4-Di-tert-butylphenol and 2,4,6-Tri-tert-butylphenol, *Ind. Eng. Chem. Res*, **45**, 6118–6126(2006).
5. Reddy B.M., Meghshyam K. P, Gunugunuri K. R, Baddam T. R, and Rao KN, Selective tert-butylation of phenol over molybdate- and tungstate-promoted zirconia catalysts, *Appl. Catal. A*, **332**, 183-191 (2007).
6. Xu L., Wu S., Guan J., Wang H., Ma Y., Ke Song H., Xu. H., Xing C., Wang Z. and Kan Q., Synthesis, characterization of hierarchical ZSM-5 zeolite catalyst and its catalytic performance for phenol tert-butylation reaction, *Catal. Commun.*, **9**, 1272-1276(2008).
7. Liao X., Chen G., Liua G, Sun L., Huo W., Zhang W and Jia M., Synthesis, characterization of COK-5 with different Si/Al ratios and their catalytic properties for the tert-butylation of phenol, *Micropor. Mesopor. Mat*, **124**, 210-217( 2009).
8. Song K., Guan J., Wu S., Yang Y., Liu B and Kan Q., Alkylation of Phenol with tert-Butanol Catalyzed by Mesoporous Material with Enhanced Acidity Synthesized from Zeolite MCM-22, *Catal. Lett.*, **126**, 333-340(2008).
9. Subramanian S., Mitra A., Satyanarayana C.V.V and Chakrabarty D.K, Para-selective butylation of phenol over silicoaluminophosphate molecular sieve SAPO-11 catalyst, *Appl. Catal. A.*, **159**, 229-240 (1997).
10. Bhatt N., Sharma P., Patel A., and Selvam P., Supported 12-tungstophosphoricacid: An efficient and selective solid acid catalyst for tert-butylation of phenol and cresols, *Cata. Comm*, **9**, 1545-1550 (2008).
11. Mizuno N and Misono M., Heterogeneous Catalysis, *Chem. Rev*, **98**, 199-218(1998).
12. Biju DM., Shanbhag G.V., Mirajkar S.P., Böhringer W, Fletcher J and Halligudi S.B., Silicotungstate-modified zirconia as an efficient catalyst for phenol tert-butylation, *J. Mol. Catal. A* , **233**, 141-146 (2005).
13. Biju DM, Shanbhag G.V, Halligudi S.B, Liao X, Chen G, Liu G, Sun Li, Huo W, Zhang W and Jia M, Phenol tert-butylation over zirconia-supported 12-molybdophosphoric acid catalyst, *J. Mol. Catal. A*, **247**, 162-170 (2006).
14. Aboul-Gheit A.K., Al Hujjajo M.A and Summan A.M., *Thermochim. Acta*, **118**, 9-16 (1987).

# Effect of interface modification on the Cure Characteristics and Mechanical Properties of Nylon-6/NBR Composites

C.Rajesh<sup>1\*</sup>

<sup>1</sup> Department of Chemistry, MES Keveeyam College Valanchery-676552, Kerala, India

\* [rajeshvlcy@rediffmail.com](mailto:rajeshvlcy@rediffmail.com)

## Abstract

The interface modification of short nylon-6 fiber reinforced NBR composites has been carried out by the incorporation of two different bonding agents, *viz.* hexamethylene tetramine-resorcinol and phthalic anhydride. The cure characteristics and mechanical properties of the bonded composites have been analyzed. The addition of bonding agents increases the maximum torque and reduces the optimum cure time and scorch time. Bonding agent added composites show superior mechanical properties than the corresponding unbonded systems. SEM studies reveal improved adhesion between fiber and rubber in bonding agent added composites.

**Keywords:** *composites, interface, bonding agent, mechanical properties*

## Introduction

The properties and performance of a fiber reinforced composite material is the result of combined behavior of the reinforcing fiber, polymeric matrix and the fiber-matrix interface. Existence of good interfacial bonding between fiber and matrix is an essential factor to achieve good fiber reinforcement. In composites, the matrix molecules may be anchored to the fiber surface by chemical reaction or adsorption which determines the extent of interfacial adhesion. Interaction at the interface can be improved either by using a bonding agent or by different surface treatments for the fiber. These additives can modify the interface by interacting either chemically or physically with both the fiber and matrix [1].

Several researchers have reported the use of different bonding agents to modify the interfacial strength of fiber-rubber composites. A tri-component dry bonding system based on hydrated silica-resorcinol-hexamethylene tetramine (H-R-H) has been used successfully in many short fiber-elastomer composites [2-10]. Dunnon [11] has evaluated the rough guidelines for the manipulation of the compounding and processing factors like

the type and amount of silica, and the amount of zinc oxide in the course of designing an optimum adhesion compound. Darwish *et al.* [12] reported the use of H-R-H as an adhesion promoter for nylon cord to nitrile rubber. They have also studied the effect of replacement of resorcinol with *o*-aminophenol, *m*-aminophenol, *p*-aminophenol and *m*-phenylene diamine. Pokluda and Osoha [13] used different types of cresol to replace resorcinol in the bonding system. Verghese *et al.* [14] reported that silica is not needed as a component in the dry bonding system when sisal fiber is used as reinforcement.

The effect of urethane resins based on polymeric 4,4'-diphenylmethane diisocyanate (MDI) and different diols on the mechanical properties of short polyester fiber reinforced polyurethane composite was studied by Suhara *et al* [15]. The urethane based bonding system affected the processability of the composites adversely. However, the tensile strength, modulus, and the abrasion resistance of the composites were improved by the urethane bonding system. Sreeja *et al.* [16] investigated the effect of urethane based bonding agent on the cure characteristics and mechanical properties of natural rubber/whole tyre reclaim–short nylon fiber composites. In our group Haseena *et al.* [17] reported the use of a two- component bonding system consisting of hexamethylene tetramine and resorcinol in short sisal/coir hybrid fiber reinforced natural rubber composites.

In our laboratory nylon 6 fiber reinforced NBR composites have been prepared and their cure characteristics and mechanical properties were analyzed [18]. The present study deals with the interface modification of these composites by using two different bonding systems, namely hexamethylene tetramine- resorcinol and phthalic anhydride. The efficiency of these bonding agents has been evaluated in terms of cure characteristics and mechanical properties.

## **Experimental**

NBR having 35% acrylonitrile was obtained from Apar Industries, Mumbai, India. Nylon 6 fiber was obtained from SRF Polymers Limited, Chennai, India in yarn form. The rubber vulcanizing agent dicumyl peroxide (DCP) was of commercial grade. Hexamethylene tetramine, resorcinol and phthalic anhydride used as bonding agents were of laboratory reagent grade.

Formulations of the mixes used in the present work are given in Table 1. Mixes A and B are cured by sulfur. Mix A contains 24 phr nylon 6 fibers of length 6 mm. B is the mix containing hexa-resorcinol as bonding agent. Mixes C, D and E are cured by DCP. Mix C contains 24 phr nylon fibers of length 6 mm. Mixes D and E contain hexa-resorcinol and phthalic anhydride respectively as bonding agents. The composites were prepared using a laboratory two roll mixing mill (150 × 300 mm). NBR was masticated on the mill for 2 minutes followed by the addition of the ingredients. The nip gap, mill roll speed ratio and the number of passes were kept the same for all the mixes. The samples were milled for sufficient time to disperse the fibers in the matrix at a mill opening of 1.25 mm.

**Table 1.** Formulations of Mixes (phr<sup>a</sup>)

	A	B	C	D	E
NBR <sup>b</sup>	100	100	100	100	100
Zinc Oxide	5	5			
Stearic Acid	2	2			
MBTS <sup>c</sup>	1.5	1.5			
TMTD <sup>d</sup>	0.5	0.5			
Sulfur	1.5	1.5			
DCP <sup>e</sup>			5	5	5
Hexa <sup>f</sup>		1.92		1.92	
Resorcinol		3.84		3.84	
Phthalic anhydride					3
Nylon Fiber, Fiber length (mm)	24, 6	24, 6	24, 6	24, 6	24, 6

<sup>a</sup>Parts per hundred rubber, <sup>b</sup>Acrylonitrile butadiene rubber, <sup>c</sup>Mercapto benzo thiazyl disulphide  
<sup>d</sup>Tetramethyl thiuram disulphide, <sup>e</sup>Dicumyl peroxide, <sup>f</sup>Hexamethylene tetramine

The cure characteristics of the mixes were investigated by using a Monsanto Rheometer R-100 at a rotational frequency of 100 cycles/ min. Vulcanization of the mixes was done at 153°C in a hydraulic press having electrically heated platens to their respective cure times as obtained from the Rheometer.

Stress-strain measurements were carried out using a Universal Testing Machine (ZWICK-1474) at a crosshead speed of 50 cm min<sup>-1</sup>. Tensile measurements of the composites were carried out using samples cut along (longitudinally oriented fiber) the

grain direction. Modulus, tensile strength, and elongation at break were determined according to ASTM test method D412-68. Hardness was measured at room temperature by using a shore-A hardness tester according to ASTM D-2240 test method. In the measurement of mechanical properties, the standard deviation was below 2%.

Samples for scanning electron micrographs (SEM) were prepared by cryogenically fracturing the samples in liquid nitrogen. The samples were sputter coated with gold and the photographs were taken using a scanning electron microscope (S-2400, Hitachi).

## Results and Discussion

### *Curing behavior*

The addition bonding agents has a considerable effect on the cure characteristics of short nylon-6 fiber reinforced NBR composites. Figure 1 represents the rheographs of mixes containing hexa-resorcinol and phthalic anhydride bonding agents (Mix D and E respectively) and that of mix without bonding agent (Mix C), cured by DCP at the optimum fiber loading. Table 2 shows the cure characteristics of sulfur and DCP vulcanized composites containing different bonding agents along with the unbonded ones. It can be seen that in DCP cured samples the torque values of mixes containing bonding agents are higher than that of mixes without bonding agent. The difference between the maximum and minimum torque value ( $M_H - M_L$ ) indicates a higher cross-linking density for mixes D and E.

**Table 2.** Cure characteristics of various mixes

Mix	Max Torque (dNm)	Min. Torque (dNm)	dT (dNm)	T <sub>90</sub> (min)	Scorch time (min)
A	19.45	0.86	18.59	3.95	0.25
B	20.82	1.22	19.60	2.30	0.20
C	27.88	1.37	26.51	30.06	1.06
D	37.08	2.71	34.37	20.75	0.59
E	33.49	6.25	27.24	17.00	0.70

In the case of resorcinol-hexa bonding agent added composite (Mix D), the higher cross link density can be attributed to the increased adhesion between the fiber and matrix

through the formation of an *in-situ* resin. During the curing of the composite, polymerization of resorcinol and hexamethylene tetramine is initiated and, as the vulcanization of rubber proceeds, the resin is formed by the condensation reaction between these two components.

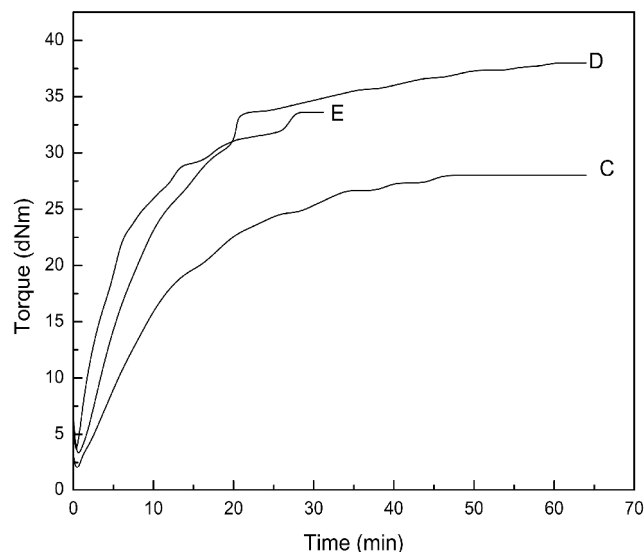
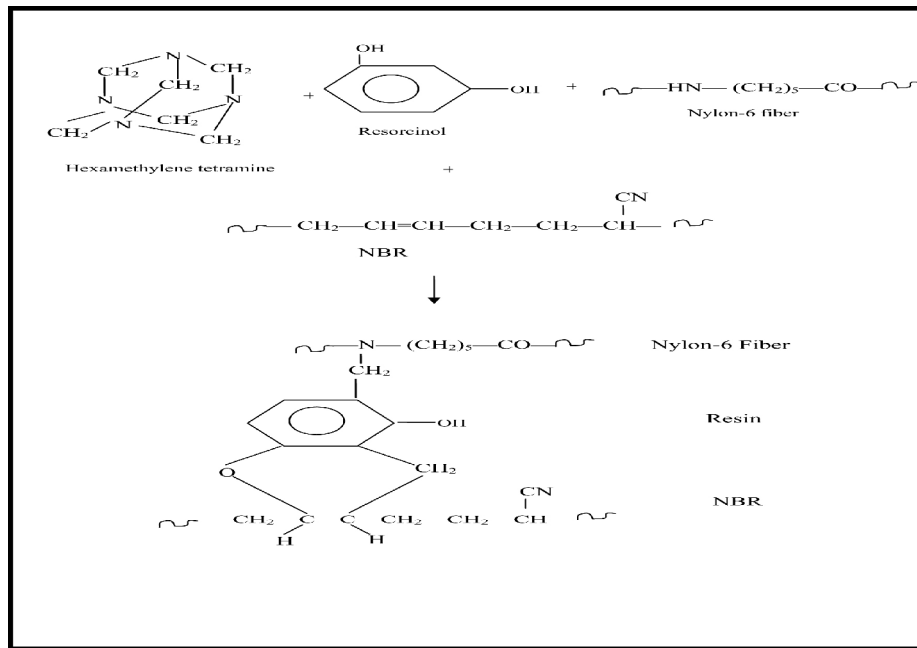
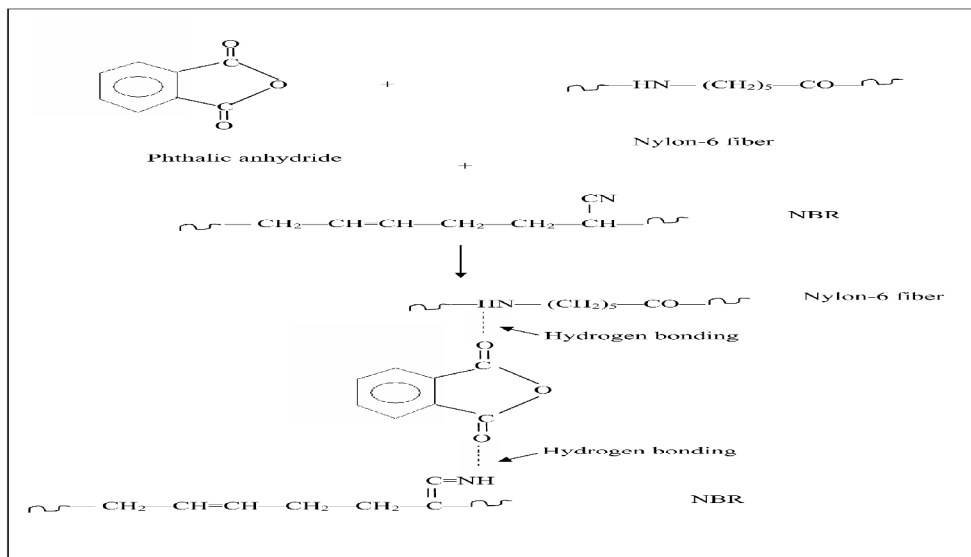


**Figure 1.** Rheographs of mixes

Meanwhile, the low molecular weight polymer species of the resin are able to diffuse into the interfacial region between the rubber and the fiber. Thus, a boundary layer is formed at the rubber surface which is rich in resin formation and it forms chemical bonds with the rubber and the fiber. Scheme.1 represents a hypothetical mechanism showing the interface bonding in hexa-resorcinol added composite. In the case of phthalic anhydride added Composite (Mix E), the higher cross-linking density can be due to the improved adhesion between fibers and matrix through intermolecular hydrogen bonding (Scheme.2). It is also found that the addition of bonding agent reduces the optimum cure time and scorch time (Table 2). However the decrease in scorch time indicates a reduction in scorch safety of the compound containing bonding agents. Table 2 shows the effect of hexa-resorcinol bonding agent on the curing behavior of composite vulcanized by sulfur. It can be seen the torque value of bonded composite (Mix B) is higher than that of the corresponding unbonded one (Mix A). The optimum cure time and scorch time were found to be reduced by the incorporation of bonding agent.



**Scheme 1.** Mechanism of interfacial bonding in composites containing hexa-resorcinol



**Scheme 2.** Mechanism of interfacial bonding in composites containing phthalic anhydride

### Mechanical Properties

Figure 2 shows the stress-strain curves for the unbonded and bonded composite systems cured by DCP. The effect of bonding agents on the mechanical properties of the composites

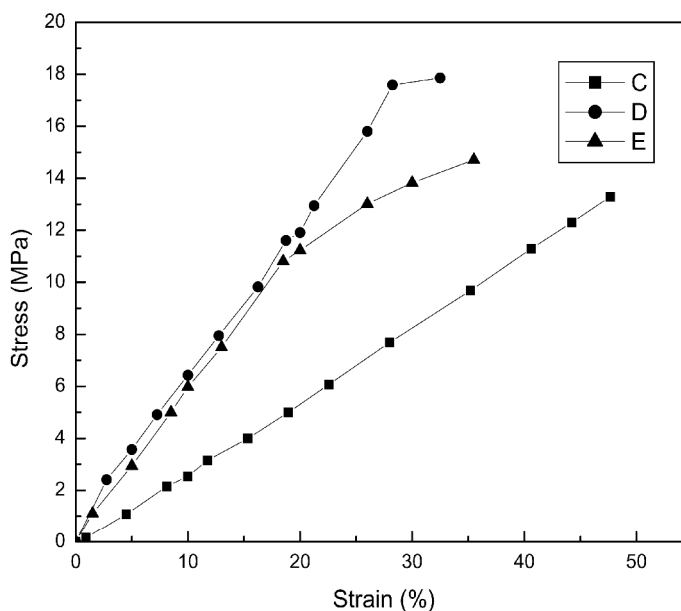


**Figure 2.** Stress vs strain curve of composites

can be understood from Table 3. It can be seen that composites containing bonding agents show superior mechanical properties than those without bonding agent. Tensile strength, tear strength, modulus and hardness of the composites were found to be increased by the

**Table 3.** Mechanical Properties of bonded and unbonded composites

	A	B	C	D	E
<b>Tensile Strength (MPa)</b>	12.32	13.72	13.295	16.46	14.64
<b>Tear Strength (kN/m)</b>	49.87	60.65	80.2	85.3	81.59
<b>Modulus (MPa) 10% elongation</b>	24.8	31.65	25.36	63.12	59.7
<b>20% elongation</b>	25.9	31.31	26.51	59.55	56.15
<b>Elongation at break (%)</b>	48	46.25	47.67	40.07	41.17
<b>Hardness-Shore A</b>	82	85	84	87	85

incorporation of bonding agent, where as the elongation at break is reduced. The improvement in tensile strength and modulus is comparatively greater for hexa-resorcinol bonded composites than phthalic anhydride bonded systems. This may be attributed to the difference in extent of interfacial interaction between the fiber and rubber resulted via the incorporation of bonding agent. It has been found that curing system plays a significant role in the enhancement in mechanical properties of the composites by the incorporation of bonding agents. It is obvious from Table 3 that the effect of hexa-resorcinol bonding agent is more pronounced in DCP cured composites than the sulfur cured one (Mixes D and B respectively). This may be attributed to the difference in type of cross links introduced by DCP and sulfur during vulcanization. As it can be seen from Figures 3 (a) and (b), DCP introduces rigid C – C linkages whereas sulfur creates mono, di and polysulfidic linkages during curing.

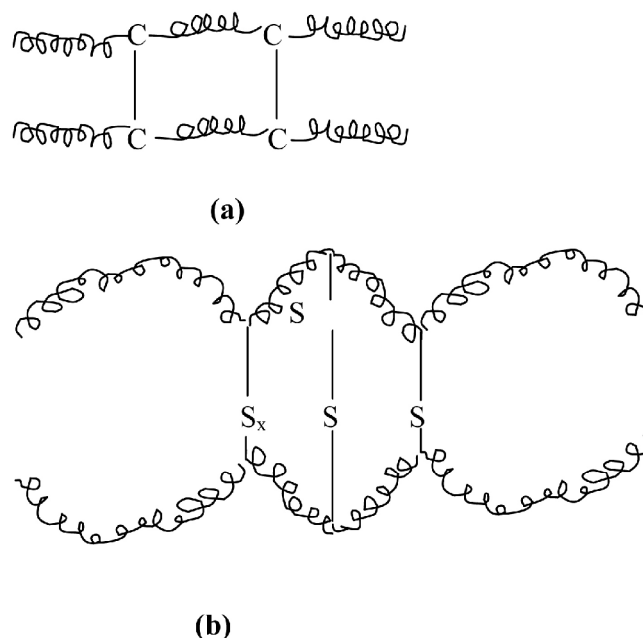
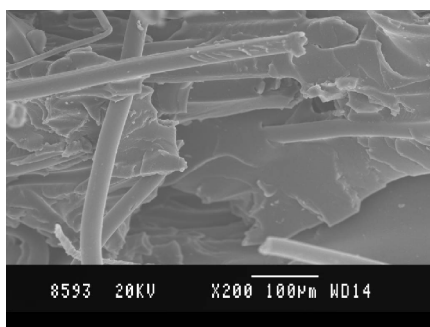


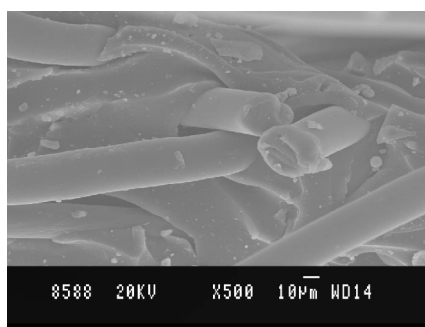
**Figure 3.** (a) C-C linkage in DCP cured composite  
 (b) Mono-, di-, and polysulfidic linkages in sulfur cured composite

The extent of interfacial adhesion has been better understood by examining the tensile fracture surfaces of the composites by scanning electron micrographs (SEM). Figure 4

(a) shows the tensile failure surface of unbonded composites (Mix A). The breakage and pull out



4 (a)



4(b)

**Figure 4** (a) SEM of tensile failure surface of unbonded composite (Mix A), (b) shows the SEM of tensile failure surface of bonding agent added composites (Mix B)

of fibers indicate poor wetting between fibers and matrix. Figure 4 (b) shows the SEM of tensile failure surface of bonding agent added composites (Mix B). It is seen that, for Mix B, the rubber particles remain adhered to the fiber surface, and also there is no considerable fiber breakage due to the better bonding between the fibers and the matrix.

## Conclusions

Hexamethylene tetramine- resorcinol and phthalic anhydride were used as bonding agents to modify the interfacial interaction in nylon 6 fiber reinforced NBR composites. The cure characteristics and mechanical properties of the bonded composites have been analyzed. The addition of bonding agents increased the maximum torque and reduced the optimum cure time and scorch time. The addition of bonding agents enhanced the tensile strength and modulus. The improvement in mechanical properties was more pronounced in DCP cured samples than in sulfur cured one. SEM studies revealed improved adhesion between the fiber and rubber in bonding agent added composites.

## References

1. Gaylord G.: *Copolymers, polyblends and composites*, Academic, New York (1975).
2. Akthar S., De P P.: Short fiber-reinforced thermoplastic elastomers from blends of natural rubber and polyethylene, *J. Appl. Polym. Sci*, **32**, 5123-5146 (1986).

3. Coran A Y., Boustany K., Hamed P.: Short-fiber-rubber composites: the properties of oriented cellulose fiber-elastomer composites, *Rubber Chem. Technol*, **47** (1974).
4. O'Conner J E.: Short fiber reinforced elastomer composite, *Rubber Chem Technol*, **50**, 945-958 (1977).
5. Roy R., Bhowmick A K., De S K.: Dynamic mechanical properties of short carbon fiber-filled styrene-isoprene-styrene block copolymer, *J. Appl. Polym. Sci*, **49**, 263-273 (1993).
6. Chakraborty S., Setua D K., De S K.: Short jute fiber reinforced carboxylated nitrile rubber, *Rubber Chem. Technol*. **55**, 1286 (1982)
7. Geethamma V G., Mathew K T., Lakshminarayanan R., Thomas S.: Composite of short coir fibers and natural rubber: effect of chemical modification, loading and orientation of fiber, *Polymer*, **39**, 1483-1493 (1998).
8. Murthy V M., De S K.: Short jute fiber reinforced rubber composites, *Rubber Chem. Technol*, **55**, 287 (1982).
9. Setua D K., Dutta B.: Short silk fiber-reinforced polychloroprene rubber composites, *J. Appl. Polym. Sci*, **29**, 3097-3114 (1984).
10. Morita E.: Reactions of resin formers in dry bonding rubber systems, *Rubber Chem. Technol*, **53**: 795 (1980).
11. Dunning D D.: *Hi-Sol Bulletin No. 40, Chemical Divn, PPG Industries Inc., Pittsburgh* (1969).
12. Darwish NA., Lawandy S N., El-Shazly., Abou-Kandil A I.: Effect of bonding systems on the adhesion of nitrile rubber to nylon cord, *Polym-Plast. Technol. Eng*, **39** (5), 793-806 (2000).
13. Pokluda., Osoha.: *International Rubber Conference (IRC), 1986, Proc., Goteborg, Sweden*, 546 (1986).
14. Varghese S., Kuriakose B., Thomas S.: Mechanical and viscoelastic properties of short fiber reinforced natural rubber composites: effects of interfacial adhesion, fiber loading, and orientation, *J. Adhesion Sci. Technol*, **8**, 235-248 (1994).
15. Suhara F., Kutty S K N., Nando G B.: Mechanical Properties of Short Polyester Fiber-Polyurethane Elastomer Composite with Different Interracial Bonding Agents, *Polym-Plast, Technol. Eng*, **37**(2), 241-252 (1998).

16. Sreeja T D., Kutty S K N.: Effect of urethane based bonding agent on the cure characteristics and mechanical properties of natural rubber/whole tyre reclaim-short nylon fiber composite, *Polym-Plast. Technol. Eng*, **41**(1), 77-89 (2002).
17. Haseena A P., Namitha., Priya Dasan K., Unnikrishnan G., Thomas S.: Investigation on interfacial adhesion of short sisal/coir hybrid fiber reinforced natural rubber composites by restricted equilibrium swelling technique, *Composite Interfaces*, **11** (7), 489-513 (2004).
18. Rajesh C., Unnikrishnan G., Purushothaman E., Thomas S.: Cure characteristics and mechanical properties of short nylon fiber reinforced nitrile rubber composites, *J. Appl. Polym. Sci*, **92**, 1023 (2004).

# EXAFS studies of Hexanitroferrate of Lead $K_2Pb[Fe(NO_2)_6]$

Padmakumar K\*

Department of Chemistry, Government Victoria College, Palakkad, Kerala, India- 678001

\*[pkkool@gmail.com](mailto:pkkool@gmail.com)

## Abstract

A detailed structural analysis of the title compound was performed using Extended X-ray absorption spectroscopy in order to understand the electronic structure of the ground state with a view to explain the magnetic and the related spectroscopic features. The structural details reported here were found to be deviating from the earlier results proposed based on the powder X-ray diffraction method.

Keywords: EXAFS, hexanitroferrate

## Introduction

Dipositive iron in its low spin state is described by a non degenerate orbital and spin ground state where the symmetry at the Iron site is close to octahedral in character. This will not give any net electron density at the site of the nucleus resulting in single narrow Mossbauer spectrum. If there are distortions from the perfect octahedral symmetry it results in the quadrupolar splitting of the Mossbauer spectral line at low temperature[1]. Temperature dependent quadrupolar splitting in Mossbauer spectroscopy resulting from the spin crossover behaviour with high spin at high temperature and low spin at low temperature is an entirely different behaviour. However the observation of the hyperfine splitting in the Mossbauer spectrum of high spin  $Fe^{2+}$  is rather unusual due to the rapid spin lattice relaxation at these temperatures where one might expect it to be observed. In an earlier report [2] it was established that the compound with a formula  $K_2Ba[Fe(NO_2)_6]$  (dipotassium barium hexanitroferrate) was found to be exhibiting unusual magnetic and electronic relaxation properties This was attributed to the  $^5E$  ground state of the ferrous ion in the high spin state originated from the Jahn-Teller distortion of the  $^5T_2$  ground state. This doubly degenerate ground state is responsible for the temperature dependent Mossbauer spectral properties of these series of compounds  $K_2M[Fe(NO_2)_6]$  where M is Pb, Ba, Sr, Ca, Zn,. The details of the structure reported earlier [3] were found to be not agreeing with the Mossbauer spectral data that we have recorded. So a detailed EXAFS data analysis was carried out at room temperature as well as at low temperature

for  $K_2Pb[Fe(NO_2)_6]$  to get an explanation for the Mossbauer spectral pattern and the associated magnetic behaviour, which can be further extended to other systems.

## Experimental

The compound was prepared according to the earlier reported procedure [4]. The purity of the compound was checked by the elemental analysis and Ir spectroscopy which concur with the earlier reported results. It should be noted here that the compounds are unstable in presence of water even though it is prepared in aqueous medium, but by quick filtration followed by drying.

*EXAFS (Extended )X-ray absorption fine structure spectroscopy) measurements:* X-ray absorption data on K-edge and  $L_{III}$  edge were collected at the Stanford Synchrotron radiation laboratory(SSRL) on beam line II-3 under dedicated ring conditions (3.0 GeV 50-100 mA) using a Si(220) double crystal monochromator. Harmonic rejection was accomplished by detuning the monochromator by 50%. The samples were ground to a fine powder, diluted with boron nitride and sealed with Kapton in Al sample holders. Spectra were measured both at 10K, using an Oxford instrument helium cryostat and at room temperature. Absorption data were collected in the transmission mode using ionizing chambers filled with Nitrogen gas. The samples were calibrated using an Iron foil internal standard with the first reflection point of the Iron foil define as 7111.2 eV. The Pb edge was calibrated by setting the first inflection point to 13055 eV. EXAFS spectra were measured by using 10eV, with 1sec. integration time on pre edge region, 0.5 steps in the edge region,  $0.05 \text{ \AA}^{-1}$  steps in the K-max  $2-17 \text{ \AA}^{-1}$  using integration times up to 8sec at  $k=T/ \text{ \AA}^{-1}$ . The total integration time per scan was 35- 40 minutes. Two spectra were averaged for each sample.

*Data analysis:* The first order polynomial was subtracted from the pre edge region and a multiple region spline was subtracted from the EXAFS region. The threshold energy ( $k=0$ ) was set to 713.0 eV. from the Iron and 13055 eV for the Lead. The EXAFS data were analysed using EXAFSPAK data analysis programs][5]. All the data were  $k^3$  weighted and the average spectra were fit between a k range of 2.0 to  $11.0 \text{ \AA}^{-1}$  for the Fe and 2.0 to  $17 \text{ \AA}^{-1}$  for Pb.

## Results and Discussion

*EXAFS data analysis:* The spectra have been recorded for different samples and were found to have excellent reproducibility. The EXFS spectra were recorded at room temperature and at 10K. All the features of the spectra were identical at both temperatures except for the broadening at room temperature. For the room temperature EXAFS the high R features are all strongly damped. This could be due to the contributions from the thermal and static damping factors which are high at high temperature. But the very immediate co-ordination environment, (such as Fe-N and Fe-O) appear identical at both the temperatures.

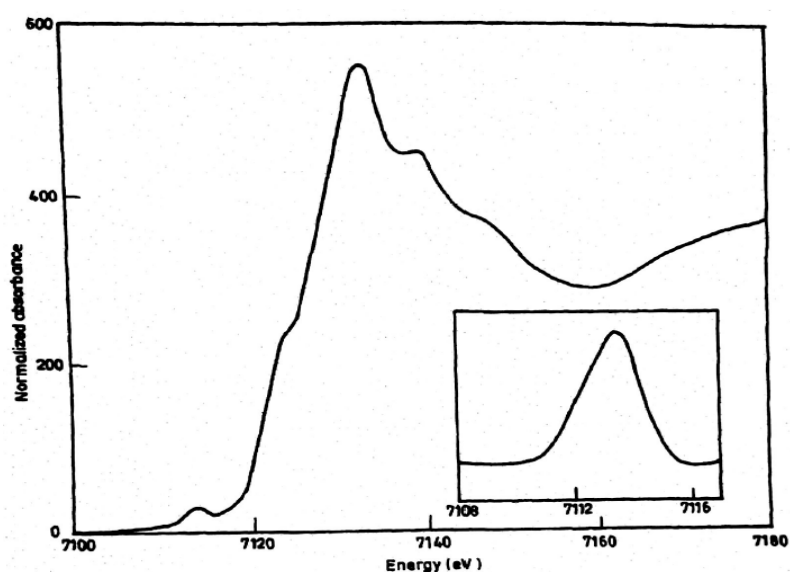


**Fig 1:** XANES spectrum of the Fe-edge region with  $1s \rightarrow 3d$  intensity expanded in the inset.

*XANES (X-ray absorption near edge spectroscopy) spectrum:* Fe XANES spectrum was compared with few other Fe spectra. There are several resolved transitions and a couple of shoulders in this region. This could be used as finger print of the local structure. The absence of any change with temperature suggests that the average environment remains the same as the temperature is raised. The spectrum of the Fe-edge is shown in Fig 1. The well resolved transition at ca 7111.3 eV is the  $1s \rightarrow 3d$  transition. The isolated background subtracted  $1s \rightarrow 3d$  transition is shown in inset. This transition which is forbidden by dipole selection rule is quadrupole allowed and is always seen for Fe (II) spectra even in centrosymmetric systems, but with a small intensity. In model studies the intensity of the  $1s \rightarrow 3d$  transition has been found to increase as the Fe site distorts perfectly from

octahedral symmetry. The pre-edge intensity gradually increases with a decrease in coordination number and the departure from a centrosymmetric co-ordination environment. This general principle has been adopted for probing the site symmetry of the metal centre in biologically important proteins [6]. This is a consequence of the 3d and 4p mixing which is allowed in distorted geometry. The intensity of the 1s→3d transition for  $K_2Pb[Fe(NO_2)_6]$  is surprisingly large, for an earlier proposed octahedral Fe(II) site. This anomalous behavior could be explained on the basis of the disorder in the material which mainly arises due to the distorted nature of the  $NO_2$  groups. It was reported that the opposite  $NO_2$  groups are lying in a plane. Thus the three sets of  $NO_2$  groups make three mutually perpendicular planes. These explanations are based on the crystal structure data available for the hexanitroferrate compound of Cu which are easily crystallisable. The Cu compound was found to undergo Jahn-Teller distortion. But the hexanitroferrate could be entirely different due to difference in electronic structure. Thus the overall distortion is manifested as a peak in the pre-edge region even though the appearance of this peak is attributed to lower co-ordination environment of the central metal atom. All the  $NO_2$  groups are distorted from the normal plane giving an overall distortion from the perfect octahedral symmetry. This distortion is also confirmed by the presence of nearly four to five peaks in the asymmetric stretch of the  $NO_2$  group, in the infrared spectrum of this compound (to be communicated). The isolated 1s→3d transition (see inset) shows a shoulder at ca 7112 eV in addition to the principle transition at ca 7113.5 eV. These most likely represent transition into different ( $1s^1$ ) ( $3d^7$ ) final states and are thus measure of 3d orbital splitting. Several more partially resolved transitions are observed in the XANES. There is a shoulder on the edge at about 7124 eV. It is impossible to say what it is due to. However, numerous studies of Cu(II) and Fe(II) complexes have shown, empirically that the transition at about this place on the edge is often correlated with the presence of a square planar or square pyramidal metal site. This transition was variously assigned as the 1s – 4p or 1s-4p +shake down. Normally we should not expect to see a transition at this energy for pseudo octahedral Fe. However in this case it is very difficult to interpret this transition in terms of a 5 co-ordination or lower than that for the central metal atom. Thus the unusual high intensity of 1s→3d transition suggests that the Fe site is distorted from the cubic crystallographic symmetry. Such distortions are not expected for a low spin Fe(II), but are quite reasonable for the high spin case. Further evidence for the high spin

character comes from the resolution of the two transitions within  $1s \rightarrow 3d$  region. Low spin Fe(II) is expected to show only one  $1s \rightarrow 3d$  transition.

*Edge Region:* The observed edge energy for this compound is slightly higher than what is expected for a normal Fe(II) complex. Comparative plots of the edge region for the various oxidation states of Fe are given Fig 2. Here again the normal interpretation is that the edge energy is a measure of the oxidation state. The energy at hlf height is typical of that found for Fe(III) complexes and is substantially (ca 2-3 eV) higher than the six coordinate Fe(II) complexes, which typically have edge energies between 7118-7122 eV[6]. As the oxidation state increase the edge energy will also be shifted to higher side. Penner-Hahn and co-workers suggest that the bond length information is the principle determinant of the edge energy rather than the simple oxidation state of the element of interest. The bond length is inversely related to the edge energy. Hence we have a first coordination sphere of six nitrogen atoms with a very short Fe-N bond. This information has been obtained from the Fe EXAFS region. Thus it is not necessarily surprising that the edge energy is usually high.

*EXAFS spectrum:* The 10K EXAFS spectra for the Fe K-edge and Pb  $L_{III}$  edge are shown in Fig 3 and the corresponding Fourier transforms are shown in Fig.4. The presence of strong outer shell scattering is apparent in the high frequencies of EXAFS and the presence of large high-R peaks in FT's. The nearest neighbour interactions are nearly identical in the room temperature spectra, however the outer shell scattering is strongly damped at room

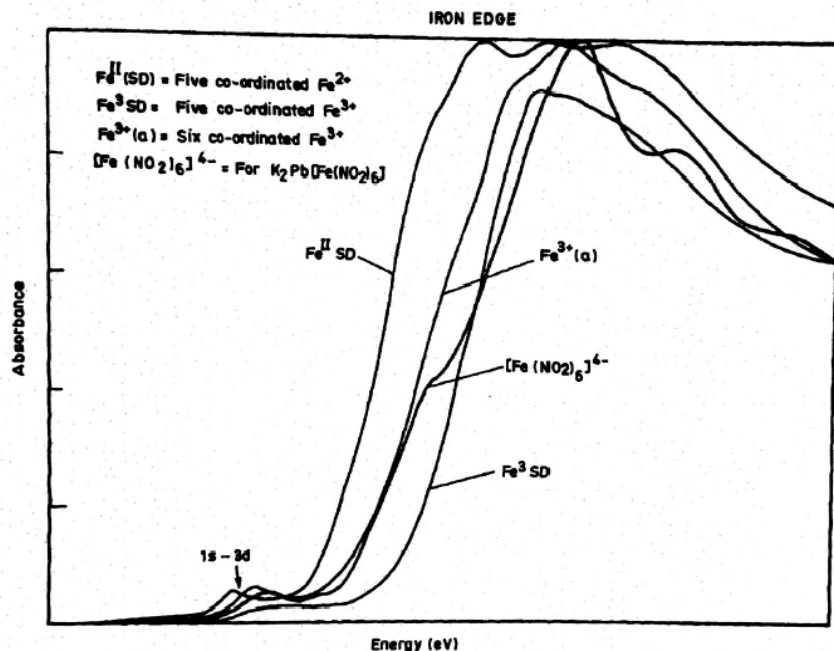


**Fig 2:** Comparative plots of the edge region of the Iron in various oxidation states.

temperature. In general the FT's are consistent with the structure expected from powder XRD pattern. According to the powder XRD pattern the Fe atom is surrounded by six nitrite N at 2 Å 12 nitrite O at 2.8 Å 8 Potassium at 4.5 Å and six Pb at 5.16 Å. In the FT all of the peaks are shifted by  $\alpha = -0.4$  Å, thus leading to the assignments indicated on Fig 4. Similarly the Pb atom is surrounded by 12 nitrite O at 2.8 Å, 6 nitrite N at 3.2 Å, 8 Potassium at 4.5 Å, and 6 Fe at 5.16 Å.

Quantitative curve fitting analysis is consistent with the structure picture. In particular there is a striking agreement between the Fe-Pb and Pb-Fe distances obtained by EXAFS (5.18 Å and 5.16 Å) as expected crystallographically (5.16 Å), (Table 1)

**Table 1:** Various bond lengths for the title compound at room temperature. (Similar values are obtained at 10K also)

Type	Distance	Type	Distance
Fe EXAFS	Å	Pb EXAFS	Å
Fe-N	1.97	Pb-O	2.77
Fe-O	2.80	Pb-N	3.22
Fe-K	4.50	Pb-K	4.33
Fe-Pb	5.26	Pb-Fe	5.24

Fits of the first FT peak (Fig 5) gave a reasonable Fe-N co-ordination number of 5-6 but an unusually short apparent bond length of 1.93 Å. (Table 2)

**Table 2:** Best fit to Iron EXAFS:

Shell	Scatterer	R Å	$\sigma^2(\text{Å}^2 \cdot 10^3)$
1	N	1.97	0.5
2	O	2.82	0.7
3	K	4.45	2.7
4	Pb	5.22	2.1

This distance is too short for a six co-ordinated Fe(II), particularly for the high spin Iron case. More typically the distances for such systems are 2.11 to 2.15 Å. A short bond length could produce a low spin Fe(II) which will be diamagnetic at all temperatures due to the presence of  $^1A_{1g}$  ground state which is non magnetic at all temperatures. But here is an Fe atom in the high spin ground state with +2 oxidation state, as proved by magnetic data (to be communicated), having a short bond length of the order of 1.97 Å. This bond length is about 0.2 Å lesser than what is calculated from crystallographic data. The apparent first shell co-ordination is about 4 which is rather puzzling. This anomaly could be due to the disorder in the Fe site which is random from one to the other. Since the overall lattice is cubic, there could be some tetragonal distortions of Fe giving 4 equatorial Fe-N at 1.95 Å and two longer axial Fe-N distances. In such a case when 1/3 distortions are long “a” 1/3 of them long “b” and 1/3 of them along “c” in different Fe centers. Such distortions are acceptable and understandable since the high spin octahedral  $\text{Fe}^{2+}$  with  $^5T_2$  ground state is expected to undergo Jahn-Teller distortion. This could lead to axial compression or elongation along the X, Y, Z co-ordinates. But the over all lattice would still look like a perfect cube. These distortions are not evident from EXAFS because of the wide distribution of Fe-N bond distances at random direction.

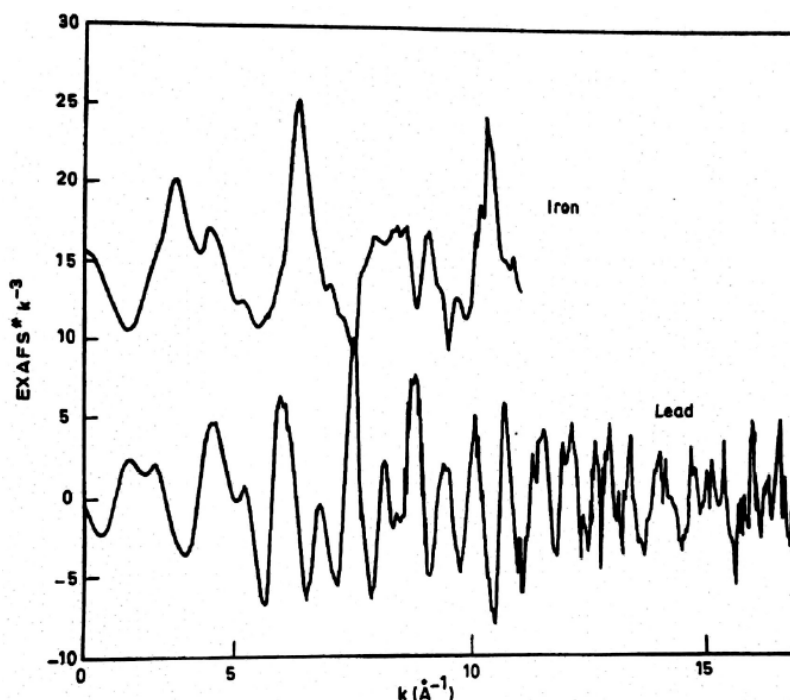


**Fig 3:** The  $k^3$  weighted EXAFS spectra of the Iron edge and the Lead edge.

We could see the outer shell oxygen very clearly. These at about 2.8 Å which are completely consistent with the known structure of the metal co-ordination nitrites, ie the Fe-N and Fe-O distances are mutually consistent, which shows most of the Fe atom co-ordinated by nitrites as required by the crystal structure. The apparent co-ordination number for the Fe-O is little low but it is approximately double the Fe-N co-ordination number. It is interesting to note here that the crystallographic parameters based on powder XRD correctly predict the Fe-O but not the Fe-N distance. But the EXAFS distances Fe-N and Fe-O are consistent which again points to some inaccuracies in the crystal structure.

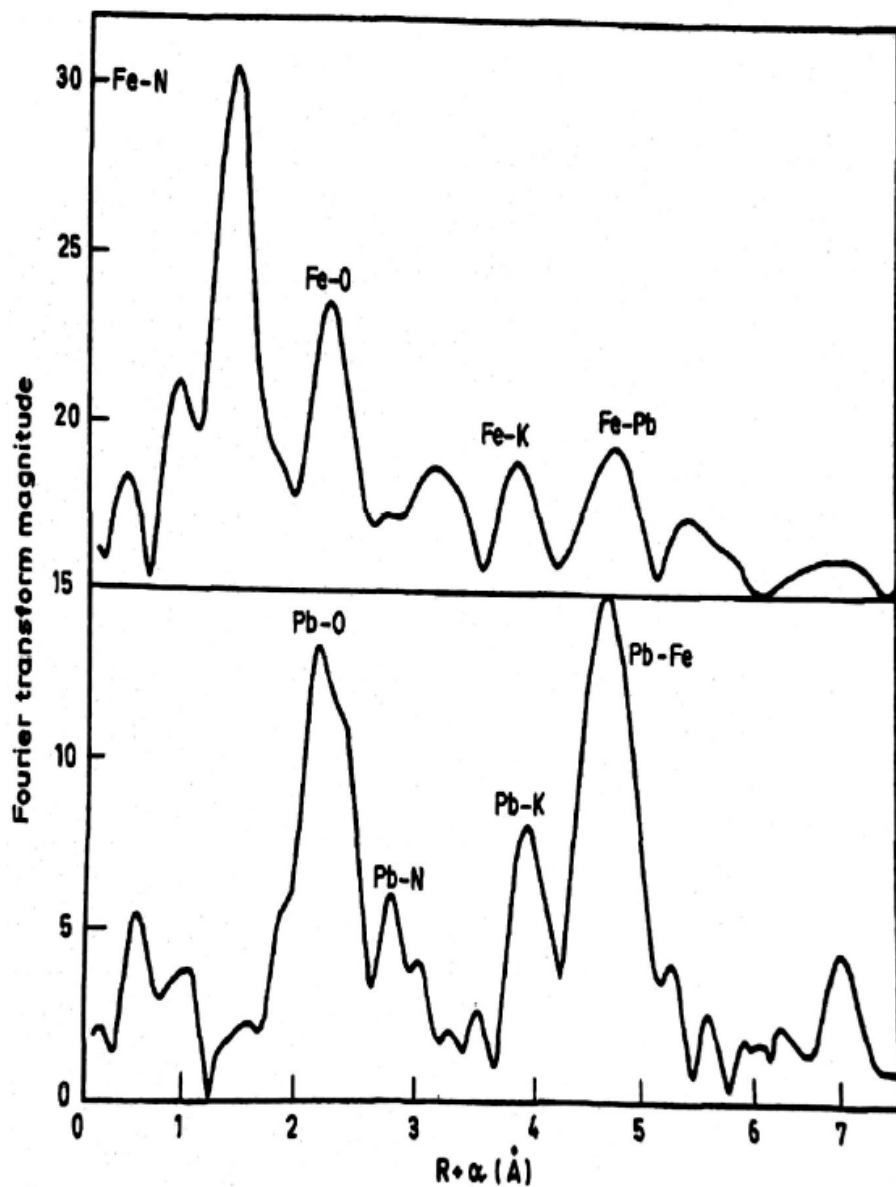
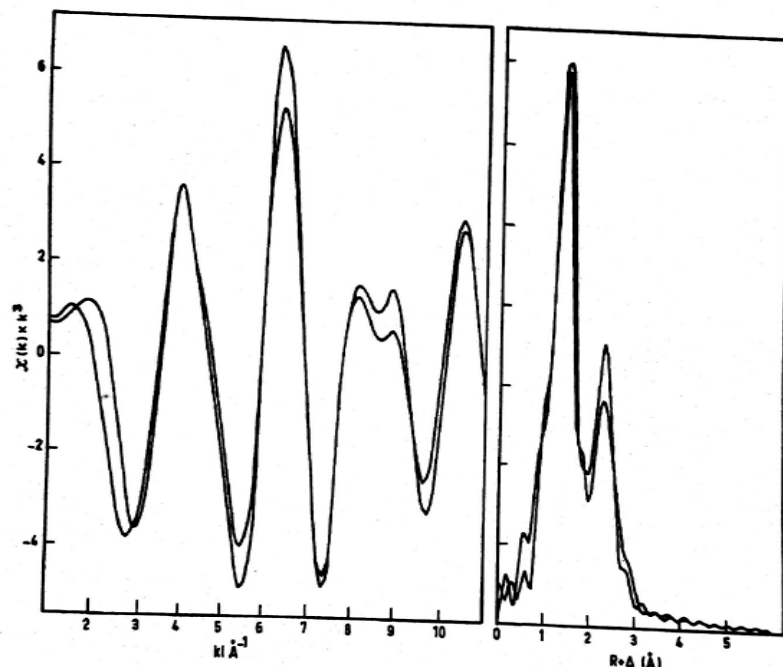


Fig 4: The fourier Transform of the  $k^3$  weighed EXAFS producing the pseudo radial distribution function for the Iron and Lead edge.



**Fig 5:** Fits to the first shell co-ordination of nitrogen and oxygen

*Outer shell:* We could see three highly reproducible peaks in the FT of the outer shell. Two of these could be fit by potassium at a ca of 4.45 Å and shell of Lead at 5.22 Å. Both of these are in good agreement with the radial distribution that is predicted from crystal structure. The apparent Fe-K and Fe-Pb co-ordination numbers are rather low which is due to the low amplitude resulting from a long distance weak interaction. The Fe-Pb distance turns out to be half of the unit cell distance which is in good agreement with the powder XRD data. This also indicates a long range order in the structure.

*Pb EXAFS;* The Pb EXAFS data are consistent with the Fe EXAFS data and the crystal structure. The Pb is in a very unusual 12 co-ordinate site with nearest neighbours being 12 oxygens from nitrite at 2.78 Å and six nitrite nitrogen atoms at 2.99 Å. This is pretty much what we see in EXAFS. We do not see any effect of distortion of the Fe site on the Pb EXAFS. This probably suggests that there is not any significant distortion of nitrites in the direction of the Pb ions, It is very surprising to see that Pb-Fe peak is 5 times higher in amplitude than the Fe-Pb peak. This is due to the destructive interference Fe EXAFS whereas it is constructive in the case of Pb. All bond distance calculated on the basis of EXAFS are shown in Table 1.

## Conclusions

In conclusion we could say that the EXAFS give the Fe-N distance as 1.95 Å. There is a possibility for long range order which is again predicted by the EXAFS results. It could also be concluded that the overall co-ordination number in the first co-ordination sphere is six. In addition to this the X-ray photoelectron spectroscopy was also used to confirm the presence and oxidation state of Lead and Iron.

## Acknowledgement

I thank Prof. Jim Penner-Hahn for recording the EXAFS spectra. UGC minor project funding (MRP(S)-565/09-10/KLCA009/UGC-SWRO) is gratefully acknowledged.

## References

- 1) Tanaka M., Tokoro T., and Aiyama Y, *J. Phys. Soc. Japan*, 21, 262 (1966).
- 2) Padmakumar K. and Manoharan P .T , *Spectrochim. Act. (A)* 56, 905-913 (2000).
- 3) Caulton K. G. and Fenski R. I., *Inorg. Chem.* 6, 562(1967).
- 4) Elliott H., Hathaway B. J., and. Slide R. C., *Inorg. Chemn*, 5, 669 (1966)
- 5) George G. N., EXAFSPAK, Data analysis program (1994).
- 6) Randall C. R., Shu L. Chiou, Y.M. Hagen, K. L., Kitajami M., Lachicotte N., Zang, Y., and Lawrence Que Jr., *Inrog. Chem* 34 (1995)1036.

## **Sol-gel preparation and characterization of nickel and cerium loaded rice husk silica catalyst: Application to the oxidation of cyclohexene**

**Femina K.S\*** , Aswini R , Anjaly Mathew , Sreeja K, Harsha M and Sneha Vijayan  
Department of Chemistry, Sree Neelakanta Govt.Sanskrit College, Pattambi , Palakkad-679306, Kerala, India.

*\*femimvpa@gmail.com*

### **Abstract**

Nickel and cerium loaded highly amorphous rice husk silica had been prepared using sol-gel method. Here, we used citric acid as the structure modifier. The prepared catalyst was characterized using FTIR, PXRD and SEM EDAX analysis. The catalyst was found to be active for the oxidation of cyclohexene using  $H_2O_2$  as oxidant under mild conditions.

**Keywords :** *Rice husk silica, sol-gel method, amorphous silica, structure modifier*

### **Introduction**

Now a day's chemists are concerned about the impacts of industrial activities on the environment, this lead them to develop new chemical pathways which are less hazardous. Solid catalysts have attracted much attention in this perspective as it provides an ecofriendly alternative to the conventional homogeneous catalyst which generates large amount of toxic by products [1-3]. The activity of solid catalyst is influenced by surface area, adsorption capacity, pore structure etc. The dispersion of active metal or metal oxides catalyst over amorphous matrix such as silica, titania improves the efficiency by increasing the effective surface area [4-5]. Silica is very attractive as a catalyst support because of its inertness, high surface area, non toxicity and ready availability etc. High quality amorphous silica can be isolated from various sources like rice husk [5-9]. Many researchers have utilized Rice Husk silica for the preparation of various metal supported catalysts for versatile chemical transformation such as oxidation, alkylation, isomerization etc. of organic compounds [12-13, 18].

The oxidation is an important step in most of the organic synthesis. The product of oxidation of Cyclohexene forms the precursors for large number of industrially important compounds. Conventional oxidation of cyclohexene and other alkenes using nitric acid or  $\text{KMnO}_4$  causes environmental pollution due to toxic by product. The oxidation with hydrogen peroxide is more economical and ecofriendly [13,16]. Generally metal oxides can catalyse the decomposition of hydrogen peroxide and the oxidation [13,18,19]. Hence, the study aim to prepare a solid catalyst by incorporating oxides of cerium and nickel over the silica rice husk derived and to study its catalytic activity towards liquid phase oxidation of cyclohexene.

## **Experimental**

### ***Preparation of Ni-Ce loaded Rice Husk silica***

Rice Husk Ash (RHA) was prepared as per procedure given in literatures [5]. It is used for the catalyst preparation. 5g RHA is stirred with 500ml 1M NaOH for 24 hrs to get sodium silicate solution. To this citric acid is added to achieve silica to citric acid molar ratio of 1 : 0.05. It is then titrated with 3M  $\text{HNO}_3$  containing cerium nitrate and nickel nitrate with constant stirring up to pH 3. The gel formed was aged for 24 h, filtered, washed several times with distilled water followed by acetone and dried in an oven at 383K for 24 h. The sample was calcined at 773 K in a muffle furnace. The xerogel obtained was ground to powder and labeled as Ni-Ce /RHS.

### ***Catalyst Characterization***

The FTIR spectra were recorded in NICOLET FT-IR Thermoscientific spectrometer in the region  $400\text{--}4,000\text{ cm}^{-1}$ . Crystal structure of the powdered sample was studied by XRD analysis. XRD patterns of the sample were recorded for  $2\theta$  between  $3\pi$  and  $80\pi$  on Bruker AXS D8 advance diffractometer employing a scanning rate of  $0.02\pi/\text{S}$  with  $\text{CuK}\alpha$  radiation ( $\lambda=1.5418\text{nm}$ ). The morphology of the catalyst was observed from SEM analysis (JEOL Model JSM- 6390LV).

### ***Catalytic reaction: Oxidation of cyclohexene***

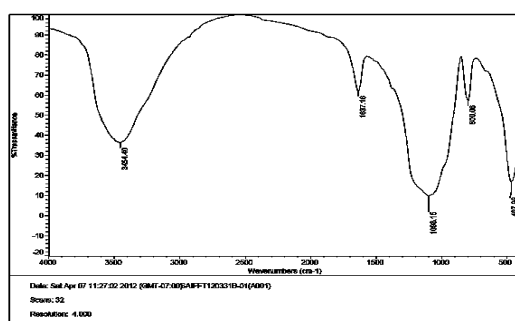
Oxidation reaction was carried out in a 50 ml double neck round bottom flask connected with a reflux condenser which is kept in an oil bath. The catalyst powder (0.1g, pre-heated at 383 K) was suspended in a mixture of 15ml acetonitrile and 1ml cyclohexene, after attaining the required reaction temperature (343 K), 5ml  $\text{H}_2\text{O}_2$  was added drop wise to the system and the reaction was carried out for 5 h. The reaction

mixture was collected, catalyst is removed by filtration, extracted with ether and is subjected to GC analysis.

## Results and discussion

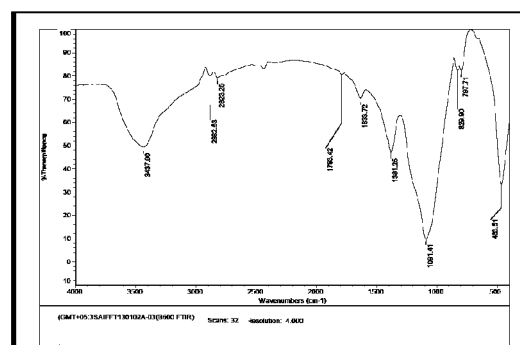
### Characterization of Ni-Ce/RHS

The FT-IR spectrum of sample Ni- Ce/ RHA was presented in Fig. 1 and it is compared with the spectra of RHS [3]. The spectra showed all the characteristic peaks of amorphous silica. There is no additional peaks corresponding to crystalline  $\text{CeO}_2$  or  $\text{NiO}$ . This suggest a uniform distribution of the metal oxide over the silica support. From the FTIR spectral analysis it is obvious that the basic structure of support is conserved during the synthesis of catalyst.

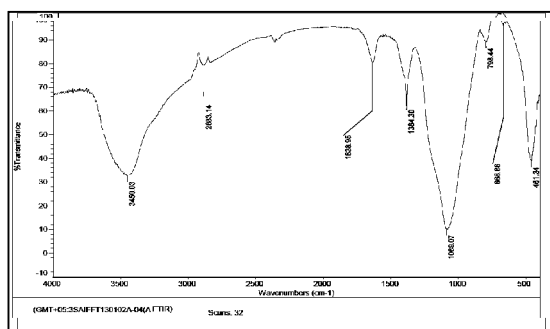


Plot created with PeakFit software version: <http://www.eslbecky.com>

Fig.1 FTIR Spectra of 10Ni-10Ce /RHS  
30Ce/RHS



FTIR spectra of 20 Ni-  
30Ce/RHS



FTIR spectra of 30 Ni-20Ce/RHS

XRD pattern of prepared Ni-Ce/RHS catalyst is shown in the Fig 2(a-c) and it is compared with that of pure silica [1-3]. The XRD pattern shows Ni-Ce/RHS has amorphous character which was observable as a broad peak in the  $2\theta$  region of  $20-30^\circ$ .

Characteristic peaks of  $\text{CeO}_2$  and  $\text{NiO}$  was not identified indicating good dispersion of the metals on the high surface area silica matrix

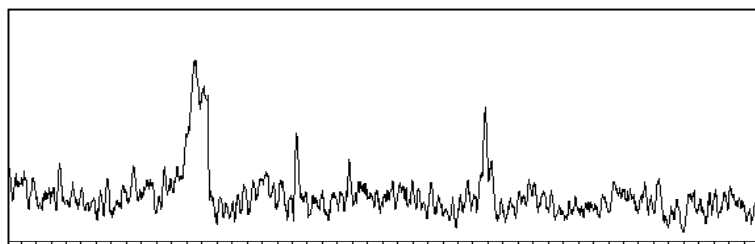


**Figure 2a.** PXRD of 20Ni-30Ce/RHS

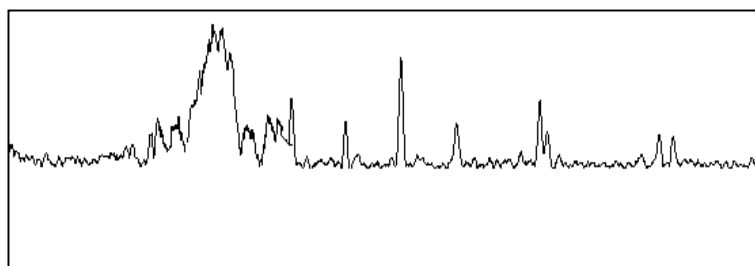


**Figure 2b.** PXRD of 30Ni-20Ce/RHS

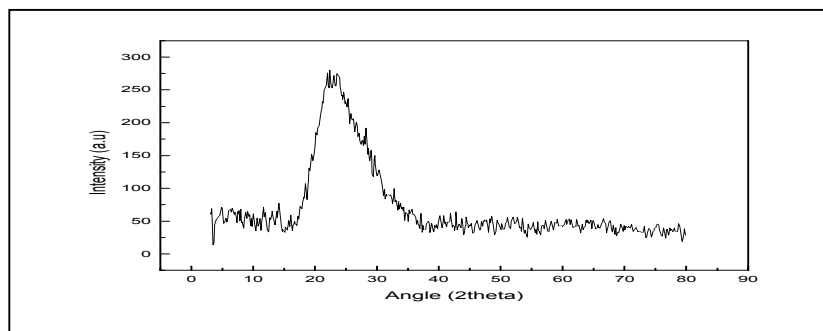


**Figure 2c.** PXRD of 10Ni-10Ce/RHS

The XRD pattern shows that RHA and metals incorporated silica catalysts has amorphous characteristics which was observable as a broad peak in the  $2\theta$  region of 20–30°. The profile of 10Ni-10Ce/RHS only shows weak and rather broad signals. Characteristic peaks of  $\text{CeO}_2$ , and  $\text{NiO}$  was not identified. For  $\text{NiO}$  the characteristic peaks appears at  $2\theta = 44.1, 51.8$  and  $76.4$  corresponding to reflection from (111), (200) and (222) planes. For the characteristic peaks  $\text{CeO}_2$  appears at  $2\theta = 44.1, 51.8$  and  $76.4$



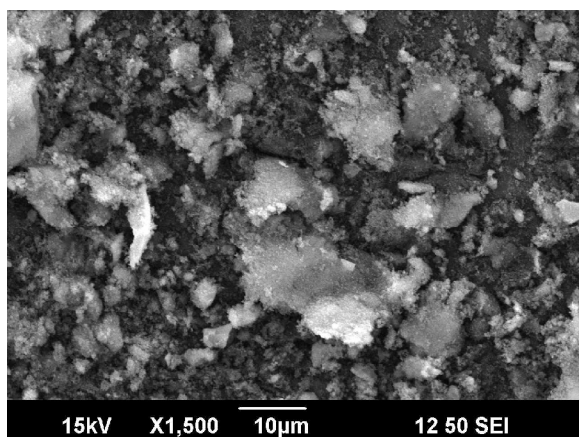


**Figure 3(c).** SEM photograph of 20Ni-30Ce /RHS

The SEM photograph revealed the morphology of Ni-Ce /RHS systems . Here citric acid imparts a limit to particle aggregation leading to well dispersed surface .The prepared system is appeared to have highly amorphous structure having large surface area and can be efficient catalyst due to easy accessibility of the active centers to the substrate molecules. Material lack long-range order but tendency for crystallization has observed in the systems having higher metal loading as small crystallites are observed in the image .The incorporation of Cerium and Nickel is further confirmed from EDX analysis data.

## 2. Catalytic activity studies

The liquid phase oxidation of cyclohexene was carried out with  $H_2O_2$  as the oxidant and acetonitrile as the solvent in presence of different Cerium and nickel loaded rice husk silica catalyst . The oxidation of cyclohexene gave a mixture of products including cyclohexene oxide , cyclohexenone and cyclohexenol. The mixed oxides catalyses the decomposition of hydrogen peroxide The use of  $H_2O_2$  being a clean and safe oxidant makes the study significant in the economical and environmental point of view.

The dependence of catalytic activity on the amount of catalyst, temperature and nature of catalyst were studied. It is found that cyclohexene conversion depends on the amount of catalyst and The cyclohexene conversion depends on the amount of catalyst used. Reactions were conducted with 100mg, 200mg and 300mg of the catalyst 30 Ce-20Ni/RHS and cyclohexene conversion is found to be increases with the amount of catalyst

The cyclohexene oxidations were conducted with different catalyst and it was observed that catalytic activity depends on the amount of metal loading. The catalytic activity was higher for 30Ce- 20Ni/RHS. The maximum conversion of cyclohexene observed was 44%.The technical refinement should further improve the efficiency of the catalyst.

**Table 3.** Percentage of cyclohexane conversion

Catalyst used	Amount in mg	Temperature	Ratio of Cyclohexene to H <sub>2</sub> O <sub>2</sub>	Duration	% of cyclohexene conversion
10Ce-10Ni	100	333K	1:2	5Hr	21
20Ce-30Ni	100				41
30Ce-20Ni	100				44
30Ce-20Ni	200				40
30Ce-20Ni	300				40

### Conclusions

Metal incorporated amorphous silica from rice husk ash had been prepared by the sol-gel technique using citric acid as structure directing agent and characterized by FTIR, XRD and SEM EDAX analysis. The Cerium and Nickel - incorporated catalyst was found to be active for the liquid phase oxidation of cyclohexene with H<sub>2</sub>O<sub>2</sub> as oxidizing agent. The catalyst efficiency was found to depend on the amount of catalyst and metal loading .The catalytic efficiency of Ni-Ce loaded silica systems can be improved and the catalysis can be extended to other organic functional groups.

### Acknowledgement

The authors would like to thank the UGC, New Delhi, India for financially supporting the research in the form of minor research project. STIC, CUSAT, Kochi, India is acknowledged for XRD, FTIR and SEM analysis.

1. Green Chemistry & Engineering: A Practical Design Approach: Jiménez-González, David J.C. Wiley, 2011.
2. Green Chemistry Fundamentals and Applications: Suresh Ameta Rakshit Ameta Apple Academic Press, 2013.

3. Principles and Practice of Heterogeneous Catalysis: John Meurig Thomas, W. John Thomas, Wiley, 1997.
4. Binitha N N., Preparation and characterization of nano silver-doped mesoporous titania photocatalysts for dye degradation, *Catalysis Today*, **147S**, S76–S80 (2009).
5. Adam F and Chew T S, A Facile Template-Free Room Temperature Synthesis of Mesoporous Wormlike Nickel Phyllosilicate, *The Open Colloid Science Journal*, **5**, 2012, **5**, 1-4 (2010).
6. Ganapati D. Yadav and George G, Single step synthesis of 4-hydroxybenzophenone via esterification and Fries rearrangement: Novelty of cesium substituted heteropoly acid supported on clay;
7. Xue, M, Hu, S Chen, H.; Fu, Y.; Shen Preparation of highly loaded and dispersed Ni/SiO<sub>2</sub> catalysts., *J. Catal. comm.*, **12**, 332-336 (2011).
8. Adam, F.; Chew, T.S; Andas, J. A simple template-free sol-gel synthesis of spherical nanosilica from agricultural biomass. *J. Sol-Gel Sci. Technol.*, **59**, 580-583 (2011),.
9. Kalpathy U , Proctor A , Shultz J, A simple method for production of pure silica from rice hull ash. *Bioresource technology*, **73**(2000) 257-262 3. Adam, F.; Fua, H.K. Malaysian Patent No: MY-136715-A, 2008.
10. Foo, KY, Hameed, B.H, Utilization of rice husk ash as novel adsorbent: A judicious recycling of the colloidal agricultural waste. *Adv. Colloid Interface Sci.*, **152**, **39-47** (2009).
11. Jang H T, Park Y, Ko Y C, Ji Yun Lee, Highly siliceous MCM-48 from rice husk ash for CO<sub>2</sub> adsorption, *Bhagiyalakshmi Margandan International Journal of Greenhouse Gas Control* **3**, 545–549 (2009).
12. Adam F, Andas J and Ismail A, Rahman, The Synthesis and Characterization of Cobalt-Rice Husk Silica Nanoparticles, *The Open Colloid Science Journal*, **4**, 12-18 (2011) Adam F, R Thankappan Oxidation of Benzene over bimetallic copper-Cerium incorporated Rice Husk Silica ., *Chemical Engineering Journal* **160**, 249–258 (2010).
13. Adam F and Retnam P Complete conversion of cyclohexane to Cyclohexanol and cyclohexanone by a simple silica chromium heterogeneous catalyst .
14. Thomas F, Holger F, Stefan B, K Albert, Carsten Silica-Supported TEMPO Catalysts: Synthesis and Application in the Anelli Oxidation of Alcohols *Bolm., Org. Chem.*, **66**,, 8154-8159 (2001).
15. Nina P, Wang YA Koltypin, Aharon Gedanken A and Srinivasan C, Mesoporous iron–titania catalyst for cyclohexane oxidation.

16. Ding, R.G, Yan, Z.F. Adsorption properties studies of the nickel catalysts for carbon dioxide reforming of methane. Fuel Chem. Div. Preprints, 46, 103-105 (2002).
17. T. Radhika, S. Sugunan, Structural and catalytic investigation of vanadia supported on ceria promoted with high surface area rice husk silica; Journal of Molecular Catalysis A: Chemical 250 169–176(2006).
18. Farook A, Anwar I, Chemical Engineering Journal The oxidation of styrene by chromium–silica heterogeneous catalyst prepared from rice husk : 160, 742–750 (2010) .

# Synthesis of Few Acridine Conjugates and Interaction With Biomolecules

Vadakkancheril S. Jisha <sup>1\*</sup>

<sup>1</sup> Department of Chemistry, MES Keveeyam College Valanchery-676552, Kerala, India  
\* [jishasomasekharan@gmail.com](mailto:jishasomasekharan@gmail.com)

## Abstract

Boronic acid substituted acridine and acridinium derivatives **1** and **2** were synthesized and investigated their photophysical properties in presence and absence of monosaccharides, nucleobases and DNA. The acridine derivatives **1** and **3** were synthesized by the condensation of diphenylamine with the corresponding benzoic acid. Quarternisation of **1** and **3** with methyl iodide in excess gave the acridinium derivatives **2** and **4** in quantitative yields. The acridine derivatives **1** and **3** exhibited absorption maximum at 357 nm while the acridinium derivatives **2** and **4** showed a characteristic absorption that extends upto 470 nm. Binding studies with sugars such as glucose and fructose shows that there is no significant change in their photophysical properties. The study of interactions with nucleobases such as guanosine shows that efficient electron transfer takes place between the nucleobase and these derivatives. The intensities of absorbance and fluorescence of the compounds decreased regularly with added DNA concentrations and their DNA association constants estimated on the basis of fluorescence titration data were found to be in the range  $10^4$ - $10^5$ . These results show that the derivatives interact with DNA through intercalation and can have potential application as DNA probes.

**Keywords:** boronic acid, interaction, biomolecules

## Introduction

Recognition of biologically important molecular species by synthetic molecular receptors has gained lot of importance for the past few years. The major classes of biomolecules in cells are proteins, nucleic acids, polysaccharides and lipids.[1] Proteins constitute the largest fraction of living matter. They are the direct products and effectors of gene action in all forms of life. Lipids serve as major structural components of membranes and as a storage form of energy rich fuel.

The nucleic acids DNA and RNA have universal function in all cells to participate in storage, transmission and translation of genetic information. Study of interaction of small molecules with DNA is an active area of research that has important biochemical and biomedical applications.[2-4] Such studies not only provide the information about

nucleic acid binding specificity, DNA conformational transitions but also are useful in understanding the molecular basis of carcinogenesis and DNA-protein interactions.

Interactions of DNA with molecules can be broadly classified into covalent and non-covalent binding modes. In the former case, molecules are linked to DNA by covalent bonds, while in the latter case, molecules bind to DNA by reversible non-covalent interactions. The non-covalent interactions of molecules with DNA include electrostatic, intercalative and groove binding as shown in Figure 1.[5, 6]

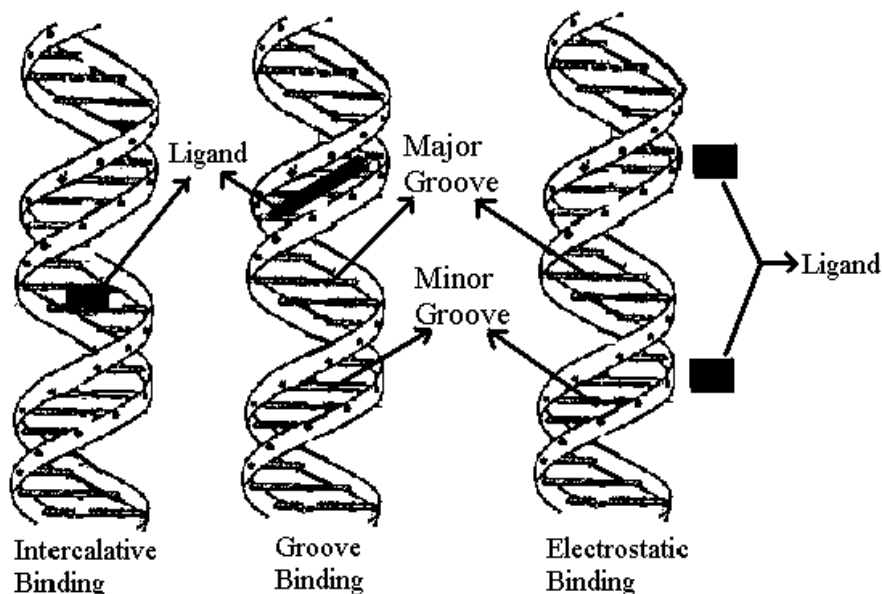


**Figure 1.** Schematic representation of different binding modes of ligands with DNA.

Several classes of molecules, which can initialize DNA modifications by various mechanisms, have been reported in the literature. Among these, photoactivated DNA cleaving agents show several advantages such as: (i) better control of reaction trigger; (ii) selectivity of the reaction centre by adjusting the wavelength of excitation and (iii) the ability to control light which helps to minimize the side reactions and thus leading to a better understanding of the reaction mechanisms.[5] Photoactivated cleaving agents are known to cleave DNA by different mechanisms initiated by the absorption of light, including electron transfer, generation of diffusible intermediates and H-atom abstraction. In the latter two cases, selectivity of the DNA cleavage is rather difficult to attain as the reactions of this type are generally non-specific, while the former one is shown to have some selectivity. Research in this direction has been focussed on two challenging aspects: (i) attaining better selectivity in the formation of DNA strand breaks and (ii) obtaining higher efficiency of the DNA cleavage.

In the case of the photoactivated DNA cleaving agents which function through electron transfer mechanism, the efficiency of the reaction depends on the excited state energy and redox potentials of the sensitizer and DNA bases, in addition to other reaction conditions. For an efficient reaction to occur, the rate of the forward electron transfer from the donor to the acceptor must be greater than the back electron transfer process. Therefore, the inefficiency associated with the DNA cleaving agents that function through electron transfer mechanism can be attributed to the existence of an efficient back electron transfer between the resultant oxidized base and the reduced sensitizer.

In order to overcome the drawback of the back electron transfer processes associated with such systems, a few examples based on cosensitization mechanism have been reported.[7-9] These systems consist of a sensitizer (intercalator) and a co-sensitizer (electron acceptor). Upon excitation, the sensitizer transfers an electron to the co-sensitizer bound on the surface of DNA (Figure 2).

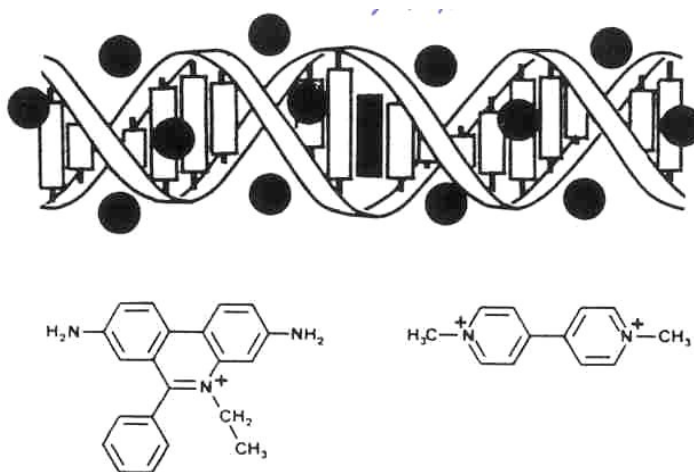


**Figure 2.** Schematic representation of binding of ethidium bromide (shown as shaded rods) and methyl viologen (shown as filled circles) with DNA.

The photosensitization involving the co-sensitizer that bound far away from the sensitizer was found to inhibit the back electron transfer to some extent and thereby increasing the efficiency of the DNA cleavage.

Small molecules that are, soluble in aqueous medium, overcome the inefficiency due to the back electron transfer, undergo strong binding interactions with DNA, induce selective and effective DNA cleavage purely through electron transfer mechanism are highly desired for biological applications.

The other major class of biomolecules, the polysaccharides have two major functions. Some like starch are storage forms of energy yielding fuels and others like cellulose function as extracellular structural elements. Body gets its energy from the metabolism of carbohydrates. Uncontrolled amounts of glucose in the body lead to many diseases. Diabetes is a chronic disease that impairs the ability of the body to manufacture or use insulin, a hormone necessary to metabolize glucose. As the chemistry of saccharides play a significant role in the metabolic pathways of living organisms, detecting the presence and concentration of biologically important sugars is necessary in a variety of medicinal and industrial contexts.[10-12]

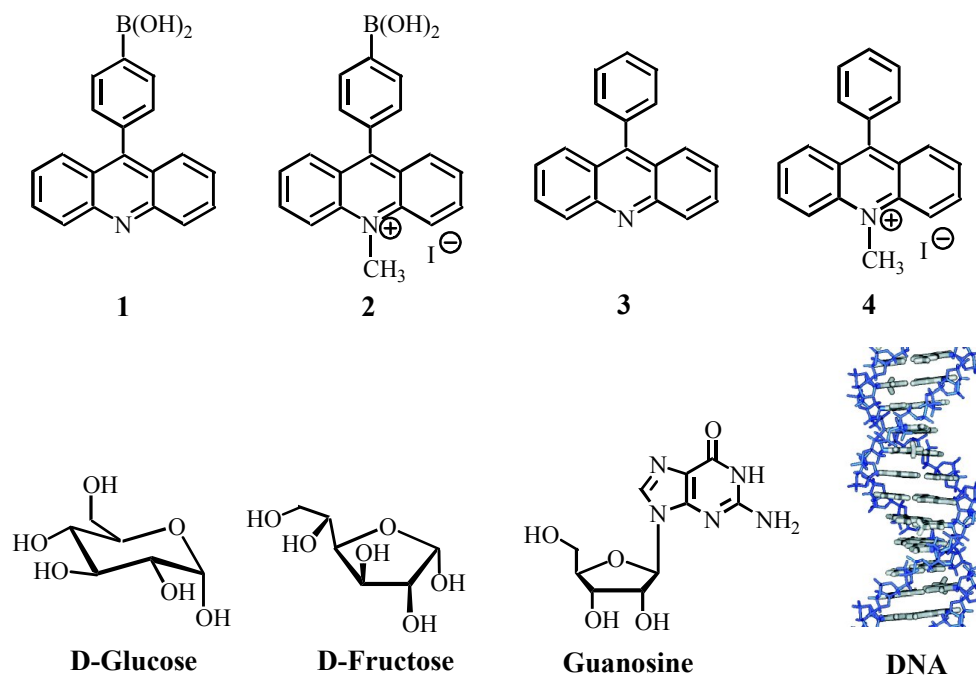


**Chart 1.** Structures of probes and analytes used in the present study.

Application range from monitoring of fermenting processes to establishing the enantiomeric purity of synthetic drugs. Current enzymatic detection methods of sugars offer specificity for only a few saccharides. Also enzyme-based sensors are unstable in harsh conditions. Many synthetic receptors are based on hydrogen bonding interactions.<sup>13-16</sup> Such interactions are efficient in non-aqueous systems but in aqueous media competitive hydrogen bonding by the solvent is a serious drawback. Few chemical sensing mechanisms have been described for saccharides as they are uncharged and neither fluorescent nor fluorescent quenchers.

Boronic acid-saccharide covalent interactions readily form in aqueous media and represent an alternative sensing mechanism in the recognition of saccharides and related molecular species.[17-19]

With these objectives synthesized acridinium derivatives **1-4** (Chart 1) and examined their photophysical and sugar and DNA binding properties.

## **Experimental Section**

### ***General Techniques***

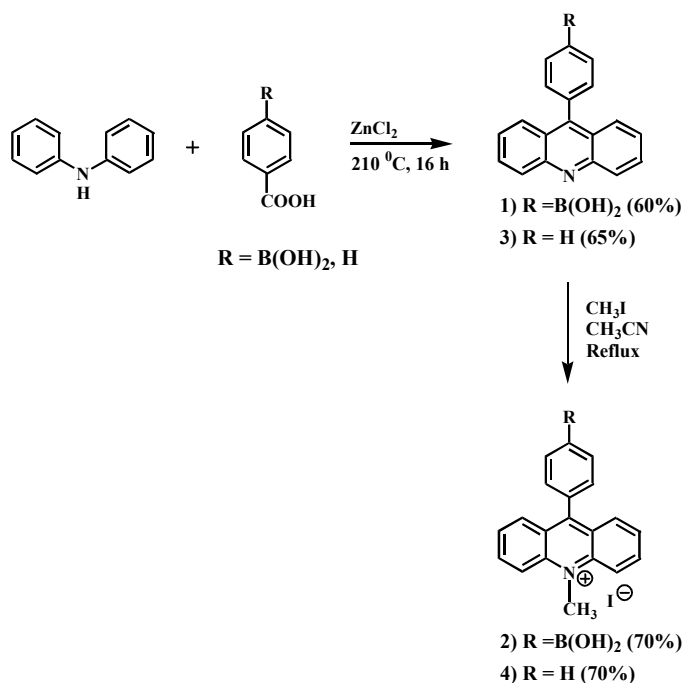
All melting points are uncorrected and were measured on a MEL-TEMP II melting point apparatus. The electronic spectra were recorded on a Shimadzu Model UV-3101PC UV-VIS-NIR Scanning Spectrophotometer.  $^1\text{H}$  and  $^{13}\text{C}$  NMR spectra were recorded on a Bruker DPX-300 MHz NMR Spectrometer using tetramethylsilane as the internal standard. The emission spectra were recorded on a Spex Fluorolog F112X Spectrofluorimeter. The fluorescence quantum yields were measured by the relative methods using optically dilute solutions with 9-aminoacridine in methanol ( $\phi_f = 0.99$ ) as the reference.[20] The fluorescence lifetimes were measured on an Edinburgh FL900CD single photon counting system and were determined by convoluting the instrumental function with a mono or biexponential decay and minimizing the  $\chi^2$  values of the fit to  $1 \pm 0.1$ .

### **Materials**

4-carboxy benzene boronic acid was obtained from Aldrich and other chemicals were obtained from local suppliers and used as received. Solution of calf thymus DNA (Pharmacia Biotech, USA) in distilled water was sonicated for 1 hour and filtered through a 0.45  $\mu\text{m}$  Millipore filter. The concentration of DNA solutions was determined by using the average extinction coefficient value of  $6600 \text{ M}^{-1}\text{cm}^{-1}$  for a single nucleotide at 260 nm<sup>[21]</sup>

### ***Synthesis***

The acridine derivatives **1** and **3** were synthesized by a modified Bernthsen procedure.[22] The quarternization of these acridine derivatives with methyl iodide in acetonitrile gave the corresponding acridinium derivatives **2** and **3** in good yields as shown in Scheme 1.



*Scheme 1*

**9-(4-phenyl boronic acid) acridine (1):** A mixture of Diphenylamine (800 mg, 4.7 mM), 4-carboxy phenyl boronic acid (800 mg, 4.8 mM) and Zinc chloride (4 g, 25.6 mM) heated at  $210^\circ\text{C}$  for 12 h. The reaction mixture was digested with 20 %  $\text{H}_2\text{SO}_4$  for 4 hours and then made alkaline with 25 % ammonia solution. It was extracted with tetrahydrofuran and the residue obtained after evaporation of the solvent was purified by column chromatography over silica gel. Elution of the column with 10 % ethylacetate-petroleum ether mixture gave **1** in 60 % yield. mp  $178\text{-}180^\circ\text{C}$ ;  $^1\text{H}$  NMR ( $\text{CDCl}_3$ , 300 MHz)  $\delta$  8.28-8.31 (2H, d), 7.69-7.8 (4H, m), 7.59-7.61 (2H, m), 7.40-7.45 (3H, m),  $^{13}\text{C}$  NMR ( $\text{CDCl}_3$ , 75 MHz)  $\delta$  148.80, 135.95, 130.41, 129.89, 129.60, 128.41, 128.31, 126.82, 125.55, 125.12. EI-HRMS 299.1011

**9-(4-phenyl) acridine (3):** A mixture of Diphenylamine (800 mg, 4.7 mM), Benzoic acid (573 mg, 4.7 mM), and Zinc chloride (4g, 25.6 mM) were heated at  $210^\circ\text{C}$  for 12 h. The reaction mixture was digested with 20 %  $\text{H}_2\text{SO}_4$  for 4 hours and then made alkaline with 25 % ammonia solution. It was extracted with tetrahydrofuran and the residue obtained after evaporation of the solvent was purified by column chromatography over silica gel. Elution of the column with 10 % ethylacetate-petroleum ether mixture gave **3** in 65 % yield. mp  $185\text{-}186^\circ\text{C}$ ;  $^1\text{H}$  NMR ( $\text{CDCl}_3$ , 300 MHz)  $\delta$  8.28-8.31 (2H, d), 7.57-7.78 (4H,

m), 7.59-7.61 (2H, m), 7.40-7.45 (4H,m), <sup>13</sup>C NMR (CDCl<sub>3</sub>, 75 MHz) δ 148.80, 135.95, 130.41, 129.89, 129.60, 128.41, 128.31, 126.82, 125.55, 125.12.

**9-(4-phenyl boronic acid)-10-methylacridinium iodide (2):** To a stirred solution of the acridine derivative 1 (60 mg, 0.2 mmol) in dry Acetonitrile (15 mL) and Benzene (5 mL), excess methyl iodide (20 mmol) was added at room temperature. The reaction mixture was refluxed for 12 h, while circulating with cold water. The precipitated product was filtered, washed with dry acetonitrile and recrystallized from dichloromethane-ethylacetate mixture to give **2** in 70 % yield. mp 245-248 °C; <sup>1</sup>H NMR (DMSO-d<sub>6</sub>, 300 MHz) δ 8.86-8.90 (2H, d), 8.44-8.50 (2H,m), 7.94-7.95 (4H,m), 7.79-7.80 (2H, m), 7.59-7.61(2H, m), 4.94 (3H, s); <sup>13</sup>C NMR (DMSO-d<sub>6</sub>, 75MHz) δ 160.54, 141.33, 138.56, 133.24, 130.26, 129.93, 129.66, 129.00, 128.08, 125.65, 119.38, 39.60.

**9-(4-phenyl)-10-methylacridinium iodide (4):** To a stirred solution of the acridine derivative 3 (50 mg, 0.2 mmol) in dry Acetonitrile (20 mL) and Benzene (5mL), excess methyl iodide (20 mmol) was added at room temperature. The reaction mixture was refluxed for 12 h, while circulating with cold water. The precipitated product was filtered, washed with dry acetonitrile and recrystallized from dichloromethane-ethylacetate mixture to give **4** in 70 % yield. mp 201-202 °C; <sup>1</sup>H NMR (DMSO-d<sub>6</sub>, 300 MHz) δ 4.93 (3H, s), 7.54-7.56 (2H, m), 7.75-7.80 (3H, m), 7.92 (4H, d, J = 3.7 Hz), 8.44-8.49 (2H, m), 8.88 (2H, d, J = 9.2 Hz); <sup>13</sup>C NMR (DMSO-d<sub>6</sub>, 75 MHz) δ 160.95, 141.76, 138.97, 133.66, 130.67, 130.35, 130.06, 129.41, 128.49, 126.08, 119.81, 39.52. EI-HRMS 441.0011

### DNA Binding Studies

The DNA binding studies of **1-4** were carried out in 10-mM phosphate buffer containing 2 mM NaCl. The association constants were calculated from the fluorescence titration data. The concentration of the free probe was determined from the equation 1,

$$C_F = C_T \left[ \frac{I}{I_0} - p \right] / (1 - p) \quad (1)$$

where,  $C_T$  is the total concentration of the added probe,  $C_F$  is the concentration of the free ligand,  $I$  and  $I_0$  are the fluorescence intensities in the presence and absence of DNA and  $p$  is the ratio of the observed fluorescence quantum yield of the probe in the bound form to that of the free form. The value of  $p$  was obtained from a plot of  $I/I_0$  vs.  $1/[DNA]$  such that the limiting fluorescence yield is given by the Y-intercept. The amount of the bound probe ( $C_B$ ) at any concentration is given by equation 2.

$$C_B = C_T - C_F \quad (2)$$

Scatchard analysis[23,24] done according to the McGhee and von Hippel[25] equation 3,

$$\frac{r}{C_F} = K(1 - nr) \left[ \frac{1 - nr}{1 - (n-1)r} \right]^{n-1} \quad (3)$$

where,  $r$  is the extent of ligand molecules bound per unit amount of macromolecule at a free ligand concentration of  $C_F$ ,  $K$  is the intrinsic binding constant to an isolated site,  $n$  is the binding site size in base pairs. The analysis was done using the plot of  $r/C_F$  vs  $r$ , where  $r$  is equal to  $C_B/[DNA]$ . The value of  $K$  can be obtained from the linear regression best fit of the data.

## Results and Discussion

### Electronic Absorption Properties

Figure 3 shows the absorption spectra of acridine derivatives **1** and **3** in 30 % v/v methanol-10 mM phosphate buffer and **2** and **4** in water. Compounds **1** and **3** exhibited characteristic acridine absorption extending up to 425 nm with a absorption maximum at 360 nm while the derivatives **2** and **4** showed the characteristic acridinium absorption that extends up to 470 nm with absorption maxima at 360 nm and 425 nm. The absorption properties of these compounds are summarized in Table 1.

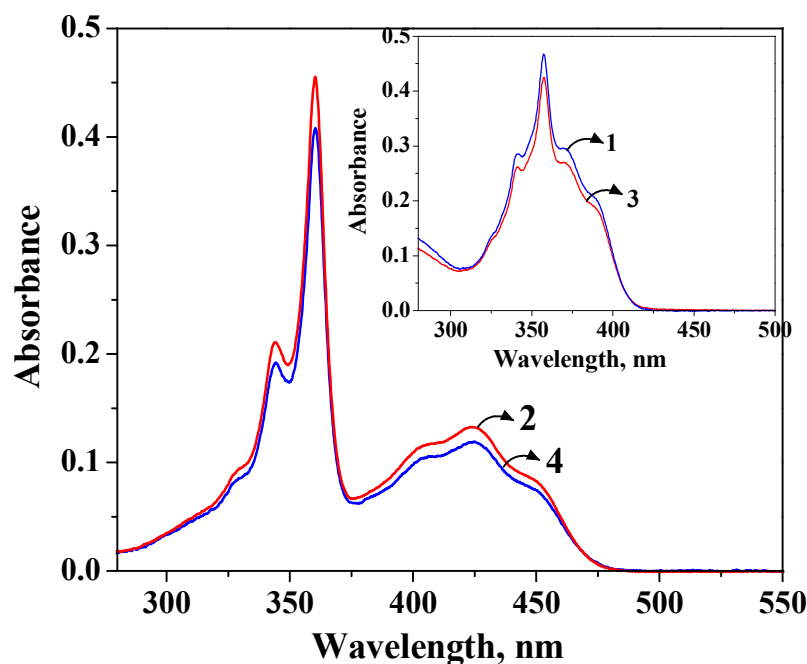


**Figure 3.** Absorption spectra of the acridinium derivatives **2** ( $2 \times 10^{-5}$  M) and **4** ( $2 \times 10^{-5}$  M) in 10 mM phosphate buffer (pH 7.4). Inset shows the absorption spectra of the acridine derivatives **1** ( $3.2 \times 10^{-5}$  M) and **3** ( $3.3 \times 10^{-5}$  M) in 30% methanol-buffer (10 mM phosphate) mixture.

### Fluorescence Emission Properties

Figure 4 shows the fluorescence emission spectra of the acridine and acridinium derivatives in 30 % v/v methanol-buffer mixture and water respectively. Table 1 summarizes the fluorescence quantum yields and lifetimes of these systems in water. Acridine derivative **1** has a fluorescence quantum yield of 0.13 and lifetime 3.1 ns while the quantum yield and lifetime of its quarternised derivative **2** is 0.08 and 1.4 ns respectively. Figure 3 shows the fluorescence decay profiles of the acridine derivatives **1** and **3** in methanol and **2** and **4** in water. All the derivatives showed single exponential decay. The fluorescence lifetimes are presented in table 1.

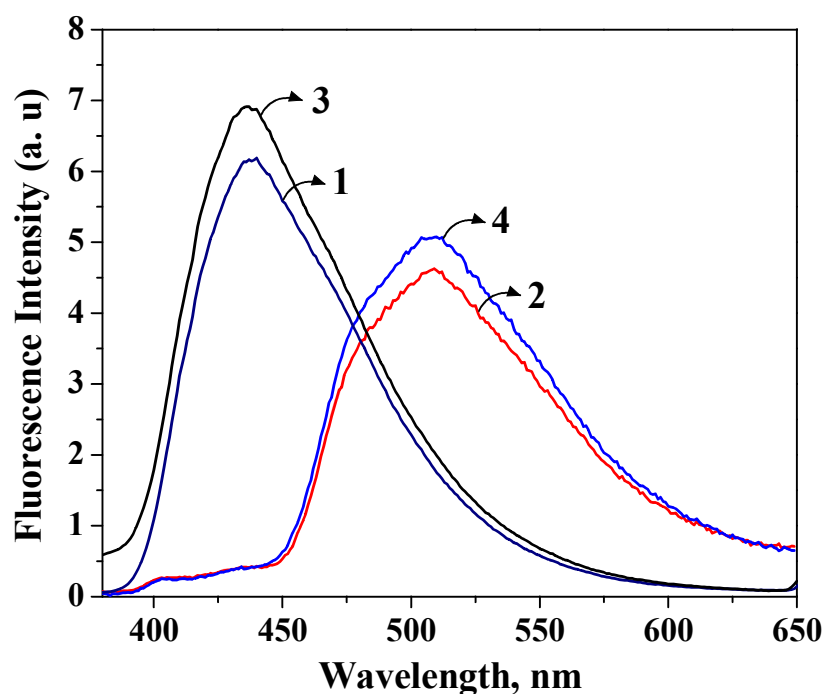


**Figure 4.** Fluorescence emission spectra of the acridine derivatives **1** and **3** in 30 % v/v methanol-10 mM phosphate buffer and acridinium derivatives **2** and **4** in 10 mM phosphate buffer (pH 7.4). Optically matched solutions (OD = 0.1) were used for spectral recording. Excitation wavelength, 355 nm.

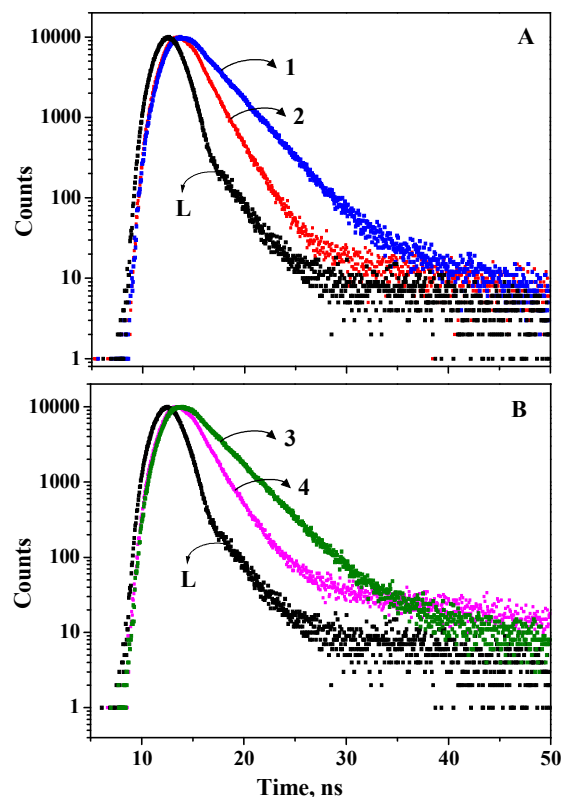


**Figure 5.** Fluorescence decay profiles of **1** and **2** (A) and **3** and **4** (B) in 10 mM phosphate buffer. L is the lamp profile; Excitation wavelength, 355 nm.

**Table 1.** Photophysical properties and DNA association constants of **1-4**.<sup>a</sup>

Compound	$\lambda_{\mu\alpha\xi}$ , nm ( $\epsilon$ , $M^{-1}cm^{-1}$ )	$\lambda_{\mu\alpha x}$ , nm	$\Phi_{\phi}^{\beta}$	$\tau$ , ns	$K_{ass}^c$	$n^d$
<b>1</b>	357 (14700)	357	0.13	3.1	$2.5 \times 10^4$	25
	341 (8600)					
<b>2</b>	360 (24000)	360	0.08	1.4	$1.2 \times 10^5$	4.5
	425 (8300)					
<b>3</b>	357 (12800)	357	0.11	2.8	$2.6 \times 10^4$	27
	341 (7600)					
<b>4</b>	361 (18300)	361	0.09	1.3	$2.5 \times 10^5$	6.2
	425 (5400)					

<sup>a</sup> Average of more than two experiments. <sup>b</sup> Fluorescence quantum yields were calculated using 9,10-dimethylacridinium iodide as standard for **2** and **4** and 9-aminoacridine for **1** and **3**, error ca.  $\pm 5\%$ . <sup>c</sup> Intrinsic DNA association constants determined by Scatchard analysis of fluorescence titration data. <sup>d</sup> Number of nucleotides occluded by the ligand.

## Sugar Binding Studies

Chromophores containing boronic acid group are known to signal the binding of sugars through different mechanisms. In order to have an idea about the interactions of the boronic acid substituted acridines with sugars, we had investigated their interactions with two monosaccharides, glucose and fructose.

Compound **1** was studied in 30 % v/v methanol-10 mM phosphate mixture while **2** was studied in 10 mM phosphate buffer. Since efficient binding with sugars occurs in alkaline media through the formation of boronate anion, we carried out pH titrations to determine the favourable pH conditions in which the binding could be investigated. Figure 4 shows the absorption and fluorescence changes of the acridinium boronic acid **2** in 10 mM phosphate buffer under different pH conditions.

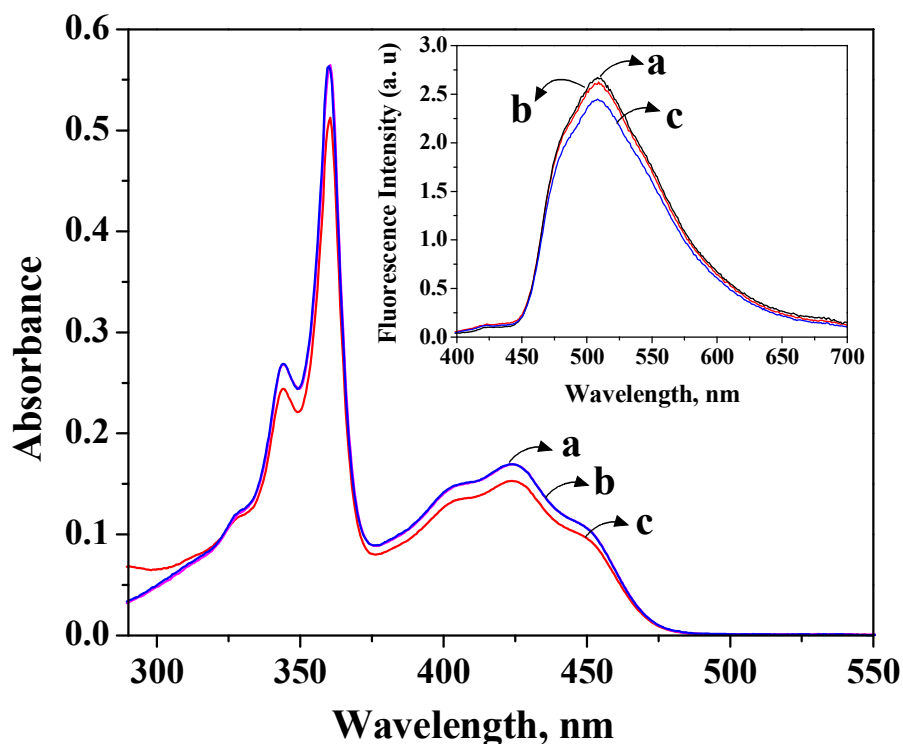


**Figure 6.** Absorption spectra of acridinium derivative **2** ( $2.2 \times 10^{-5}$  M) in 10 mM phosphate buffer under different pH conditions. pH, a) 3.1, b) 7.4 and c) 9.6. Inset shows the corresponding changes in fluorescence spectra. Excitation wavelength, 355 nm.

It was found that at pH 9.6 slight change occurs in the absorption spectra at 300 nm. This is due to the formation of the acridan derivative by the OH<sup>-</sup> attack at the 9-position of the acridinium ring. Because of this reason we could not go beyond pH 9.6. In the case of derivative **1** sugar binding studies were carried out at pH 10.43. Figures 7 - 10

shows the changes in absorption and fluorescence of **1** and **2**. Both the compounds did not show any significant changes on the addition of monosaccharides glucose and fructose.

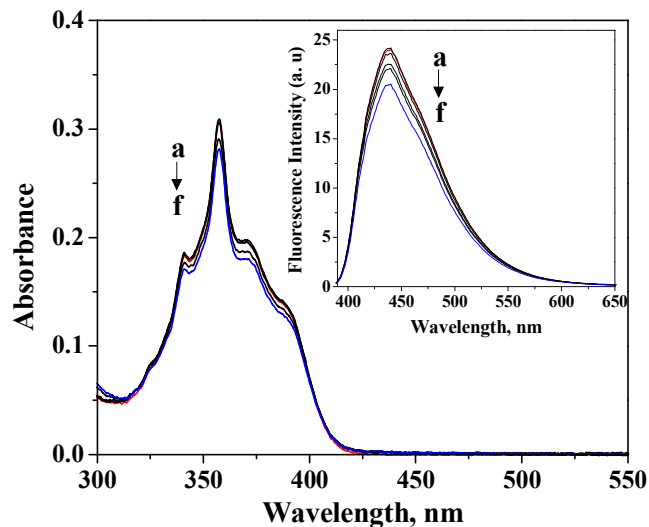


**Figure 7.** Change in absorption spectra of **1** ( $2.07 \times 10^{-5}$  M) with increasing fructose concentration in 10 mM phosphate buffer (pH 9.6). Inset shows the corresponding changes in the fluorescence spectra. [Fructose], a) 0, b) 4.81, c) 9.62, d) 19.21, e) 60.58 and f) 100 mM. Excitation wavelength, 330 nm.

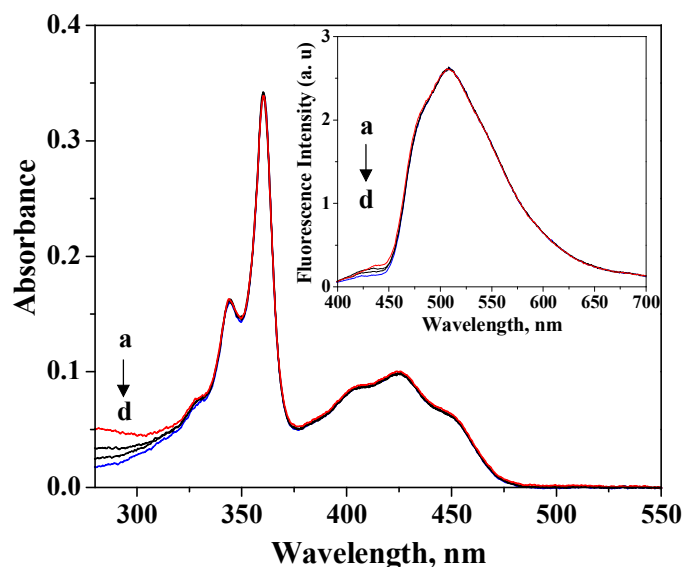


**Figure 8.** Change in absorption spectra of **2** ( $1.4 \times 10^{-5}$  M) with increasing fructose concentration in 10 mM phosphate buffer (pH = 9.6). Inset shows the corresponding changes in the fluorescence spectra. [Fructose], a) 0, b) 4.6, c) 28 and d) 100 mM. Excitation wavelength, 370 nm.

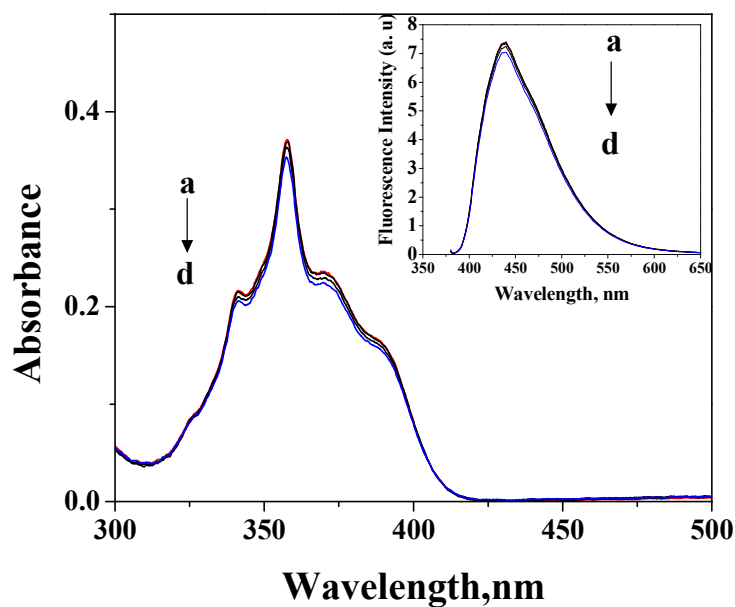


**Figure 9.** Change in absorption spectra of **1** ( $2.4 \times 10^{-5}$  mM) with increasing glucose concentration in 10 mM phosphate buffer pH 9.6. Inset shows the corresponding changes in the fluorescence spectra. [Glucose], a) 0, b) 2.5, c) 5.05, d) 17.60, e) 50 mM. Excitation wavelength, 330nm.

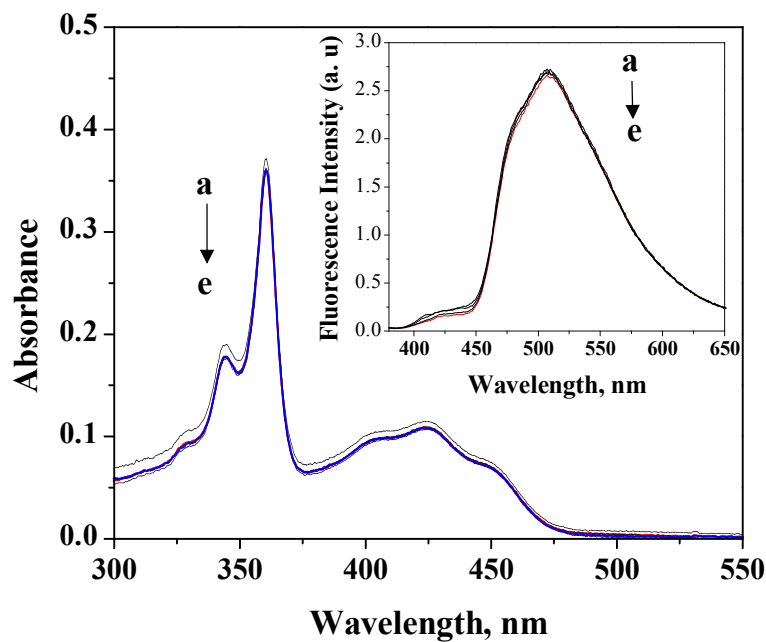


**Figure 10.** Change in absorption spectra of **2** ( $1.4 \times 10^{-5}$  M) with increasing glucose concentration in 10 mM phosphate buffer pH 9.6. Inset shows the corresponding changes in the fluorescence spectra. [Glucose], a) 0, b) 4.69, c) 9.37, d) 18.7, e) 64.8 and f) 100 mM. Excitation wavelength, 370 nm.

### Intermolecular electron transfer studies with DNA bases

In the case of DNA modifications induced by the electron transfer mechanism, the oxidation by sensitizers play a major role. Several molecules are known to oxidize DNA bases with varying degrees of selectivity. In order to understand the efficiency of the acridinium derivatives as DNA oxidizing agents, we have examined the bimolecular quenching properties of these derivatives with guanosine.

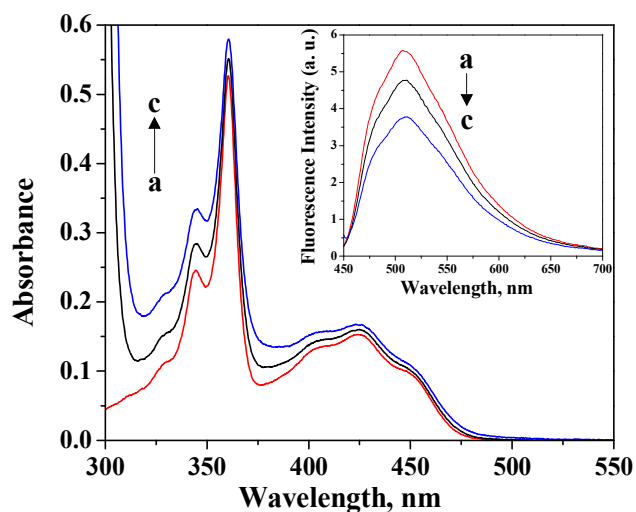


**Figure 11.** Change in absorption spectra of **4** with increasing guanosine concentration in 10 mM phosphate buffer (pH 7.4). Inset shows the corresponding changes in the fluorescence spectra. [Guanosine], a) 0 b) 5.4, c) 13 mM. Excitation wavelength, 440 nm.

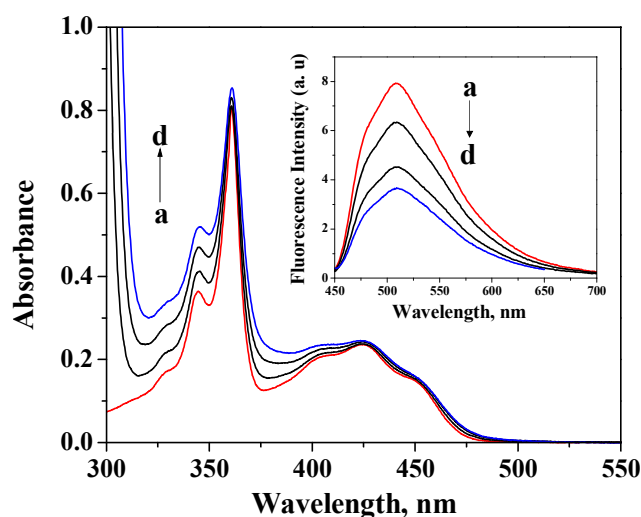


**Figure 12.** Change in absorption spectra of **2** with increasing guanosine concentration in 10 mM phosphate buffer (pH 7.4). Inset shows the corresponding changes in the fluorescence spectra. [Guanosine], a) 0 b) 6.6, c) 16.4, d) 25.2 mM. Excitation wavelength, 440 nm.

Figures 11 and 12 shows the change in fluorescence emission and absorption of compounds **2** and **4** respectively with varying concentrations of guanosine.

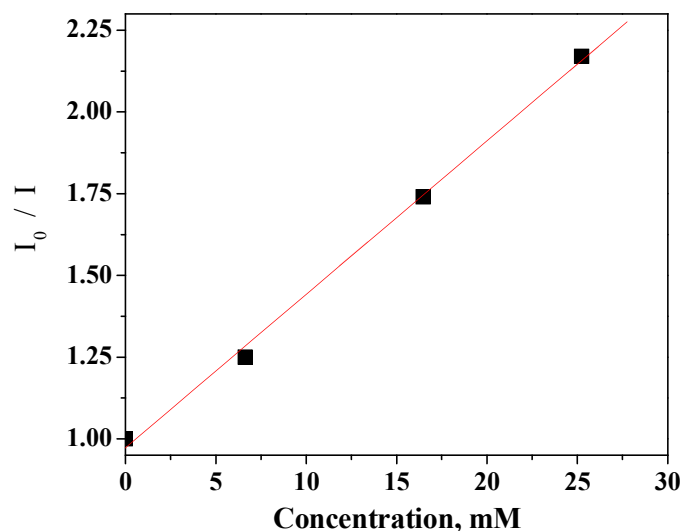


**Figure 13.** Change in fluorescence properties of **2** with increasing guanosine concentration in 10 mM phosphate buffer (pH 7.4).

Figure 13 shows the Stern-Volmer plot for the quenching in emission of **2** by guanosine. The bimolecular quenching rate constant was calculated using the Stern-Volmer equation,

$$I_0/I = 1 + K_{sv} [Q]$$

where,

$$K_{sv} = k_q \times \tau$$

and  $I_0$  and  $I$  are the fluorescence intensity in the absence and presence of quencher (Q),  $K_{sv}$  is the Stern-Volmer constant,  $k_q$  is the quenching rate constant and  $\tau$  is the singlet lifetime in the absence of quencher.

Quenching rate constant was calculated to be  $3.3 \times 10^7 \text{ M}^{-1}\text{s}^{-1}$  for the acridinium boronic acid derivative **2**.

### DNA binding Properties

Acridinium derivatives can bind to DNA by intercalation as well as by electrostatic interactions. In order to understand their DNA binding interactions, we have investigated the DNA binding properties of **1-4** in 10 mM buffer containing 2 mM NaCl.

The interaction of these molecules with DNA was studied using UV absorption and fluorescence techniques. Figure 14 shows the change in the absorption spectrum of the acridine boronic acid derivative **1** with added DNA concentrations. The corresponding changes in the fluorescence spectra are shown in the inset. Figures 15 and 16 shows the change in absorption and fluorescence of **2** and **3** with increasing DNA concentrations. The addition of CT DNA resulted in a strong decrease in the absorption of the acridinium chromophore, along with a red shift of 3 nm. Both these changes are characteristic of intercalative mode of interaction.

The association constants of the complexes between **1-4** and DNA were determined by fluorescence titration experiments, according to the method of McGhee and von Hippel by using the data points of the Scatchard plot. These results are summarized in Table 1. The acridine boronic acid derivative **1** showed a binding constant of  $2.5 \times 10^4$  while the acridinium derivative has a binding constant of  $1.2 \times 10^5$ .

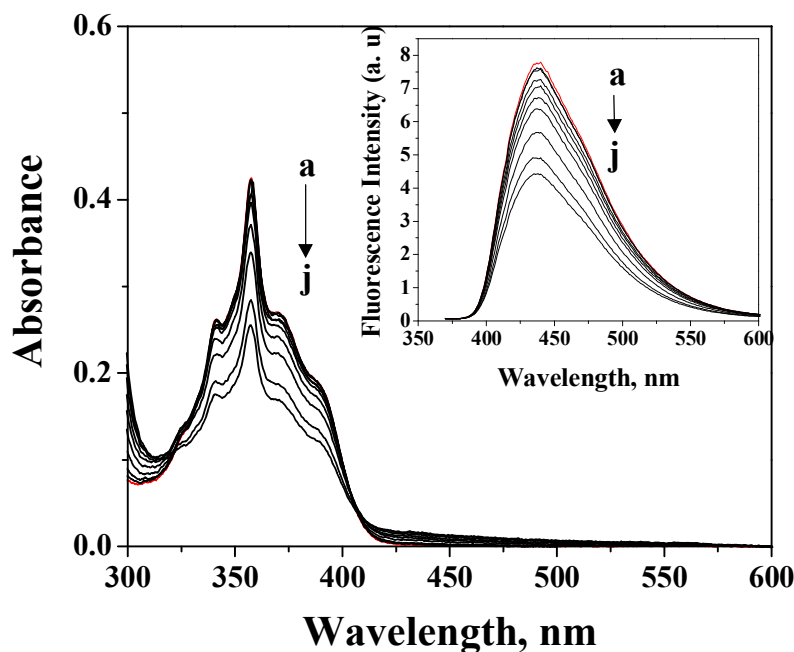


**Figure 14.** Change in absorption spectra of **1** ( $2.72 \times 10^{-5}$  mM) with increasing DNA concentration in 30 % v/v methanol-10 mM phosphate buffer (pH 7.4). Inset shows the corresponding changes in the fluorescence spectra. . [DNA], a) 0, b) 0.01, c) 0.04, d) 0.1, e) 0.2 f) 0.23 g) 0.3, h) 0.34, i) 0.4, j) 0.44 mM. Excitation wavelength, 330 nm

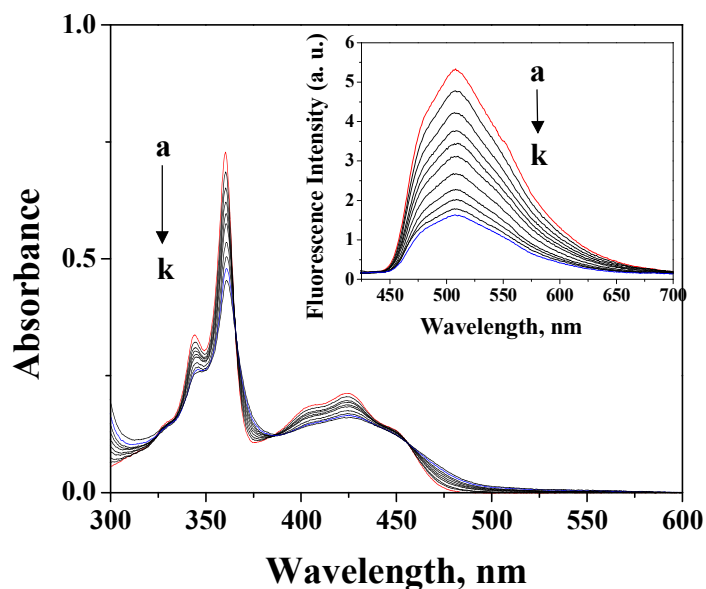


**Figure 15.** Change in absorption spectra of **2** ( $3 \times 10^{-5}$  mM) with increasing DNA concentration in 10 mM phosphate buffer (pH 7.4). Inset shows the corresponding changes in the fluorescence spectra. [DNA], a) 0, b) 0.03, c) 0.05, d) 0.08, e) 0.1 f) 0.13 g) 0.2, h) 0.23, i) 0.3 , j) 0.32, k) 0.4 mM. Excitation wavelength, 355 nm.

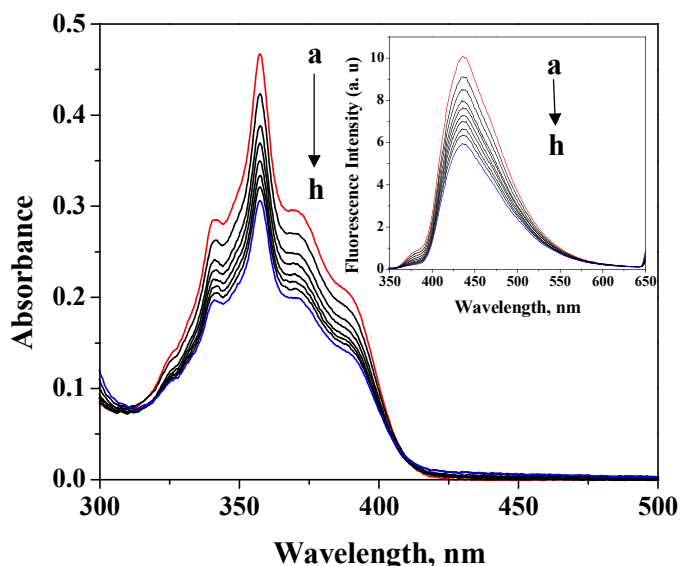


**Figure 16.** Change in absorption spectra of **3** ( $3.6 \times 10^{-5}$  mM) with increasing DNA concentration in 30 % v/v methanol-10 mM phosphate buffer (pH 7.4). Inset shows the corresponding changes in the fluorescence spectra. [DNA], a) 0, b) 0.01, c) 0.03, d) 0.04, e) 0.05 f) 0.08 g) 0.1, h) 0.2 mM. Excitation wavelength, 330 nm

## Conclusions

In summary, synthesized a few novel phenyl acridine boronic acid derivatives and studied their photophysical, sugar and DNA binding properties. The acridine derivatives **1** and **3** gave characteristic absorption extending up to 425 nm and the acridinium

derivatives gave characteristic absorption that extends upto 470 nm. While these derivatives showed negligible binding with sugars, the DNA binding studies indicate that they bind with DNA by the intercalative mode. These results show that the acridine derivatives **1-4**, which show high affinity for DNA, can have potential application as DNA probes.

## References

1. Lehninger, A. L; in *Principles of Biochemistry*; Worth Publishers Inc., New York, , p 54. (1984).
2. Bischofberger, N.; Shea, R. G. in *Nucleic Acid Targeted Drug Design*; Propst, C. L.; Perun, T. J. Eds.; Dekker, New York, p 579, (1992).
3. Tidd, D. M. in *Molecular Aspects of Anticancer Drug-DNA Interactions, Vol. 1*; Neidle, S.; Waring, M. Eds.; CRC, Boca Raton, FL, p 272, (1993).
4. Pullman, B.; Jortner, J. in *Molecular Basis of Specificity in Nucleic Acid –Drug Interactions, Vol. 1*, CRC, Ann Arbor, MI, (1993).
5. Armitage, B. Chem. Rev. **98**, 1171, (1998).
6. *Nucleic Acids in Chemistry and Biology*, II<sup>nd</sup> ed; Blackburn, G. M., Gait, M. J. Oxford, New York, p 329, (1996).
7. Dunn, D. A.; Lin, V. H.; Kochevar, I. E. *Biochemistry* **31**, 11620,(1992).
8. Atherton, S. J.; Beaumont, P. C. *J. Phys. Chem.* **91**, 3993, (1987).
9. Rogerz, J. E.; Weiss, S. J.; Kelly, L. A. *J. Am. Chem. Soc.* **122**, 427, (2000).
10. Fedoak, R. N.; Gershon, M. D.; Field, M. *Gastroenterology* **96**, 37, (1989).
11. Yasuda, H.; Kurokawa, T.; Fuji, Y.; Yamashita, A.; Ishibashi, S. *Biochim. Biophys. Acta.* **1990**, *114*, 1021. Elsa, L. J.; Rosenberg, L. E. *J. Clin. Invest.* **48**, 1845, (1969).
12. Huang, C. Y.; Cabell, L. A.; Lynch, V.; Anslyn, E. V. *J. Am. Chem. Soc.* **114**, 1900, (1992).
13. Huang, C. Y.; Cabell, L. A.; Lynch, V.; Anslyn, E. V. *J. Am. Chem. Soc.* **116**, 2778, (1994).
14. Kikuchi, Y.; Tanaka, Y.; Sutarto, S.; Koboyashi, K.; Toi, H.; Aoyama, Y. *J. Am. Chem. Soc.* **114**, 10302, (1992).
15. Bonar-Law, R. P.; Davis, A. P.; Murray, B. A. *Angew. Chem., Int. Ed. Engl.* **29**, 1407, (1990).

16. Yoon, J.; Czarnik, A. W. *J. Am. Chem. Soc.* **114**, 5874, (1992).
17. James, T. D.; Sandanayake, K. R. A. S.; Shinkai, S. *Angew. Chem., Int. Ed. Engl.* **29**, 1407, (1990).
18. Suenga, H.; Mikami, M.; Sandanayake, K. R. A. S.; Shinkai, S. *Tetrahedron Lett.* **36**, 4825, (1995).
19. Weber, G.; Teale, F. W.J. *Trans. Faraday. Soc.* **53**, 646,(1957).
20. Baguley, B. C.; Falkenhaus, E. M. *Nucleic Acids Res.* **5**, 161-171, (1978).
21. Bernthsen, A. *Justus Liebigs Ann. Chem.* **224**, 1, (1884).
22. Scatchard, G. *Ann. N.Y. Acad. Sci.* **51**, 660, (1949).
23. McGhee, J. D.; von Hippel, P. H. *J. Mol. Biol.* **86**, 469, (1974).
24. Adam, W.; Cadet, J.; Dall'Acqua, F.; Epe, B.; Ramaiah, D.; Saha-Moller, C. R. *Angew. Chem. Int. Ed. Engl.* **34**, 107, (1995).

## Studies on the Effect of Struktol 40 Ms Flakes on the Heavily Filled Vulcanization of EPDM Rubber

Ameerali P. K.<sup>1\*</sup>, Muraleedharan Nair<sup>2</sup> and Divya P<sup>3</sup>

1. Department of Chemistry, Markaz Arts and Science College Athavanad, Kerala
2. Common Facility Service Centre, Manjeri, Kerala
3. Department of Chemistry, MES Keveeyam College Valanchery

\*sreeragam22@gmail.com

### Abstract

Effect of STRUKTOL 40 MS FLAKES on the heavily filled vulcanizates of EPDM rubber were studied. A formulation is taken in which EPDM is selected as base polymer. Sulphur is used as the vulcanizing agent, Precipitated calcium carbonate and Silica are used as fillers and a plasticizer STRUKTOL 40 MS FLAKES is selected and used in representative formulation in different quantities and all other ingredients normally used in rubber compounding are added.

**Keywords:** EPDM, STRUKTOL, vulcanisates

### Introduction

EPDM is an elastomer made by the sterio specific copolymerization of ethylene and propylene. It has no unsaturation, cannot be vulcanized with sulphur, but can be cured with peroxides. There are two types of ethylene propylene rubber- EPM and EPDM. These so called poly olefin rubbers are produced in two main types. Saturated copolymers (EPM) and Unsaturated terpolymers (EPDM)

Even though EPM and EPDM is elastomers have been available for more than 30 years, the technology for this products, both their production and their application, is still under development. The most widely used process is solution polymerization, in which the polymer is produced in a hydrocarbon solvent. EPM and EPDM as manufactured today are rubbers based on early work of Natta and co-workers. Generally an EPM contains 60 mol % of ethylene, 40 mol% of propylene. Analogous EPDM polymer contains in addition, 1.5 mol% of non conjugated diene such as cyclopentadiene. The co-monomers statistically distributed along the molecular chain.

EPDMs are EPDs that posses unsaturation. The unsaturation is introduced by copolymerizing ethylene and propylene with a third monomer, which is a non conjugated diene. The dienes are so structured that only one of the double bond will

polymerise and the un reacted double bond act as a site for sulphur crosslinking. This latter unsaturation is also so designated that it does not become part of the polymer backbone but a side group. As a consequence, the terpolymer retains the excellent ozone resistance that the copolymer processes. The three co-monomers employed in industry to introduce unsaturation are Dicyclopentadiene (DCPD), Ethylene norbornene (ENB) and 1,4 hexadiene

EPM is saturated synthetic elastomer since it does not contain any saturation. It is inherently resistant to degradation by heat, light, oxygen and ozone. EPDM which contains pendant unsaturation, is only slightly able to ageing than EPM. The properties of EPM copolymers are dependent on the relative content of ethylene unit in the copolymer chain and the variation in the co-monomer composition of different chains. EPM and EPDM polymers with greater than 60% ethylene are increasingly crystalline and are tough. EPM can be vulcanized radically with peroxides. A small amount of third diene monomer in EPDM permits conventional vulcanization with sulphur and other vulcanization system like resins at the pendant sites of unsaturation. In EPM/EPDM compounds mechanical properties depends on the composition of elastomers and the type and amount of fillers.

The resistant to heat and ageing of EPM/EPDM is much better than that of SBR and NR. EPM/EPDM vulcanizates have an excellent resistant to inorganic or highly polar fluids, such as dilute acids, alkalies and alcohol. However the resistance to aliphatic, aromatic or chlorinated hydrocarbon is very poor. The electrical insulating and dielectric properties of the poor EPM/EPDM are extra ordinary, but in compounds they are also strongly dependent on the choice of compounding ingredients. Among the synthetic elastomers, EPM and EPDM are the fastest growing elastomers, due to their excellent ozone resistance in comparison to the diene elastomers. This growth still comes from replacement of these commodity rubbers by virtue of their ozone and thermal resistance. Another face of the growth is that EPDM rubber can be extended with fillers and plasticizers to an extremely high level in comparison with other elastomers and still maintain excellent processibility and properties in end use articles.

In the present work EPDM is selected as main matrix. The various compounding ingredients used in this work are 1) Activator 2) Accelerator 3) Vulcanizing agent 4) filler.

Rubber products are exposed to different climatic conditions in its normal use. The synthetic rubber EPDM itself is not having the desired properties of different

products. In order to improve these properties we have to mix rubber with different additives such as activators, accelerators, fillers, vulcanizing agents etc. a formulation is taken in which EPDM is selected as base polymer. Sulphur is used as the vulcanizing agent, Precipitated calcium carbonate and Silica are used as fillers and all other ingredients normally used in rubber compounding are added. In first mix no filler is added. In second, third, fourth and fifth formulations PCC is added and in sixth, seventh, eighth and ninth formulations Silica is added as filler. The effect of the STRUKTOL 40 MS FLAKES (Homogenizer) on the heavily filled vulcanizates of EPDM rubber are studied. In the present work a combination of accelerator 'F' is used. It is a combination of mercapto benzothiazole (MBT) and diphenyl guanidine (DPG).

MBT is a good accelerator with specific gravity 1.42 and sharp odors and is not poisonous. It is soluble in water, but soluble in alkali, alcohol, acetone, ether and benzene. If the amount of filler in the compound is less than 1% accelerator is sufficient but with more filler 1.5% accelerator is required and then 2 – 2.5% sulphur is sufficient. 2.5 % sulphur is used when carbon black or china clay are used as fillers. DPG is one of the common accelerator for vulcanization of rubber in combination with thiazole and sulphanamides. Though it does not show better activity than thiouram and dithiocarbamates, it has better stability. It is used as a complexing agent for the detection of metals organic bases. It is used as a secondary form stabilizer in silico fluoride foam process.

Most of the precipitated calcium carbonate(PCC)are made from limestone. The carbonate is first converted back into another calcium compound and this is later converted to the carbonate under the condition that permits the control of particle size. The limestone is first burned to quick lime which is then slaked to get milk of lime. The milk of lime is then treated with carbon dioxide from the kiln or better with sodium carbonate solution to get calcium carbonate. The precipitate is filtered, washed,dried and powdered. The particle size of precipitated calcium carbonate is below 0.1m and it is a semi reinforcing filler .

STRUKTOL 40 MS FLAK is a homogenizer cum tackifier of rubber compound. It is a mixture of dark aromatic and aliphatic hydrocarbon resins. It improves the homogeneity of polymer blends. It improves the processing behavior in internal mixtures, on open mills and during calendaring. It provides good compound tack.

In the present work we prepared different EPDM rubber mixes for studying the effect of STRUKTOL 40 MS FLAKES on the heavily filled vulcanizates of EPDM

rubber. Cure characteristics of all the above mixes will be studied. Tensile properties such as tensile strength, elongation at break, modulus and Physical properties such as durometer hardness, density are also will be studied. The suitability of the rubber mixes prepared in industrial application will be explored.

## Experimental

The rubber compounds prepared in this study were based on EPDM. EPDM -502 is a commercial products of Herdillia Unimers Ltd(Mumbai, India). Since basic properties such as molecular weight distribution and the content of non rubber constituents of rubber are subjected to variation through seasonal changes, methods of preparation etc, rubber from the same lot has been used for the whole experiment. The rubber chemicals such as sulphur, zinc oxide, stearic acid, PCC, Silica, a combination of accelerators 'F' and a homogenizer STRUKTOL 40 MS were used in this study and all these chemicals were supplied by CFSC Manjeri.

Rubber compound preparation: The rubber compounds of EPDM, cross linking system and filler were prepared on a two roll mixing mill. Mastication of polymer done separately between hot rolls of the mill at 800c as per the recipe given below. The different fillers used in the present work is PCC and Silica.

**Table 1 Compounding**

Ingredients	1	2	3	4	5	6	7	8	9
EPDM -502	100	100	100	100	100	100	100	100	100
Sulphur	1.75	1.75	1.75	1.75	1.75	1.75	1.75	1.75	1.75
ZnO	4	4	4	4	4	4	4	4	4
Stearic acid	2	2	2	2	2	2	2	2	2
F	1.5	1.5	1.5	1.5	1.5	1.5	1.5	1.5	1.5
PCC	-	100	100	100	100	-	-	-	-
Silica	-	-	-	-	-	50	50	50	50
Struktol 40 ms flakes	-	-	2	4	6	-	2	4	6

The compounding time for each EPDM mix was maintained for 15 – 25 minutes. Rheometric properties such as optimum cure T90 maximum and minimum torque (ML and MH) and scorch time TS2 of the mixes were studied by using GOTTFERT ELASTOGRAPH “VARIO”. The vulcanization of blends was performed on hydraulic press under pressure of 30 tonnes and at temperature of 150°C.

The desired amount of rubber is cut from the sheet and then placed at the nip of two roll mixing mill. It is then passed through the nip until it softens. Then the ingredients are added one by one. Activators like zinc oxide and stearic acid is added first. After that combination accelerator ‘F’ is added, at last sulfur is added and mixed well. During mixing, the mix is to cut from the sides to get better mix. After proper dispersion the compound is sheeted out as 2.5 to 3.5 mm thickness and grained direction is marked. The sheet can be used for molding and testing.

The Rheometer used in present work is GOTTFERT ELASTOGRAPH rheometer. After maturation the rubber sheet is cut using a press then it is placed in the cavity present in the rheometer. Then the machine will plot a graph as the curing proceeds. The cure time of two specimens are measured individually, then average is taken. This value can be used as the cure for molding. Hydraulic press has an important role in rubber industry. It is mainly used for compression molding. Hydraulic press utilizes hydraulic energy for its operation. The mold should be held between heated platens of the press. A prepared quantity of molding compound is placed in the mold usually by hand and placed in the press. The press process with sufficient pressure to be minimizes or prevents flash. The compound softens and flow inside the mould to get the required shape, the chemical are then occurs at internal mould temperature 150°C. The press is then opened after required cure time and molding removed. The mold is removed from the press and opened the bench to taken out the product. Before molding aalittle silicone oil is applied inside the mold to prevent sticking.

Tensile properties of different mixes were examined using an Instron Universal Testing machine (model 4411; Instron Ltd, Buckinghamshire, UK)) at a crosshead speed of 500mm/min. The tensile tests were conducted according to the ASTM D 412–87 test procedures using dumbbell-shaped test pieces.

Test Specimen: Dumb bell shaped test specimens are used for the measurement of tensile properties. The type one model of 1 dumb bell of ISO 37 with 6mm wide centre portion and preferable cut from 2mm thick sheet is used for the measurement of tensile properties. The dimensions of test pieces are,

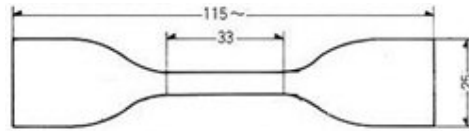


**Table 2: Dumbbell Dimension**

	Dimension	In mm
A	Overall length(minimum)	115.0
B	Width of the ends	25.0 – 1.0
C	Length of the narrow portion	33.0 – 0.4
D	Width of the narrow portion	6.0 – 0.4
E	Transition radius outside	14.0 – 1.0
F	Transition radius inside	25.0 – 2.0

Measurement of test piece: The thickness of the test piece is measured by micrometer gauge. The width between cutting edges of the narrow central part of the die is measured to the nearest point 0.5mm.

Determination of Tensile Strain Properties: The dumbbell test piece is inserted into the grip of the tensile testing machine, taking care to adjust it symmetric so that the tension will be distributed uniformly over the cross section. If tension is greater on one side of the test piece than the other benchmark will not remain parallel and the maximum strength of the rubber will not be developed. Then the machine is started and the distance between the centers of bench marks is measured as required to the nearest 1mm taking care avoiding parallax, until the test piece breaks. If necessary note the load on the test piece as required. The testing is carried out at  $27 \pm 2^\circ\text{C}$ .

Physical Properties: The hardness (Shore A) of samples was measured by using Durometer (ModexIndia Pvt. Ltd, Mumbai, India) according to ASTM 2240 – 86. The durometer is placed at three different places of the specimen and then apply force and measure the value then the average value of hardness is taken.

Specific Gravity of each sample was measured using Densimeter (DENSIMETER MD-200S Scale capacity is 0.01-200g). A sample is placed on the sensor. The sample should be lighter than 200g and smaller than 60'80'30mm. Then the weight of the sample is shown and then press memory after stable mark appears. MD-200S starts to memories the average weight of the sample in the air. Memory mark appears on the display. Stable

mark blinks on and off and dashes disappears one by one on the screen. Then stable mark appears on the display, which indicates that MD-200S has memorized average weight of the sample in air. The display returns to Zero when the sample is removed from the sensor. The sample is gently put on the basket by tweezers. Then the weight of the sample in water will be shown on the display. Memory is pressed after stable mark appears; MD-200S starts to calculate density of the sample. Stable mark blinks on and off while dashes disappear one by one. In this period, no vibration should be applied on MD-200S. Then, the value density of the sample appears on the display and the value is noted. The sample is taken out of water by tweezers without dripping water on any part of the sensor. When the measurement is finished, the memory button is pressed to return to zero.

### Results and Discussion

The study of effect of Struktol 40 MS Flakes on the heavily filled vulcanizates of EPDM Rubber are carried out as per the recipe shown in table 1.

Ingredients	1	2	3	4	5	6	7	8	9
EPDM -502	100	100	100	100	100	100	100	100	100
Sulphur	1.75	1.75	1.75	1.75	1.75	1.75	1.75	1.75	1.75
ZnO	4	4	4	4	4	4	4	4	4
Stearic acid	2	2	2	2	2	2	2	2	2
F	1.5	1.5	1.5	1.5	1.5	1.5	1.5	1.5	1.5
PCC	-	100	100	100	100	-	-	-	-
Silica	-	-	-	-	-	50	50	50	50
Struktol 40 ms flakes	-	-	2	4	6	-	2	4	6

Cure characteristics of samples prepared are carried out at 160°C, are given in Table 3. The rheometer used in the present work is 'Gottfert Elastograph'. The cure characteristics such as T<sub>90</sub>, TS<sub>2</sub>, ML and MH of the seven mixes are determined and are tabulated in Table 4.

**Table 4:** Cure characteristics of various mixes

Sample	T90
1	20.85
2	17
3	16.8
4	15.9
5	15.3
6	20.1
7	20.6
8	21.25
9	21.5

T<sub>90</sub> is the time required for the 90% curing of rubber sample. Sulfur is used as the curing agent. It is found that for PCC (PCC & Struktol 40 MS Flakes)filled EPDM vulcanisates the cure time get decreased. That is the cure rate increased. It may be due to the alkaline character of PCC. For Silica (Silica & Struktol 40 MS Flakes) filled EPDM vulcanisates the cure time get increased. That is the cure rate get decreased. It may be due to the acidic character of Silica.

The mechanical properties of nine mixes were studied using Universal Testing Machine (INSTRON 4411). The tensile properties such as tensile strength, elongation at break, modulus were determined and the results are given in Table 5 and graph 2 and 3/

**Table 5:** Mechanical properties of different PCC & Silica (with Struktol 40 MS Flakes) filled EPDM vulcanisates

Sample	Tensile strength	Modulus at 100%	Elongation at break
Mix 1	1.17	0.41	114.92
Mix 2	1.84	0.99	198.58
Mix 3	1.86	1.02	236.57
Mix 4	2.04	1.13	298.61
Mix 5	2.16	1.19	337.75
Mix 6	5.57	2.16	457.13
Mix 7	12.86	2.63	510.15
Mix 8	13.98	2.77	531.07
Mix 9	15.16	2.83	690.77

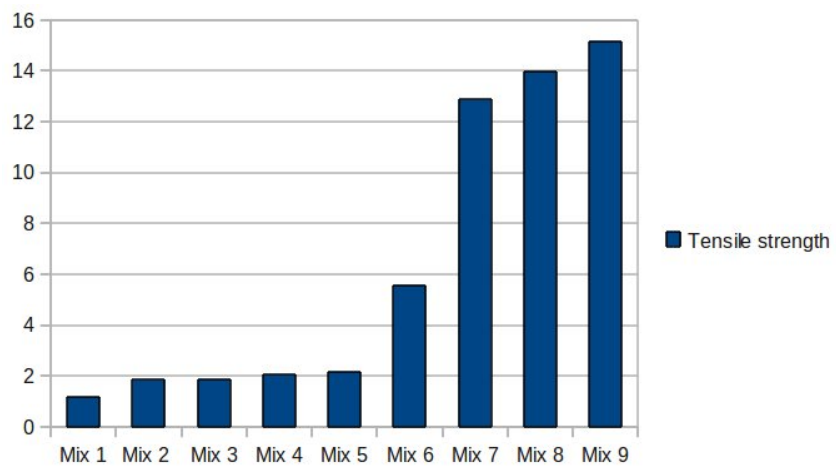


Fig 1. Variation in tensile strength of different EPDM mixes

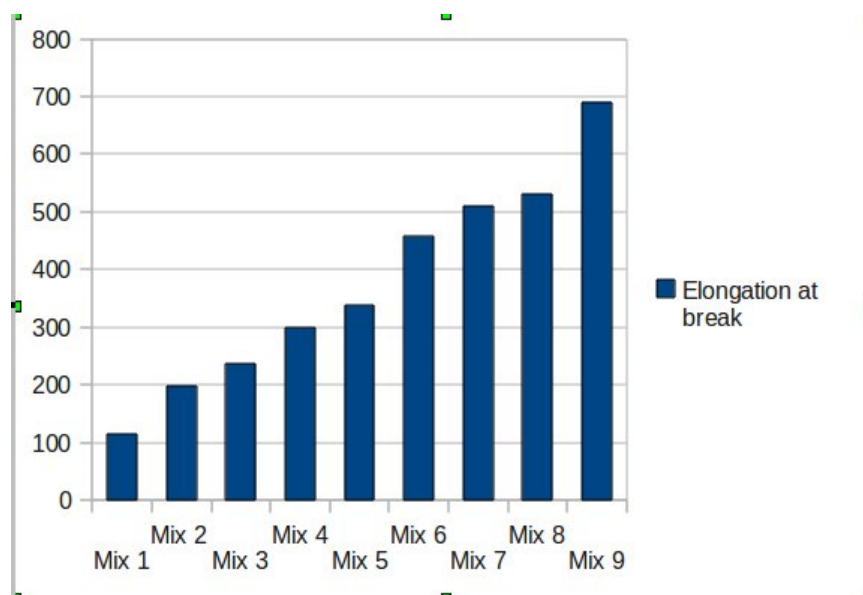
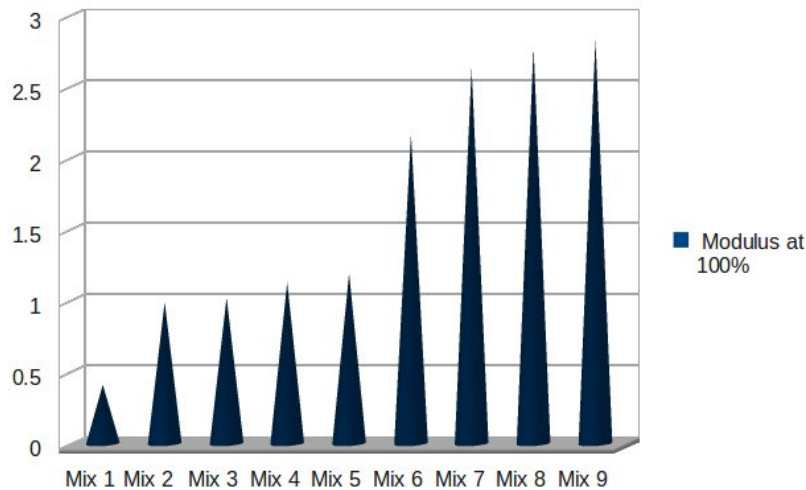


Fig 2. Variation in elongation at break of different EPDM Mixes



**Fig 3.** Variation of modulus at 100% of different

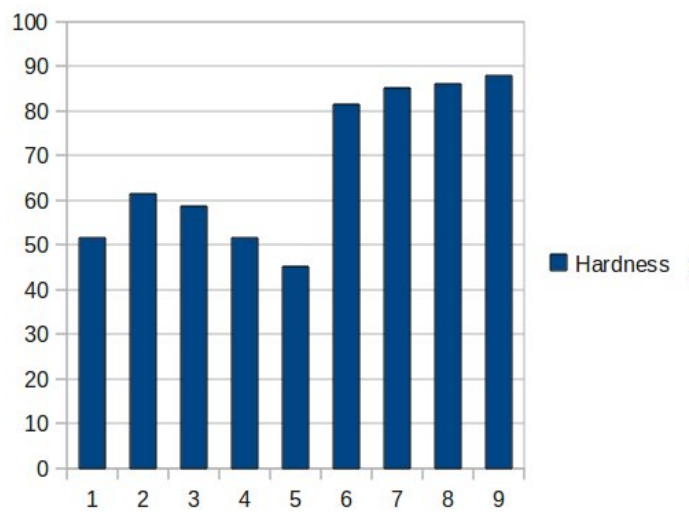
Tensile properties include tensile strength, elongation and tensile modulus. These properties are determined by stretching standard test pieces at a constant rate using a tensile machine. Tensile strength is expressed in MPa or N/mm<sup>2</sup>, required to rupture a standard test piece by stretching at a constant rate. Elongation is defined as the extension produced by force applied to standard specimen and expressed as a percentage of the original length. Ultimate elongation or elongation at break is the elongation at the time of rupture and is determined simultaneously with the tensile strength test. Tensile modulus as applied to elastomer is defined as the force expressed in N/mm<sup>2</sup> required producing certain elongation. From the table it is very clear that Silica filled (with the presence of Struktol 40 MS Flakes) EPDM vulcanisates show higher tensile strength than PCC filled (with Struktol 40 MS Flakes) EPDM vulcanisates. Silica is a good reinforcing filler and PCC is a poor reinforcing filler. On increasing the amount of Silica, tensile strength increases.

Clay filled mixes have high E.B value. E.B increases with increasing clay content. But in the case of PCC filled compounds 50phr of filler loading has the highest E.B. PCC filled compounds show high modulus also.

Hardness is tested using a hardness tester called Shore A durometer. Specific gravity of various mixes is determined using a densimeter. The hardness and specific gravity of various mixes are tabulated in Table 6.

**Table-6** Physical properties of different EPDM mixes:

Sample	Hardness	Specific Gravity
1	51.5	0.8945
2	61.4	1.318
3	58.66	1.201
4	51.5	1.2755
5	45.25	1.282
6	81.5	1.074
7	85.16	1.0855
8	86	1.09
9	87.8	1.094

**Fig 4.** Variation in hardness of different PCC and clay filled EPDM mixes.

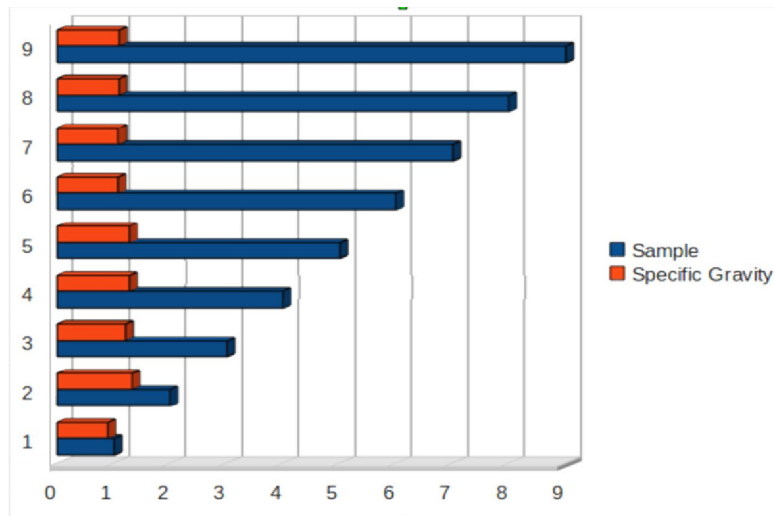


**Figure.5** Variation in Specific gravity of different EPDM mixes.

Hardness applied to elastomer is defined as the resistance of the surface of penetration by an indenter of specified dimension under specified condition. Specific gravity of rubber compound is a contribution of specific gravities of ingredients used in each formulation. In the seven formulations studied they differ only in the quantity of two ingredients and hence close values are observed.

Comparing PCC and clay filled samples it is clear that PCC filled EPDM vulcanisates show higher hardness than mix with non-reinforcing filler clay.

Hardness

increases with increasing filler loading. Specific gravity also increases with increasing filler

loading. Tear strength of various mixes shown in Table 7

**Table 7:** Tear strength of various mixes

Sample	Tear Strength	Relative Volume loss
1	1.89	158.7394
2	2.87	280.1995
3	3.46	309.19998
4	3.52	278.3073
5	3.59	85.3829
6	9.95	86.6787
7	14.02	86.7029
8	15.645	73.2055
9	13.50	72.9378

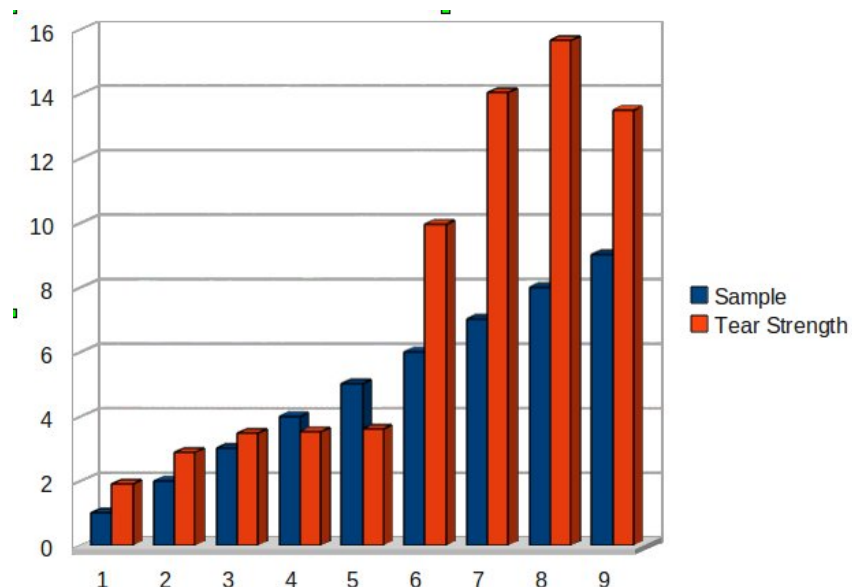


**Figure 6.** Variation in tear strength of different EPDM mixes

Silica & Struktol 40 MSFlakes filled EPDM vulcanisates show high tear strength than PCC & Struktol 40 MS Flakes filled EPDM vulcanisates. On increasing filler content tear strength also increases.

## Conclusions

In the present work two types of fillers and a plasticizer Struktol 40 MS Flakes are selected and used in representative formulation in different quantities. Mechanical properties and physical properties of different mixes are measured and compared. Mix-1 does not contain any filler or plasticizer. Mix 2(100 PCC, Zero gm 40 MS), mix 3(100PCC,2 gm 40 MS) , mix 4(100 PCC,4 gm 40 MS) and mix 5(100 PCC,6 gm 40 MS) shows an increase in cure rate due to the alkaline nature of filler. Mix 6(50 Silica,0 gm 40 MS), mix 7(50 Silica,2 gm 40 MS),mix 8(50 Silica,4 gm 40 MS) and mix 9(50 Silica,6 gm 40 MS) shows a decreasing cure rate due to acidic nature of the filler. Slow curing always gives better mechanical properties. The compound safety of mixes defined in terms of scorch time. Higher the scorch values better the compound safety. Silica filled EPDM mixes show higher scorch value than other mixes. From this study it was found

that Silica filled EPDM vulcanisates have given high tensile properties compared with poor reinforcing filler PCC. The tensile strength of un filled EPDM mix found to be very low. This is due to poor unsaturation of synthetic rubber. Among the nine mixes Silica filled mix (with 6 gm 40 MS) gives highest hardness value due to reinforcing character of filler. The tear strength of PCC and Silica filled mixes are also studied and found that Silica filled compounds have high tear strength than PCC filled ones. The EPDM compounds developed could be used for those products required better aging resistance, enhanced tensile and physical properties. Roofing membranes, rail pad, gaskets are some examples.

### References

1. Fred W Barlow, Rubber Compounding : Principles, Materials and .
2. James E Mark, Science and Technology of
3. J.R White , Rubber Technologists Handbook
4. V.R. Gowariker, N.V Viswanathan. Jayadev Sreedha, Text Book of Polymer science.
5. Joel. R.Fried , Polymer Science and Technology.
6. Hand book of Plastic Test methods – R.P. Brown
7. C. M Blow, Rubber Technology and manufactures.
8. Billmeyer, Textbook of Polymer Science, John Wiley.
9. Vishu Shah, Plastic Testing and Technology, John Wiley

## **In vivo Analgesic activity of ethanolic extract of medicinal plant *Hypericum mysorense* Aerial part**

**Anusha P.<sup>1\*</sup> and Gurusamy R<sup>1</sup>**

<sup>1</sup>Department of Biotechnology Vivekanandha College of Engineering for Women, Tiruchengode, Namakkal, Tamil Nadu, India

\* [anukrishna@rediffmail.com](mailto:anukrishna@rediffmail.com)

### **Abstract**

India has a rich tradition of plant-based knowledge on healthcare. A large number of plants/plant extracts/decoctions or pastes are used by the community in India for treatment of pain, cuts, wounds, and burns. The present study attempts to analyze the analgesic activity of *Hypericum mysorense*, an herbaceous plant which belongs to the family of *Hypericaceae*. *H. mysorense* which has many biological activities was found by WIGHT & ARN. The aerial part of *Hypericum mysorense* plant was extracted by Soxhlet extraction method. Ethanolic extract of the plant was prepared and qualitative test was performed. Analgesic activity of plant was tested on Swiss albino mice (15-50gm), the mice were divided into 4 groups [Group I negative control, Group II standard, Group III received alcoholic extract (200mg/kg body weight, p.o.). Group IV received alcoholic extract (400mg/kg body weight, p.o.). The analgesic activity of the ethanolic extract of the aerial part of *Hypericum mysorense* was investigated on mice using Eddy's hot plate method and Acetic acid induced writhing method. Tramadol and Indomethacine were used as the standard drug. The result showed that the administration of the extract lowered the number of writhing and increased the reaction time towards pain. Thus the present finding suggested that, though the extract had analgesic activity, a detailed study is required to establish it as a potent analgesic to be used in drug formulation.

**Keywords:** *hypericum mysorense*, *Mice*, *Eddy's hot plate*, *analgesiometer*, *acetic acid induced Writhing method*.

### **Introduction**

Plant plays a major role as potential source of therapeutic agent and traditional herbal systems of medicine, resulted in the revival of primordial medicine. Scientific authentication of medicinal plants is indispensable for future herbal drugs with fewer side effects. [Thankamani V *et al.*, 2011] Due to adverse side effects caused by NSAIDs and

opiates, the use of these drugs as analgesic agents have not been booming in all the cases. Therefore, analgesic drugs lacking those effects are being searched all over as an alternative to NSAIDs and opiates.[Zulfiker *et al.*, 2010]

*Hypericum mysorense* Wight and Arn is well known for its therapeutic potentials and antifungal activities. The analgesic properties of *Hypericum mysorense* has not been scientifically evaluated so far. Hence, the present work was undertaken to evaluate the effect of ethanolic extract of aerial part of *Hypericum mysorense* on Swiss Albino mice.[Pulok K Mukharjee *et al.*,2000]

## Materials And Methods

### Collection and authentication of plant:

Plant was collected from Nilgiri district of Tamil Nadu, India and authenticated by Botanist.



**Fig.1:** Picture showing the morphology of *Hypericum mysorense*

### Preparation of ethanolic extract *Hypericum mysorense* plant:

After authentication, aerial part of the plant material was shade dried, until it was free from moisture. The plant material was subjected to size reduction to obtain a coarse powder. About 500 gm of air dried powdered material was taken in 1000ml soxhlet apparatus and defatted with petroleum ether which was followed by ethanolic (90%) extract preparation from the same material. The extract was concentrated by distillation; the temperature (40-60°C) was maintained on an electric heating mantel with thermostat control. Appearance of colourless solvent in the siphon tube was taken as the end point of extraction (approximately 15-20 cycles). The extract was then concentrated to 3/4<sup>th</sup> of its original volume by using rotavapour apparatus. The concentrated extract was then taken in a China dish and evaporated on a thermostat controlled water bath till it

forms a thick paste. The thick mass was kept for vacuum drying in a desiccator till get free from moisture and the average yield obtained was 14%. The colour and consistency of ethanolic extract was noted and it was subjected to preliminary phytochemical and pharmacological studies.

#### **Phytochemical screening:**

Phytochemical screening of the prepared extracts was conducted with various qualitative tests to identify the presence of chemical constituents. To perform the tests the following chemicals and reagents were used: Carbohydrates with Molisch's test, glycoside with water and sodium hydroxide solution, saponins with the capability of producing suds, steroids with chloroform and sulphuric acid, flavonoids with Mg and HCl, tannins with ferric chloride solution, gum with Molish reagents and concentrated sulfuric acid. Alkaloids were tested with Mayer's reagent, Hager's reagent and Dagendorff's reagent. These were identified by characteristic color changes using standard procedures. [Zulfiker *et al.*, 2010]

#### **Animal Study:**

##### **1) Eddy's Hot Plate Method:**

Eddy's Hot plate was maintained at  $55 \pm 1^\circ\text{C}$ . Male Swiss albino mice of either sex were randomly divided in 4 groups of 5 mice each. The animals were placed on the hot plate and the basal reaction time taken to cause a discomfort (licking of paw or jumping response whichever appeared first) was recorded at 0 min. Cut-off period of 15 seconds was established to prevent damage to the paws.

- Group 1 : Control mice received propylene glycol (5 ml/kg).
- Group 2 : Standard drug treated group which received tramadol (40 mg/kg).
- Group 3 : Mice received ethanolic ext 200mg/kg.
- Group 4 : Mice received ethanolic ext 400mg/kg.

The reaction time in seconds was noted at 15, 75 and 135 mins after the treatment. Changes in reaction time were noted.

##### **2) Acetic acid –Induced Writhing in Mice:**

Male Swiss albino mice (over night fasted) were divided into 4 groups of 5 mice each for various treatments.

- Group 1 : Control mice received Acetic acid solution 0.6% v/v (10 ml/kg)
- Group 2 : Standard drug treated group which received indomethacine (5 mg/kg).
- Group 3 : Mice received ethanolic ext 200mg/kg.
- Group 4 : Mice received ethanolic ext 400mg/kg.

Acetic acid solution 0.6% v/v (10 ml/kg) was injected by intra peritoneal route one hour after the treatment and number of writhes (i.e. index of pain reaction against chemical stimuli characterized by abdominal muscle contraction together with turning of trunk and extension of hind limbs) was counted over a period of 20 min [Tambe *et al.*, 2010]. The percentage inhibition was determined for each experimental group as follows:

$$\text{Percentage inhibition} = 1 - [\text{NRt} / \text{NRc}] \times 100$$

NRt = Number of writhing in experimental group

NRc = Number of writhing in control group.

#### Statistical Analysis

The results are expressed as mean  $\pm$  SEM. Result with P<0.001 and P<0.01 were considered significant

### Result

#### Phytochemical Screening

The results of phytochemical screening are given in Table 1. Phytochemical analysis of the plant extracts revealed the presence of alkaloids, carbohydrates, glycoside, tannins, Protein and aminoacids, Saponins and flavanoids.

**Table 1: Qualitative Chemical Analysis Report**

SI.No	Phytoconstituents	<i>Hypericum mysorense</i>
1	Alkaloids	+
2	Glycosides	+++
3	Sterols	-
4	Tannins	+
5	Resins	-
6	Carbohydrates	++
7	Proteins and amino acids	+
8	Saponins	++
9	Gum and mucilage	-
10	Flavonoids	+++
11	Vitamin-C	-

### Animal Study

Mice of either sex weighing between 15-50 gm were kept on a hot plate ( $55\pm 0.5^{\circ}\text{C}$ ), the time for Intraperitoneal administration of *Hypericum mysorense* aerial parts extracts in the Hot Plate test (200 and 400 mg/kg, Table:2), and acetic acid induced abdominal constriction Test (200 and 400 mg/kg, Table:3) showed significant analgesic activity. These results indicated that a significant analgesic activity is present at both dose levels. In both models 400mg/kg dose showed more significant analgesic activity compared to 200 mg/kg plant extract and standard drug. The analgesic activity shown by *Hypericum mysorense* aerial parts extract in various models indicated that the plant extract might possess centrally and peripherally mediated analgesic properties.

**Table 2: Analgesic Activity (Hot Plate Method) Of *Hypericum mysorense* Aerial Parts**

Extracts in Mice				
Groups	0	15	75	135
Control	4.012± 0.568	2.83± 0.13	4.424± 0.485	4.46± 0.179
Standard	4.728±0.067	13.372±0.407 ***	9.748±0.129 ***	8.148±0.335 ***
Extract 200mg / kg	5.69± 0.133***	5.564±0.643**	6.552±0.51 ***	5.592±0.452 **
Extract 400mg / kg	5.988± 0.21***	7.888± 0.576***	9.75±0.258 ***	6.168± 0.188***
GROUPS	Control	Standard	GROUP 3 EXTRACT	GROUP 3 EXTRACT

Vs control \*\*\*  $p < 0.001$ ; \*\*  $p < 0.01$ ;

**Table 3: Analgesic Activity (Writhing Method) Of *Hypericum mysorense* Aerial Parts Extracts in Mice**

Mean	45.4 ± 0.510	7.6 ± 0.245***	20.8 ± 0.490***	17.8 ± 0.735***
% of inhibition	-	83.25991	54.18502	60.79295

Vs control \*\*\* p<0.001

## Discussion

The analgesic efficacy of *H. mysorensis* aerial part extracts was evaluated by Eddy's hot plate method and Acetic acid induced writhing method.

In the present study *Hypericum mysorensis* significantly increased the reaction time in the hot-plate test suggesting its central analgesic activity; the probable mechanism could be the inhibition of prostaglandin synthesis. Prostaglandins play a significant role in different phases of inflammatory reactions and elicit pain by direct stimulation of sensory nerve endings and also sensitize sensory nerve endings to other pain provoking stimuli. [Jayarama Reddy et al., 2010]

In acetic acid induced writhing method, dilute acetic acid produced pain reaction that is characterized as writhing response. Constriction of abdomen, turning of trunk (twist) and extension of hind limbs (at least once) are considered as writhing reaction to chemically induced pain. Acetic acid induced writhing test is known as a visceral pain model nociception. Based on the results obtained from the present study, it can be inferred that all the test extracts had effective central and peripheral analgesic actions.

Preliminary qualitative phytochemical screening revealed the presence of alkaloids, carbohydrates, glycosides, tannins, protein and amino acids, saponins and flavonoids.. Flavonoids were reported to have a role in analgesic activity primarily by targeting prostaglandins. There are also reports on the role of tannins in anti-nociceptive activity. [Zulfiker et al., 2010]. Besides these alkaloids are also well known for their ability to inhibit pain perception. Therefore, it is assumed that these compounds may be responsible for the observed analgesic activity Narcotic analgesics inhibit both peripheral and central mechanism of pain, while NSAIDs inhibit only peripheral pain. The plant

extracts of *H.mysorensis* exhibited both types of pain inhibition. The analgesic effect of the plants in both models suggested that they have been acting through central and peripheral mechanism

### Conclusion

The findings in this study suggested that *Hypericum mysorensis* possess both central and peripheral analgesic properties. The results have been obtained by cautiously controlled experiments with laboratory animals where psychological factors can presumably be ruled out. In all the tests the responses have been assessed by actual measurement and not by subjective comparisons which may be influenced by the observer. Therefore the statistical validity of the findings has been proven and they provide a scientific foundation for the use of the biologically active ingredients in *Hypericum mysorensis* for analgesic activity and explain the clinical effectiveness of the *Hypericum mysorensis*.

### Acknowledgements

The author is thankful to KMCH College of Pharmacy, Tamil Nadu, India for providing necessary facilities and guidance all throughout this work.

### References

1. Thankamani V, Misra Chandra Shekhar, Kumar Pratyush, Sagadevan Lipin Dev Mundur, James Joel and Veetil Arun Kumar Thaliyil ; Analgesic activity of the methanolic extract of *Alstonia scholaris*; International Research Journal of Pharmacy., 2(8), pp 117-118,(2011).
2. Zulfiker AHM, Mahbubur Rahman M, Kamal Hossain M, Hamid K, Mazumder MEH, Sohel Rana M ; In-vivo analgesic activity of ethanolic extracts of two medicinal plants - *Scoparia dulcis* L. and *Ficus racemosa* Linn; Biology and Medicine, 2(2), pp. 42-48,(2010).
3. Pulok K Mukherjee and Suresh B ; Studies on In-vivo Wound Healing activity of leaf extract of *Hypericum mysorensis* with different wound model in Rats; Natural Product Science., 6(2),pp. 73-78 (2000).
4. Tambe D A, Chaudhari T B, Chaudhari S R ; Analgesic activity of *Caralluma adscendens* Roxb (Aerial part); International Journal of Pharma. Research and Development-online (IJPRD)., vol-2, issue-7, (2010).
5. Jayarama Reddy, Gnanasekaran D, Vijay D and Ranganathan T V ; Invitro studies on asthmatic, analgesic and anti convulsant activities of the medicinal plant *Bryonia laciniosa*.Linn; International Journal of Drug Discovery., 2(2),pp. 01-10,(2000).

# Pyrrole incorporated Schiff Base Macrocycles

Divia P. <sup>1\*</sup>

<sup>1</sup> Department of Chemistry, MES Keveeyam College Valanchery-676552, Kerala, India  
\* *sreeragam22@gmail.com*

## Abstract

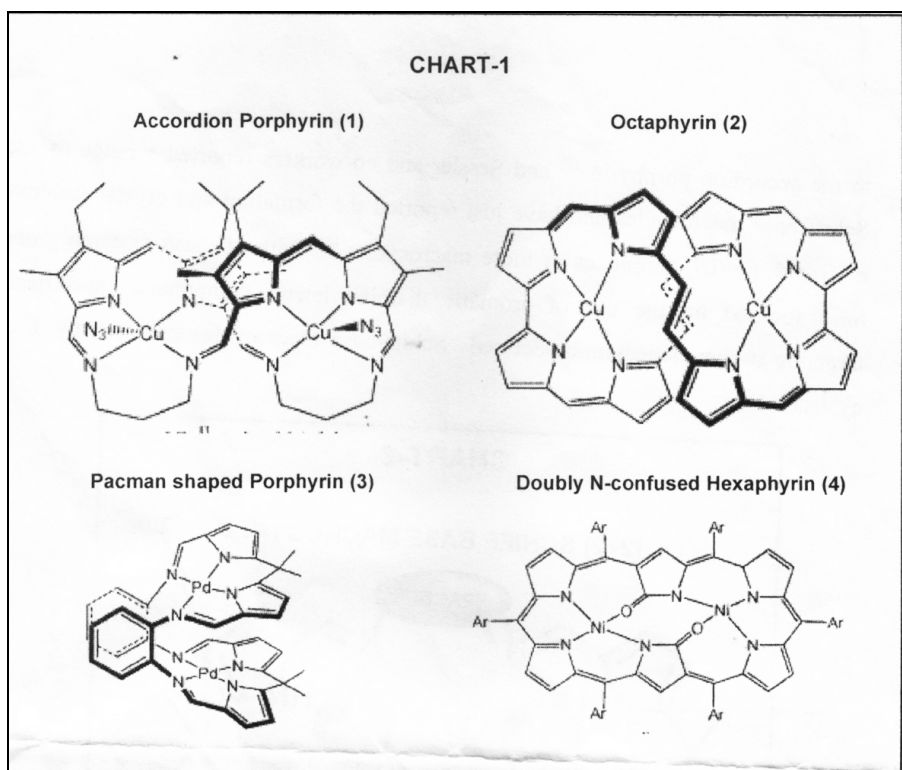
Syntheses of various [2+2] diiminodipyrromethane macrocycle by the condensation of 5, 5<sup>1</sup>-dimethyl-1,9diformyl dipyrromethane with aliphatic diamines are described. The structures of the macrocycle were characterized by <sup>1</sup>H NMR spectral analysis. The coordination chemistry was performed by using Ni(II) salt with these macrocyclic Schiff bases.

**Keywords:** *Expanded porphyrins, Schiff-base macrocycles, 5, 5<sup>1</sup>-dimethyl-1,9diformyl dipyrromethane, diamines, [2+2] diiminodipyrromethane macrocycle.*

## Introduction

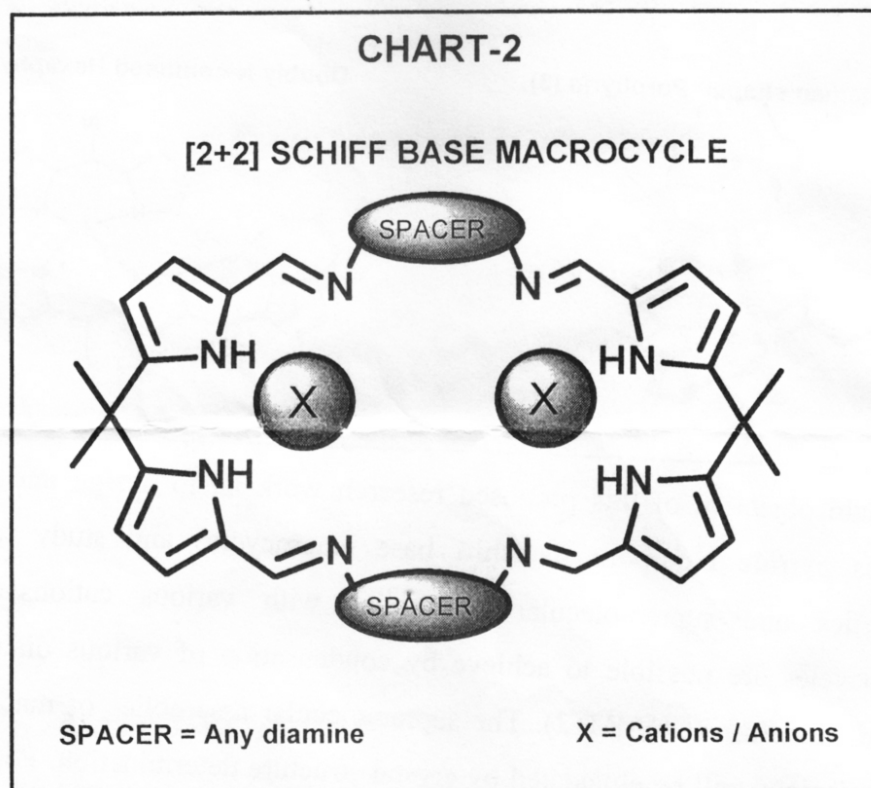
Much of the interest in porphyrins and expanded porphyrins lies in the exploration and refinement of their rich metallation chemistry, and in the development of the complexes for use in the range of applications such as photodynamic therapy (PDT), X-ray radiation therapy and magnetic resonance imaging (MRI). Our interest lies primarily in the development of porphyrin like polydentate ligands that provide access to di- and poly-metallic transition metal complexes with interesting magnetic, electrochemical or catalytic properties. Pyrrole-containing ligands, including porphyrins, can act as anion-binding agents and such studies on our pyrrole-containing ligands are also being pursued.

Almost every element in the periodic table has been incorporated into a porphyrin at some stage and the chemistry of porphyrins is clearly well established and exploited. However due to the limited cavity size, porphyrins generally co-ordinate to only one metal ion, via the four pyrrolic nitrogen atoms. The larger polypyrrolic macrocycles, the expanded porphyrins, which generally contain either more than four pyrrolic unit or a larger number of meso like bridging atoms or both, can in principle complex more than one metal ion but in practice, the development of the dimetallic expanded porphyrin complexes has been remarkably slow.



The dimetallic expanded porphyrins fall into distinctly differing classes(CHART-1), including the accordion porphyrins/dipyrromethene-based Schiff base macrocycles(1), octaphyrins (2), Pac-Man shaped porphyrins/dipyrromethane based Schiff base macrocycles(3), doubly N-confused hexaphyrins(4) and other polypyrrolic macrocycles. Of these, the accordion porphyrins, first described by Bowman-James and co-workers in 1984, which generate catalytically active dimetallic first row transition metal complexes that are functional models for dinuclear metalloenzymes captured our attention. This class of expanded porphyrins has not yet been fully exploited so we decided to try and develop related Schiff-base macrocycles and dinuclear complexes<sup>[1]</sup>

The main objective of this proposed work is to design and syntheses of various pyrrole incorporated Schiff base macrocycles and study their receptor properties and supramolecular assemblies with various cations/anions. Such macrocycles are possible to achieve by condensation of various dialdehydes with various diamines(CHART 2). The supramolecular assemblies of macrocycles with cations/anions will be elucidated by crystal structure determination. Possible binding modes will be predicted through solution analyses.

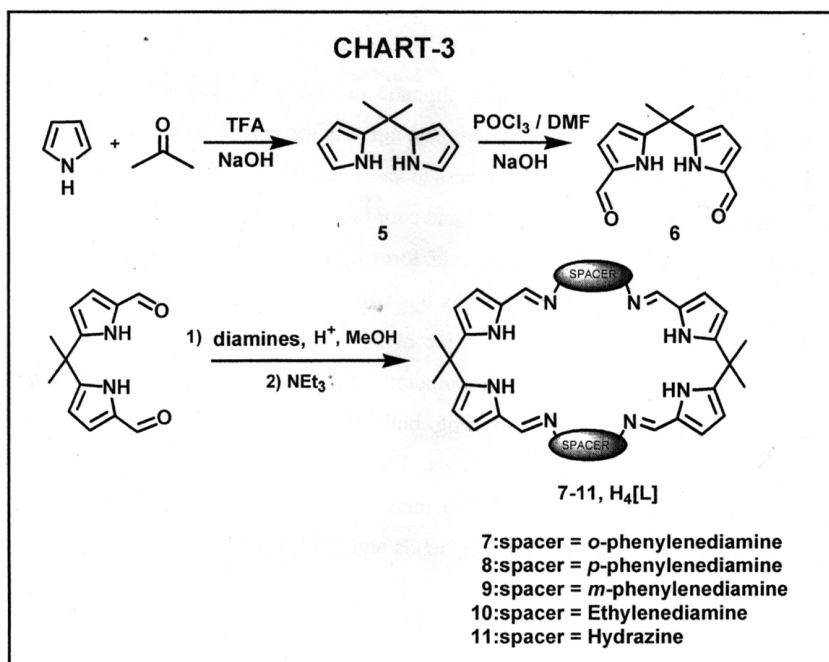


More coordinative flexibility and modularity of design, and also relative simplicity of synthetic routes to cofacial and expanded porphyrins, focus has shifted to the development of Schiff-base porphyrin analogues as binucleating ligands for transition metals. Love's group and Sessler's group are mainly focused on this area of research. Recently, Love and co-workers reported the formation of two Pac-Man shaped dipalladium(II)Schiff-base macrocyclic complexes, which are closely related the accordion porphyrin and<sup>[2]</sup> Sessler and co-workers reported a range of such Schiff base macrocycles and have just reported the formation and crystal structures of five diiron(III) complexes of these macrocycles.<sup>[3,4]</sup> Both of these research group have focused on the use of aromatic diamine lateral components, specifically targeting *o*-phenylenediamine – derived Schiff-base macrocycles prepared by direct cyclisation.

### Results and Discussion

To do our work, we targeted the head unit as 5, 5<sup>1</sup>-dimethyl-1, 9-diformyldipyrromethane (6), because of two reasons. (a) The synthesis of the precursor, 5, 5<sup>1</sup>-dimethyldipyrromethane (5) was known and Vilsmeier-Haack formylation of dipyrromethane with POCl<sub>3</sub>/DMF in CH<sub>2</sub>Cl<sub>2</sub> gives required dialdehyde<sup>[5,6]</sup> and (b) the

meso carbon in the dipyrromethane (dpm) unit is doubly substituted which will prevent its oxidation to dipyrromethene. We used the similar methodology of Love group to synthesise new members of Schiff- based calix [4] pyrrole type macrocycles(7-11) with various diamines and found that the synthetic methodology is successfully worked out. The structures of the macrocycles and the starting materials were characterized by FAB mass and  $^1\text{H}$  NMR spectral analyses. (CHART 3)



The addition of *p*-toluenesulfonic acid to a stirred mixture of dialdehydes and diamines in methanol followed by neutralisation with triethylamine ( $\text{NEt}_3$ ) quantitatively yields the free ligands  $\text{H}_4[\text{L}]$ , Schiff based calix[4] pyrrole, 7-10, as poorly soluble amorphous powders, although addition of a protic solvent such as  $\text{d}_4$ -methanol to a slurry of  $\text{H}_4[\text{L}]$  in  $\text{CDCl}_3$  results in immediate dissolution.

$\text{H}_4[\text{L}]$  with ethylene diamine spacer  $\text{H}_4[\text{L}]^{\text{Et}}$ : White amorphous powder

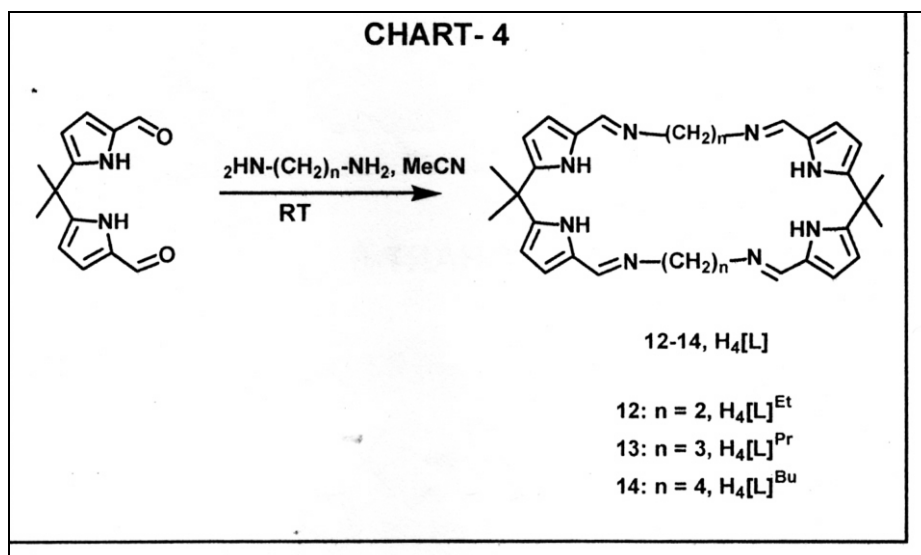
The  $^1\text{H}$  NMR spectrum reveals the retention of the characteristic resonance of the imine protons at 7.9 ppm. Pyrrolic  $\beta$ -CH protons resonate between 6.39 and 6.049 ppm respectively. Ethylene protons resonate at 3.73 ppm. Methyl groups at 1.66 ppm and pyrrolic NH signals not seen due to internal H-bonding between pyrrolic protons and imine Nitrogen. Here the spectrum reveals the symmetry within the macrocycle, as the signals are observed for a quarter of the macrocycle meanings that the two ends and two faces of macrocyclic rings are equivalent in solution at room temperature.

$\text{H}_4[\text{L}]$  with hydrazine spacer  $\text{H}_4[\text{L}]^{\text{Hy}}$ : yellow amorphous powder soluble in DMSO

The  $^1\text{H}$  NMR spectrum  $\text{H}_4[\text{L}]^{\text{Hy}}$  was taken in  $\text{DMSO-d}_6$ . Spectrum shows degenerate pyrrolic NH and imine protons, because  $\text{DMSO-d}_6$  H-bonding between pyrrolic protons and imine Nitrogen. Pyrrolic NH protons resonate at 11.25ppm. Imine protons resonate at 8.3. Pyrrolic  $\beta\text{-CH}$  protons resonate between 5.94 and 6.47ppm respectively Methyl groups at 1.70ppm. also the spectrum reveals the symmetry within the macrocycle, as the signals are observed for a quarter of the macrocycle meanings that the two ends and two faces of macrocyclic rings are equivalent in solution at room temperature.

Even more recently, Sally Brooker group reported the synthesis and characterisation of two dicopper(II) and two dinickel(II) macrocyclic complexes, prepared by the metal ion template [2+2] condensation of 5,5-dimethyl-1,9-diformyl dipyrromethane(6) with two aliphatic diamines, 1,3-diaminopropane and 1,4-diaminobutane.<sup>[1]</sup> Introduction of a template agent is the most reliable method to prevent oligocondensation and switch the process towards forming macrocyclic Schiff-bases. Use of metal ions with different ionic radii and coordination requirements makes it possible to control the structure of the macrocycle formed. However, template synthesis of the macrocyclic Schiff-bases on metal ions has two substantial disadvantages. First, rather often, it doesn't allow one to synthesize metal free macrocyclic Schiff bases. Second template synthesis from dicarbonyl compounds and diamines usually affords symmetric macrocyclic complexes. Other starting building blocks have to be used to obtain nonsymmetric macrocyclic Schiff-bases. During the last two decades, considerable efforts have been made for developing metal-free methods for furnishing macrocycles starting from various dicarbonyl compounds and diamines in addition to standard metal template protocols.

By keeping this in mind, we have done the similar type of condensation reaction without using acid catalyst in acetonitrile medium and found that methodology successfully worked out for the formation of metal free parent macrocycles(12-14).<sup>[7]</sup> A solution of dialdehyde in  $\text{CH}_3\text{CN}$  was added to a stirred solution of diamine in  $\text{CH}_3\text{CN}$  over a period of one hour. The mixture was stirred overnight and the precipitate filtered off, washed with acetonitrile and recrystallised from  $\text{CHCl}_3/\text{CH}_3\text{CN}$ . The structures of the macrocycles were characterized by  $^1\text{H}$  NMR spectral analysis. (CHART-4)



The <sup>1</sup>H NMR spectrum H<sub>4</sub>[L]<sup>Pr</sup>: White amorphous powder

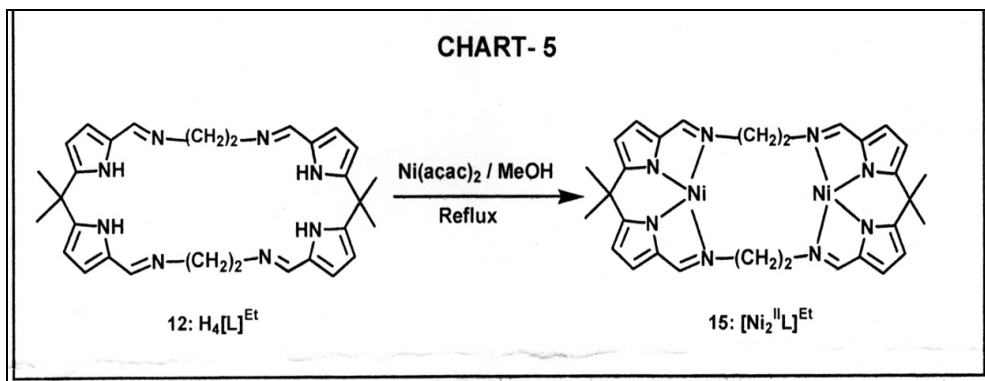
Addition of a protic solvent such as d<sub>4</sub>-methanol to a slurry of H<sub>4</sub>[L]<sup>Pr</sup> in CDCl<sub>3</sub> results in immediate dissolution. The <sup>1</sup>H NMR spectrum reveals the retention of the characteristic resonance of the imine protons at 7.91 ppm. Pyrrolic β-CH protons resonate between 6.12 and 6.42 ppm respectively. Propylene protons resonate at 3.43 ppm and 1.83 ppm. Methyl groups at 1.69 ppm and pyrrolic NH signals not seen due to internal H-bonding between pyrrolic protons and imine Nitrogen. Here the spectrum reveals the symmetry within the macrocycle, as the signals are observed for a quarter of the macrocycle meanings that the two ends and two faces of macrocyclic rings are equivalent in solution at room temperature.

The <sup>1</sup>H NMR spectrum H<sub>4</sub>[L]<sup>Bu</sup>: White amorphous powder

Addition of a protic solvent such as d<sub>4</sub>-methanol to a slurry of H<sub>4</sub>[L]<sup>Bu</sup> in CDCl<sub>3</sub> results in immediate dissolution. The <sup>1</sup>H NMR spectrum reveals the retention of the characteristic resonance of the imine protons at 7.84 ppm. Pyrrolic β-CH protons resonate between 6.09 and 6.35 ppm respectively. Butyl protons resonate at 3.45 ppm and 1.61 ppm respectively. Methyl groups at 1.69 ppm and pyrrolic NH signals not seen due to internal H-bonding between pyrrolic protons and imine Nitrogen. Here the spectrum reveals the symmetry within the macrocycle, as the signals are observed for a quarter of the macrocycle meanings that the two ends and two faces of macrocyclic rings are equivalent in solution at room temperature.

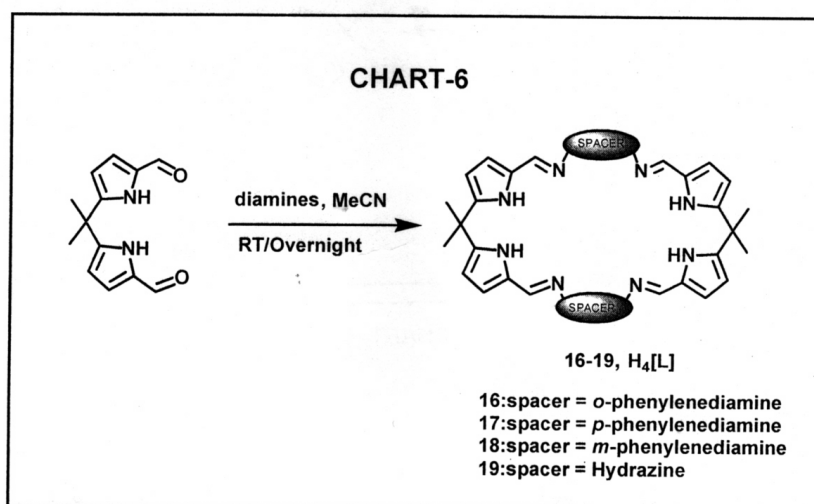
The cationic property was examined by the reaction between the metal free macrocyclic Schiff base, **12** and Ni(II) salt. Addition of Net<sub>3</sub> to a stirred mixture of nickel

acetylacetonate, Ni (acac)<sub>2</sub> and macrocycle in CH<sub>3</sub>OH under reflux condition results in clean generation of orange dinickel compound (**15**) in quantitative yield (CHART-5).



<sup>1</sup>H NMR spectra obtained in CDCl<sub>3</sub>. The <sup>1</sup>H NMR spectra shows shift in δ values from the corresponding metal free ligand. The <sup>1</sup>H NMR spectrum reveals the retention of the characteristic resonance of the imine protons at 7.22 ppm. Pyrrolic β-CH protons resonate between 6.7 and 6.15 ppm respectively. Ethylene protons resonate at 3.52 ppm and 3.20 ppm respectively. Methyl groups at 1.54 ppm and pyrrolic NH signals not seen. Here the spectrum reveals the symmetry within the macrocycle, as the signals are observed for a quarter of the macrocycle meanings that the two ends and two faces of macrocyclic rings are equivalent in solution at room temperature. The absence of NH protons in the <sup>1</sup>H NMR spectral signals and the corresponding upfield shifts in the imine protons and pyrrolic CH proton signals suggested the Ni(II) coordination.

The condensation reaction between 5, 5<sup>1</sup>-dimethyl-1,9-diformyl dipyrromethane (**6**) with aromatic diamines and hydrazine (**16-19**) respectively in acetonitrile medium is currently underway in our laboratory. (CHART-6)



### Conclusions

In summary, we have demonstrated the synthesis of metal free macrocyclic Schiff bases by the condensation of 5, 5<sup>1</sup>-dimethyl-1,9-diformyl dipyrromethane with aliphatic diamines. The structures of the macrocycle were characterized by <sup>1</sup>H NMR spectral analysis. The spectral analyses suggested that the macrocycles are highly symmetric. The coordination chemistry was performed by using Ni(II) salt. The spectral analyses of this metal complex shows that in CDCl<sub>3</sub> solution they are highly symmetrical and diamagnetic. The complexation of Ni(II) by [2+2] diiminodipyrromethane macrocycle reveals that the flexible framework of these new macrocycles can accommodate a variety of transition metals and f-block elements. The relative simplicity of the synthesis and high yields afforded mean that multigram quantities can be readily prepared. The X-ray crystal structure determination will confirm the [2+2] cyclisation and supramolecular assemblies with cations which is currently underway in our laboratory.

**Acknowledgement:** I wish to express my very sincere thanks to Dr.A.Srinivasan NIIST,CSIR for supervising the project work and his continuous constructive suggestions. I thanks to NIIST-CSIR for the fellowship. I greatly acknowledge Mrs.Viji and Mrs.Sowmini, NIIST,CSIR for recording the FAB and NMR spectra.

### REFERNCES

1. Rongqing Li; Peter.D.W.Boyd; Saly Brooker; *Inorg.Chim.Acta* ,**357**,3360, (2004).
2. Gonzlo;Givaja;Martin Schroder; Janson.B.Love,*Chem.Commn.*,2508(2003).
3. Sessler,J.L.; *J.PorphyrinsPhthalocyanines*,**7**,97(2003).
4. Veauthier, J.M.; Sessler,J.L, *Inorg.Chem.*, **43**, 1220(2004).
5. Littler.B.J.; Lindsey.J.S, *J.Org.Chem.*, **64**, 1391(1996).
6. Wickramasinghe.A; Smith.K.M., *Tetrahedron*, **57**,4261(2001)
7. Ray.J.Butcher,*Journal of Organometallic Chem.*,**689**,1452 (2004)

# Sorption Behaviour of Polyethylene/Chitosan Composites in Polar and Non Polar Solvents

Mubeena Thaikkadan<sup>1</sup>, Sunil Kumar M<sup>2</sup> and C.Rajesh<sup>1\*</sup>

<sup>1</sup> Department of Chemistry, MES Keveeyam College Valanchery-676552, Kerala, India

<sup>2</sup> Department of Chemistry, National Institute of Technology, Calicut-673601, Kerala, India

\* [rajeshvlcy@rediffmail.com](mailto:rajeshvlcy@rediffmail.com)

## Abstract

Many technologically important processes are done upon the design of polymers with tailored characteristics of permeability and selectivity towards fluid molecules. The dimensional stability and integrity of the polymeric materials in presence of aggressive liquids are very important as far as their wide variety of applications such as separation process, controlled release of drugs and pesticides, food packaging, encapsulation of electronic circuits, etc. are concerned. Extensive research work going on run the field of diffusion and permeation of gases, vapours and liquids through polymers.

Several reports are available concerning the polyethylene-solvent interaction. These studies are extremely important in the continued improvement of gaskets, hoses, protective apparel and food packaging. The present project investigates the sorption behavior of polyethylene/chitosan composites in polar and non-polar solvents. Composites of polyethylene with different loading of chitosan were prepared, and sorption of polyethylene/ chitosan composites were studied in four different solvents. Solvents used are Xylene, Toluene, Dimethyl sulphoxide and Dimethyl formamide. It was found that the sorption is higher for non-polar solvents than the polar solvents.

**Keywords:** *polyethylene/chitosan composites, sorption behavior, polar and nonpolar solvents*

## Introduction

Polyethylene or polythene is approximately 80 million metric tons. Its primary uses are in packaging (bags, plastic films, geomembranes, containers including bottles etc.) Many kinds of polyethylene are known, most having the chemical formula  $(C_2H_4)_n$

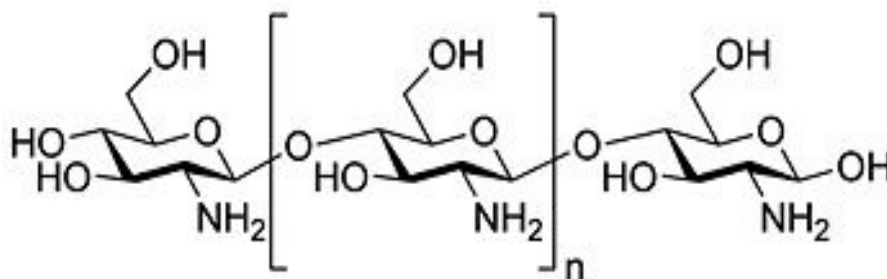
H<sub>2</sub>. Thus polyethylene is a mixture of similar organic compounds that differ only in terms of the values of n. Polyethylene is a thermoplastic consisting of long hydrocarbon chains.

Polyethylene is classified into several categories based on density, branching and crystallinity[1]. Properties of polyethylene depend on the extent and type of branching and molecular weight. Polyethylene is classified mainly into High density polyethylene(HDPE), Low density polyethylene(LDPE) and Linear low density polyethylene(LLDPE).

HDPE is 90% crystalline and is much stiffer than LDPE and has a higher tensile strength and hardness. LLDPE is a linear polymer with significant branches. LLDPE is prepared by copolymerization of ethylene and alpha olefin like 1-butene, 1-hexene. It has higher tensile strength, impact strength than LDPE. LDPE is only 40% crystalline. Solvents cannot dissolve it at room temperature. LDPE is produced by the high pressure polymerization of ethylene, using oxygen as initiator. LDPE has branching. Most LDPE, LLDPE and HDPE grades have excellent chemical resistance, meaning that it is not attacked by strong acids or strong bases. It is also resistant to gentle oxidant and reducing agents.

Polyethylene burns slowly with a blue flame having a yellow tip and gives off an odor of Paraffin. The material continues burning on removal of the flame source and produces a drip. Crystalline samples do not dissolve at room temperature. Polyethylene usually can be dissolved at elevated temperatures in aromatic hydrocarbons such as toluene, xylene or in chlorinated solvents such as trichloroethane or trichlorobenzene [2]. Its mechanical properties depend significantly on variables such as the extent and type of branching, the crystal structure and the molecular weights[3].

Chitin is a white, hard, inelastic nitrogenous polysaccharide found in the exoskeleton as well as in the internal structure of invertebrates[4]. The waste of this natural polymer is a major source of surface pollution in coastal areas. Chitosan is mostly obtained by the deacetylation of chitin. This is a more useful and interesting bioactive polymer. The production of chitosan from crustacean shells obtained as a food industry waste is economically feasible. Scheme 1.1 shows the structure of chitosan.



Scheme 1.1: Structure of chitosan

Chitin and chitosan are the naturally abundant and renewable polymers having excellent properties such as biodegradability, biocompatibility, non-toxicity, and adsorption of heavy metals [5]. Despite its biodegradability, it has many reactive amino side groups. Which offer possibilities of chemical modifications, formation of large variety of useful derivatives that are commercially available or can be made available via graft reactions and ionic interactions. Chitin and chitosan are considerably versatile and promising biomaterials. Chitin is the second most natural polysaccharide after cellulose on the earth [6]. Various efforts have been made to prepare functional derivative of chitosan by chemical modifications like graft reaction and ionic interactions. Only few of them are found to dissolve in conventional organic solvents. Chitosan is soluble in aqueous solutions of some acids, and some selective N-alkylation and N-acylation have also been attempted. Modification of the chemical structure of chitin and chitosan to improve the solubility in conventional organic solvent has been studied by many researchers [7].

Composites can be defined as materials that consist of two or more chemically and physically different phases separated by a distinct interface [8]. It is evident that the material advances have been the key to significant breakthroughs throughout the history. The Stone Age, Iron Age, the industrial revolution, the nuclear age, the electronic revolution, the aerospace of today; all have critically resulted from breakthroughs in material technology. A composite material is a combined material created from two or more components, selected filler or reinforcing agent and a compatible matrix, in order to obtain specific characteristics or a property that was not there before. The matrix is the continuous phase, and the reinforcement constitutes the dispersed phase. It is the behavior and properties of the interface that generally control the properties of the composites [9].

Conventional polyethylene products are non-biodegradable and will remain hundreds of years in soil. The increased costs of solid waste disposal methods as well as potential hazard from waste incineration are severe problems. Recycling of polymeric waste proves to be a better solution for this problem, but it is very costly. Moreover the recycled products have poor mechanical properties. Now researchers are on to develop materials with better biodegradable and more environment friendly nature. Polymer blends and composites with natural polymers as one of the components have been developed by many researchers, but these are not yet commercialized. Disadvantage in blending or reinforcing natural polymers with synthetic polymer is their incompatibility with the matrix, which is caused by the immiscibility of the hydrophilic natural polymers with the hydrophobic synthetic polymers.

Biodegradability enhancement of polyethylene is the one of the major research area which has been actively pursued. In all these studies biodegradability enhancement of polyethylene has not been achieved by physical or chemical modifications. Synthetic plasticizers cannot be used as they are non-biodegradable, irritating, corrosive and even toxic. Glycerol, ethylene glycol, propylene glycol, diethylene glycol and triethylene glycol are most used plasticizers, but their volatility, UV susceptibility, leaching, migration and insufficient lubrication and suspected carcinogenic effect on a number of living organisms have been reported. Vegetable oils are potential substitute for mineral oils in these regards. Fatty acids obtained from palm oil processing consist of a mixture of myristic, palmitic, stearic, lauric, oleic and linoleic acids. These acids are long stearic chain compounds containing an even number of carbon atoms  $C_{10}$ - $C_{18}$ . Hence palm oil can improve flexibility, processability, and filler dispersion of the composite films.

In recent years, there has been a marked increase in the interest in biodegradable polymer materials for the use in packaging, agriculture, medicine, and other areas. Different biodegradable composite films have been fabricated by several researchers. Meifang et al. [10] prepared the graft copolymer, chitosan-g-polyethylene glycol (PEG) through graft polymerization of PEG chains to chitosan due to the esterification reaction between PEG and 6-O-succinate-N-phthaloyl-chitosan (PHCSSA). The graft copolymer with porous structure was observed from scanning electron micrographs. Minfang [11] prepared the sub-micrometer porous membrane from chitosan/polyethylene glycol. The content of PEG and the crosslinking agent has significant effects on the pore structure,

swellability, and mechanical properties of the membranes. The membrane is pH sensitive, exhibiting reversibility and rapid response in swelling to pH changes.

Zhang et.al [12] evaluated the biocompatibility of chitosan modified by several methods, at the cellular and protein levels using different physical and biological methods. The results provide a theoretical basis for screening biomaterials. Felinto et.al[13] prepared the membranes of polyethylene glycol (PEG 300 and 400) and chitosan under ultraviolet light (UV) and  $\gamma$ -radiation curing, at room temperature. The hydrogels were characterized by FTIR spectroscopic, UV absorption spectroscopy, thermal analysis and scanning electronic microscopy. The hydrogel with PEG 300 showed unusual swelling behavior. Tomoki et.al [14] prepared the Chitosan membrane by the casting method in combination with N-acetylation reaction. Deacetylation degree decreased linearly with increasing added amounts of acetic anhydride.

The biodegradability of LDPE can be improved by using palm oil as a plasticizer and chitosan. Palm oil being a renewable resource, it is biodegradable, non-toxic and a more effective coupling agent. In addition the envisaged filler chitosan has antimicrobial activity against a wide range target organisms. The combination of filler with plasticizer is proposed to improve the antibacterial properties of the composite for packaging application.

The presence of solvents in polymer composites assumes significance, since most Polymers after swelling in the solvent shows a reduction in its properties. Therefore polymer for commercial application should be chemically resistant and retain their mechanical strength and dimensional stability on contact with solvents. Thus the phenomenon plays a prominent role in many industrial and engineering applications of polymers.

The objectives of the project is to study the sorption behavior of polyethylene/chitosan composites in polar solvents, such as Dimethyl formamide and Dimethyl sulphoxide, and to study the sorption behavior in non-polar solvents such as Xylene and Toluene using equilibrium swelling technique.

## **Experimental**

The formulations of the mixes used in the present work are given in Table given below

**Table 1: Formulations of composites**

Sample	LDPE(g)	Chitosan (wt%)	Dicumyl peroxid e	Maliec anhydri de (wt.%)	Palmoil (wt%)
A	40	—	0.5	2	2.5
B	40	5	0.5	2	2.5
C	40	10	0.5	2	2.5
D	40	15	0.5	2	2.5

Maleic anhydride (2 wt.%) as a coupling agent (their amounts in the system have been optimized by checking their mechanical properties), varying amount of the bio-filler (5, 10 and 15) and palm oil(2.5%) as plasticizers were added in 2 min time intervals to the LDPE. Mixing was continued for another 4 min. Mixes have been prepared under shear deformation in a rotor disperser.

The composites obtained from melt mixing were compressed using an electrically heated hydraulic press for 3 min at 150 °C under a pressure of 200 kg/cm<sup>2</sup>. The average thickness of the composite films was 0.14 ± 0.01 mm. After pressing, the samples were allowed to cool at room temperature.

For swelling studies, circular specimens were punched out from the composite sheet by using a sharp steel die having a diameter of 2.5 cm. The weighed dried specimens were immersed in polar aprotic solvents such as N,N-dimethyl formamide (DMF), dimethyl sulphoxide (DMSO) and non-polar solvents such as xylene and toluene contained in diffusion test bottles, kept in room temperature. After a particular time, they were removed from the solvent and wiped by using tissue papers. The weight of these specimen after swelling in the solvents were determined by using a highly sensitive electronic balance at regular intervals until no further increase in solvent uptake was detected; i.e., weighing was done until equilibrium sorption was reached.

The swelling coefficient is an index showing the extent to which the samples swell. The polyethylene/chitosan were swollen in a suitable solvent at room temperature and the swelling coefficient was evaluated by equation.1 [15]

$$\text{Swelling coefficient } (\alpha) = \frac{W_2 - W_1}{W_1} \times \frac{1}{\rho_s} \dots \dots \dots (1)$$

Where  $W_1$ , the initial weight of the sample,  $W_2$ , the final or swollen weight of the sample and  $\rho_s$ , the density of the solvent used

The uptake of liquid during swelling has been expressed as moles of liquid sorbed by 100 g of the polymer composite. This method has been found to be more convenient for the comparison of sorption data. The mole percentage uptake,  $Q_t$ , for the composite samples has been determined as equation.2 [16, 17],

$$Q_t = \frac{W_2 - W_1 / M_s}{W_1} \times 100 \dots \dots \dots (.2)$$

Where  $M_s$  is the molecular weight of the solvent. The sorption data was evaluated by plotting the mole percentage uptake ( $Q_t$ ) of the solvent versus the square root of the time of immersion in different solvents.

**Results and Discussion**

The phenomenon of transport through rubbery polymers is controlled by the polymer structure, its cross-link density, the mode of cross-linking, the presence of fillers, their interaction with the polymer matrix, temperature, etc. Figure 1 shows that the sorption curves of the polyethylene/chitosan composites (A) in DMF, where  $Q_t$  value is plotted against the square root of time of sorption.

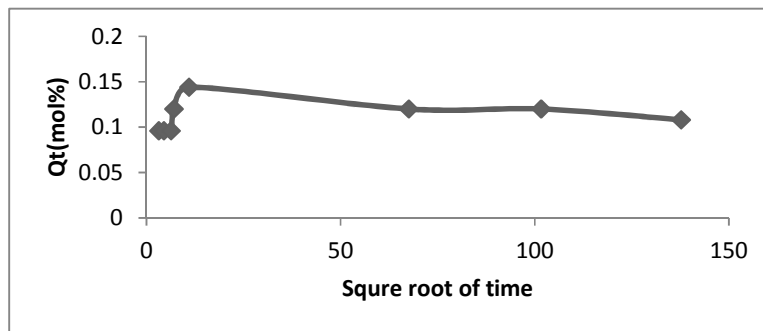


**Figure.1:**Transport of DMF through polyethylene/chitosan composite

It can be seen from the figure that initially there is an increase in  $Q_t$  value with time, and then  $Q_t$  become constant. Figure.2 show that the sorption curves of the

polyethylene/chitosan composite (B) in DMSO, where  $Q_t$  value is plotted against the square root of time of sorption.

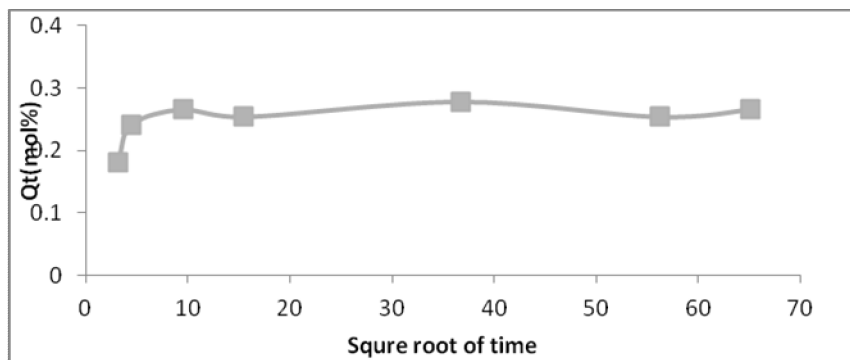


**Figure .2:** Transport of DMSO through polyethylene/chitosan composites

It can be seen from the figure, initially there is an increase in  $Q_t$  value with time, and then takes a constant value. All the composites follow the same trend. Table.1 shows the swelling coefficient values of the composites in both DMF and DMSO. Comparison of swelling coefficient in DMF and DMSO are given in figure.3 also.

**Table.2:** Swelling coefficient values of DMF and DMSO

Sample	DMF	DMSO
A	0.0871	0.2019
B	0.0740	0.1038
C	0.0376	0.0943
D	0.0195	0.0801

It can be seen that there is a decrease in the swelling coefficient values with increase in chitosan content. Swelling coefficient value is found to be higher for DMSO than DMF in the case of all composites. From the swelling coefficient values of the composites, it can be seen that as the loading of the filler increases, the swelling coefficient value decreases. Upon the incorporation of chitosan in to polyethylene matrix, the solvent uptake behavior decreases due to the reduction in the free volume available for transport.

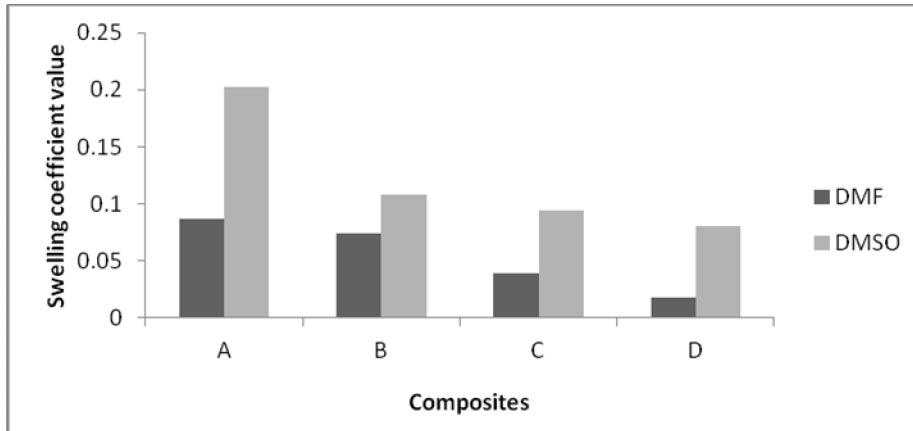


**Figure.3:** Effect of filler content on swelling coefficient values.

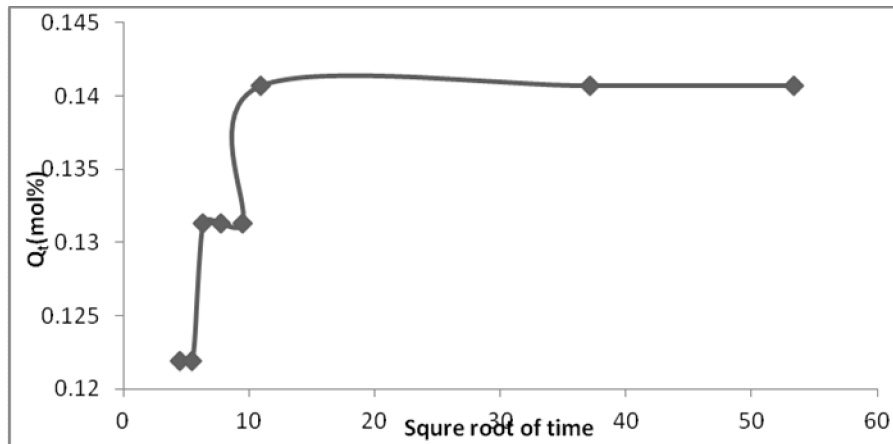


**Figure.4:** Transport of Xylene through polyethylene/chitosan composite

Figure 4 shows the sorption curve of polyethylene/chitosan (A) composites in xylene, where  $Q_t$  is plotted against square root of time of sorption. Initially there is an increase and reaches a constant value. All composites take the same path. Figure .5 shows that the sorption curve of the polyethylene/chitosan composites (B) in Toluene.

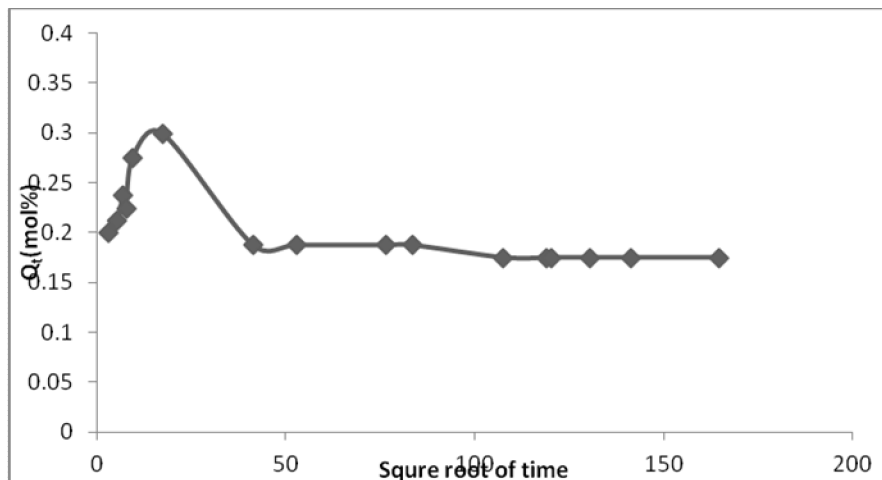


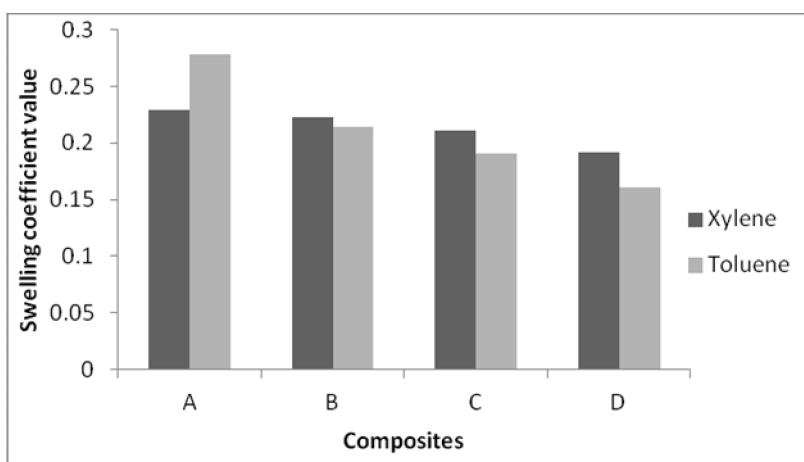
**Figure.5:** Transport of Toluene through polyethylene/chitosan composite

Initially there is an increase, then decreases and reaches a constant value. All composites take the same path. Table.3 shows the swelling coefficient values of the composites in both Xylene and Toluene. Figure .6 shows the comparison of swelling coefficient values of xylene and toluene.

**Table.3:**Swelling coefficient values of xylene and toluene.

Sample	Toluene	Xylene
A	0.2775	0.2298
B	0.2143	0.2229
C	0.1904	0.2111
D	0.1611	0.1915

It can be seen from the figure that there is a decrease in swelling coefficient value when increasing chitosan content. Swelling coefficient value of gum sample in xylene is lower than that in toluene which can be due to the increase in size of the solvent molecule. From the swelling coefficient values of the composites, it can be seen that as the loading of the filler increases, the swelling coefficient value decreases. Upon the incorporation of chitosan into polyethylene matrix, the solvent uptake behavior decreases due to the reduction in the free volume available for transport.

**Figure. 6:** Comparison of swelling coefficient values of Xylene and Toluene

Sorption of polyethylene/chitosan composites is higher for non-polar solvents, since polyethylene is non-polar. Figure.7 compare the swelling coefficient value in non-polar and polar solvents (Xylene and DMSO). From the figure it can be seen that swelling coefficient is higher for non- polar solvents than polar solvents for all composites.

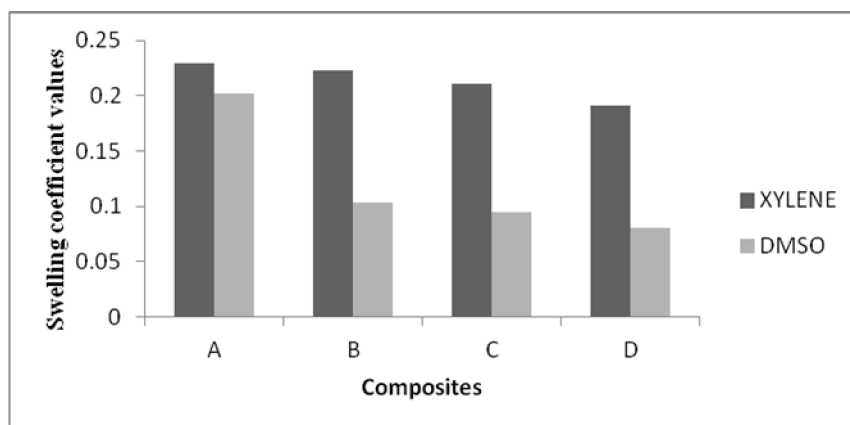


**Figure. 7:** compare the swelling coefficient value in non-polar and polar solvents

## Conclusions

The restricted equilibrium swelling behavior of polyethylene/chitosan composites was investigated with special reference to the effect of chitosan content. The equilibrium sorption value and swelling coefficient have been calculated. Sorption is higher for non-polar solvents than for polar solvents. In non-polar solvents Xylene has the highest swelling coefficient value and in non-polar solvents sorption is highest for DMSO. Swelling coefficient value decreases with increase in chitosan content, due to decrease in free volume for sorption.

## References

1. Gupta, A., Kumar, V., *J. Europ. polym.*, **43**, 2011
2. Levis, J., Barlz, M., *J. Enviorn. sci. technol.*, **45**, 2011
3. Website: [www.spelman.edu](http://www.spelman.edu)
4. Kurita, K., *Chemistry and application of chitin and chitosan*, Kodansio scientific Ltd, Tokyo, 2001
5. Domard, A., Muzzarelli, R.A., *Advances in chitin science*, university of Potsdam, German, 2000
6. Schwartz, M., *Composites materials*, Prentice Hall PTR, UpperSaddle, USA, 1997
7. Lubin, G., *Hand book of composites*, VanNostrandReinhold, New York, 1982
8. Strong, A.B., *High performance and Engineering Thermoplastic composites*, Technomicpub. Co, pennsylvania, 1993

9. Krishnamoorthy.R., Richard,A.,vaia,eds.ISBN:0841237689 publisher,American chemical society copyright,2001
10. Sanjay,K.,Mazumadar,Composites manufacturing materials product and process engineering,CRC Press LLS,USA, ,2002
11. Minfeng,Z.,Zhengping,F.,*J.Mem.Sci.*, **245**, 2004
12. Zhang,M., Li,X.H.,Gong,Y.D., Zhao,N.M.,Zhang,X.F.,*J.Bio.mat.*, **23**, 2002
13. Felinto,M.C.F.C.,Parra,D.F., Da Silva,C.C.,Angerami,J.,Oliveira,M.J.A.,LugãoA.B.,*J.Nuc. Instr. Meth.*, **265**, 2007,
14. Tomoki,T.,Masanao,I.,Isao,S.,*J. Bio.mat. Engi.*,**36**, 2007
15. Toti,U.S.,Kariduraganavar,M.Y.,Soppimath,M.Y., and Aminabhavi, T.,*J. Appl. Polym. Sci.***83**, 259–272 ,2002.
16. Geethamma,V.G., andThomas,S., *J. Adhes. Sci. Technol.* **18**, 951–966 2004.
17. Khinnavar,S., and Aminabhavi,T.M.,*J. Appl. Polym. Sci.* **42**, 232
18. Paul,S.A., Boudenne,A., Ibos,L., Candau,Y., Joseph,K., and Thomas,S., *Composites Part A*, 39,2008
19. Joseph,P.V.,*Computer Sciences Technology*, 62,2002
20. John,M.A.,Francis,B.,Varughese,K.T.,andThomas,S., *Composites Part A*, 39, ,2008
21. Bledzki, A.K., and Gassan, J., *Progress in Polymer Science*, 24, 1999
22. Jayanarayanan,K., Jose,T., Thomas,T., and Joseph,K.,*J.Europ. Polym.*, **45**,2009
23. Paul,S.A., Joseph,K., Mathew,J.D.G., Pothen,L.A., and Thomas,S. *Composites Part A*, 41,2010
24. Bergeret, A., and Bozec, M.P., *Polymer Composites*,25,2004
25. Liu,D., McDaid,A.D., and Xie,D.Q. *Mechatronics*, 21, 2011
26. Geethamma,V.G., Thomas Mathew,K., Lakshminarayanan,R., and Thomas, S. *Polymer*,39,1998

## Development of LDPE/Low Molecular Weight Chitosan Composite Films for Packaging Applications

## **Abstract**

Biodegradable composite films based on low density polyethylene (LDPE) and bio filler-low molecular weight chitosan were prepared by using a rotor disperser. In these formulations low molecular weight chitosan, maleic anhydride (MA) and dicumyl peroxide (DCP) have been used as the biodegradable component, the coupling agent and the free radical initiator respectively. Film microstructure was characterized by Field Emission Scanning Electron Microscope (FESEM) and X-ray diffraction (XRD). Sorption (saline water and petrol) and biodegradation of the films has also been investigated. The investigated properties of composite films were found to vary with the amount of low molecular weight chitosan in the LDPE matrix. The saline water uptake and biodegradation rate was found to increase with increased chitosan loading whereas percentage crystallinity was found to decrease. From the specified characterisation it was found that addition of low molecular weight chitosan in LDPE prove to be a novel combination in increasing the biodegradability of the LDPE based composite films. The prepared composite films invoke potential applications in food-packaging

**Keywords:** *LDPE, Chitosan, Biodegradability, Food Packing*

## **Introduction**

There has been increasing interest in the development of antimicrobial packaging materials. The use of biodegradable and renewable polymers in an attempt to replace plastic packaging materials would replace environmental pollution. Chitosan with antibacterial and antifungal properties, is one of the most promising and abundant resources for this purpose. Chitosan as poor resistance to water transmission because of their hydrophilic nature. Hence, there is a major drawback in using chitosan as packaging material, so there is a necessity for the composite with other synthetic polymer for packaging.

Polymer based material used in wide range of applications [1]. For many applications, polymer materials need set of properties, but single polymer cannot fulfill. To satisfy these problems is to mix two or more polymer. These compounds are known as polymer blends. Polymer blends have interesting and challenging industrial and technological area. Many blends are used in packaging industry. Plastics are

manufactured and designed to resist the environmental degradation and also more economical than metal, wood and glasses in terms of manufacturing costs and energy required. Due to these issues, plastics resins have become one of the most popular materials used in packaging [2]. The durability, strength, low cost, water and chemical resistance, welding properties, lesser energy and heavy chemicals requirements in manufactures, fewer atmosphere emissions and light weight are advantage of plastic materials, cause these material most preferable especially in packaging industries.

Synthetic polymers have become technologically significant since the 1940's and packaging is one industry that has been revolutionized by oil, based polymers such as polyethylene (PE), polypropylene (PP), polystyrene (PS), polyethylene terephthalate (PET) and polyvinyl chloride (PVC). Synthetic plastic such as polyethylene and polypropylene have a very low water vapour transmission rate and they are totally non-bio degradable, and therefore lead to environmental pollution. There has been an increased interest in enhancing the bio-degradability of synthetic plastic by blending them with low cost natural bio-polymers. Blending of LDPE with a natural bio-polymer such as chitosan will enhance the bio-degradability of the material.

All natural phenomenon can cause materials degradation. Heat, light, short wave length electromagnetic radiation, chemicals and interaction with bacteria, fungi can damage materials. Degradation is a process that results in change in the properties of materials, which reduces the ability of the material to perform its intended function [2-4]. Degradation processes are categorizing into several groups, such as chemical, mechanical/physical and biological. Material degradation such as thermal damage or chemical reaction, which are either entirely physical/chemical in nature co-exist with combined forms of materials degradation, such as corrosive wear. Environmental conditions also exert a strong effect on material degradation and there are three basic degradation mechanisms that can be identified which are scissions of inter monomer linkages in the back bone, and ionic ally catalyzed attack on side chains [5].

The degradation of polymers may proceed by one or more mechanism including bio-degradation, photo-degradation or thermal degradation, depending on the polymer environment and desired application. The combination of different factor from the environment, such as sunlight, heat and humidity also has synergistic effects on the degradation [6].

Bio-degradable plastics have been intensively studied in recent years [7-11] and have been commercialized into various products such as garbage bag, composting yard

waste bags, grocery bags and agriculture mulches. Plastic packaging demand will increase more rapidly based on good opportunity for both flexible and rigid packaging. Flexible packaging advance will be fuelled by rapid growth for pouches and protective packaging. The rapidly expanding stand-up pouch segment will enable flexible packaging to gain share in a number of rigid packaging, application. In rigid plastic packaging, best opportunities are anticipated for trays, tubs and cups.

Over the last 30 years there has been a growing interest in bio-degradable polymers. Bio-degradable polymers can be divided to two main categories which are naturally occurring bio-degradable polymers and synthetic bio-polymers [12]. Naturally occurring bio-degradable polymers include polysaccharides such as, starch, cellulose. Chitin/chitosan, pullulan, levan, konjate, and elsinan. In this compound, simple sugar such as glucose, fructose, and maltose are the basic unit [12].

Synthetic bio-degradable polymers are normally polymers with hydrolysable backbone or polymers that are sensitive to photo degradation. Polystyrene is the polymer with hydrolysable backbone. The most attractive feature of the biopolymer based material is their total biodegradability. As a result they fit perfectly well in the ecosystem and save the world from growing ecological pollution caused by non-biodegradable plastics, which are essentially petroleum based. A number of aerobic and anaerobic micro organisms have been identified for bio-degradation [13].

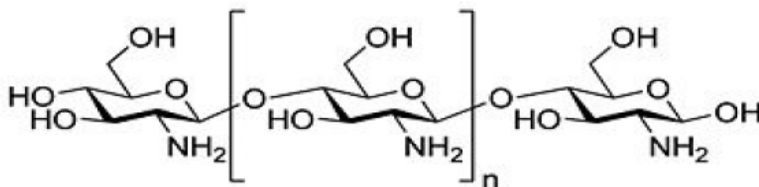
The mixing of two or more polymers to improve their properties is known as polymer blending. And such compound is known as polymer blends. Blend system can be classified based on any of the following considerations, the physical state of the component polymers, the mutually inert or reactive nature between the components, the thermodynamics of the blend system, and any improvement in the property of the blend. Various mixing equipments, e.g., roll mill, intermix (plastic order, Banbury etc...) and twin screw extruders, are used to prepare polymer blends. In roll milling, the mixing of polymers can be accomplished by squeezing the stock between rolls.

Reaction injection moulding (RIM) of polymers and elastomers is worth mentioning for the reactive processing of blends. It involves the mixing of two or more reactive components, injecting the mix into the mould, allowing it there for chemical reactions under static conditions, and finally ejecting out the solid product. Special design of the mix head takes care of the requirement of short yet efficient mixing cycle.

The term biocompatibility has been defined as the ability of a material to perform with an appropriate host response in a specific biological application. The concept of

biocompatibility might be extended to consider the carcinogenic potential of a material its direct interaction with the immunological system of the host. Testing for in-vitro cytotoxic ensures the biocompatibility of materials like polymer blends for external applications. A negative result indicates that a blend is free of harmful extractable or has an insufficient quantity of them to cause quite effects under exaggerated conditions with isolated cells. On the other hand, a positive cytotoxicity test result can be taken as an early warning sign that a material contains one or more extractable substances that could be of clinical importance. In such cases, further investigation is required to determine the utility of a blend material.

Morphology of composites is very much influenced by processing condition. Many properties of composites depend on the nature of the arrangement of the two phases. One phase may be dispersed in a matrix of the other, and in this case the matrix phase dominates in controlling the properties. The morphological parameters can be obtained from spectroscopic and microscopic analysis. Imaging of the face structure is possible by optical or electrical microscopes such as, scanning electron microscope (SEM). Many physical and chemical interactions in a composite system which control the morphology can be examined by X-ray diffraction (XRD).



SEM was carried out to determine the dispersion of fibre in the matrix, adhesion between fibre and matrix and to detect the presence of any micro defect. SEM micrographs of fracture surfaces of different LDPE- chitosan composites clearly indicate that the differences in micro structure of the various composites. The degradation by microorganism is termed as biodegradation. There are two major steps in the biodegradation process. The first step involves the depolymerisation or chain cleavage of the polymers to oligomers, and the second step is resulting mineralization of these oligomers [5]. The depolymerisation step normally occurs outside the microorganism and involves both endo and exo-enzymes. Endo enzymes cause random scission on the main chain, while the exo-enzyme causes sequential cleavage of the terminal monomer in the polymer main chain. Once depolymerised, sufficiently small sized oligomeric fragments are formed. These fragments are transported into the cell where they are mineralized [5].

Mineralized is defined as the conversion of the polymers into biomass, minerals, water, CO<sub>2</sub>, CH<sub>4</sub> and N<sub>2</sub>.

The rate of biodegradation was found to be affected by several factors polymers environment, organisms utilized and the nature of the polymeric material are three main factors affecting biodegradation.

All micro organisms have an optimum temperature at which maximum growth rate occurs and thus highest enzyme kinetics exist [14]. If the temperature in the environment becomes, higher than the optimum temperature of micro organism, then the denaturing of enzymes and other proteins in the micro organism take place. In this case the rate of biodegradation is reduced [15]. An optimum pH value also will affect the rate of biodegradation. A micro organism also needs a certain amount of nutrients from its environment to allow it to grow. Therefore, the concentration of nutrients is essential to the rate of biodegradation in terrestrial environments [15]. One of the main problems in land fill sites is that there is lack of oxygen and moisture in the environment, the micro organisms cannot grow.

Nature of polymer-substance also affects the rate of biodegradation. Increased branching in polymeric materials will reduce the rate of degradation. Maximising the linearity of the molecule reduces steric hindrance facilitates the maximum susceptibility of the molecule to enzymatic attack and promote micro organism assimilation. How molecular plastics are susceptible to degradation, due to the ability to transport into a microbial cell [16]. Composite materials combine and maintain two or more distinct phases to produce a material that has properties far superior than either of the base material. Composite materials have been used in construction for thousands of years. Biocomposite is a material formed by a matrix (resin) and a reinforcement of natural fibers (usually derived from plants or cellulose). With wide-ranging uses from environment-friendly biodegradable composites to biomedical composites for drug/gene delivery, tissue engineering applications and cosmetic orthodontics. They often mimic the structures of the living materials involved in the process in addition to the strengthening properties of the matrix that was used but still providing biocompatibility, e.g. in creating scaffolds in bone tissue engineering. Those markets are significantly rising, mainly because of the increase in oil price, and recycling and environment necessities.

Bio fillers are naturally occurring biodegradable polymers used to make polymer composites. A polymer composite is a solid material in which the bio- filler is uniformly dispersed in a matrix. The matrix can be a non-degradable polymer such as LDPE, PP

etc... The biological materials used as fillers are polysaccharides, proteins, lipids and their derivatives. Specifically, within polysaccharides cellulose derivatives, chitosan, starch, Iginate, carrageenan and pectin are preferred because of their high film forming capacity [17]. Other fillers are: zein, soy, whey, wheal, gluten (proteins), bee wax, camauba wax, free fatty acids (lipids/fats). Incorporation of natural fiber fillers into plastics such as polyethylene and polypropylene can reduce the overall usage of these petroleum-derived materials.

Chitosan is a natural polycationic polysaccharide derived from chitin. Chitosan possesses antimicrobial activity and filmogenic properties, besides being biocompatible and biodegradable. Chitosan films have been successfully probed at an experimental level on food such as, eggs, fruits, vegetable, dairy products and meat, where it has been observed that the chitosan treatment offers protection against contamination and microbial spoilage, ncreasing the food quality and self life. Chitosan has an antimicrobial effect on bacteria such as, staphylococcus, aurens, listeria monocylogenes, pseudomonas aeruginosa etc.

Three mechanisms have been proposed as an explanation to chitosan's antimicrobial properties. In the first one, the positive charges present in the polymeric chain of chitosan due to its amino group, interact with the negative charges from the residues of macromolecules in the membranes of microbial cells, interfacing with the nutrient exchange between exterior and interior of cell. The second mechanism proposes that chitosan acts as a chelating agent, while the third mechanism establishes that chitosan of low molecular weight is capable of entering the cells nucleus itself, interacting with the DNA, interfering with the messenger RNA, affecting the synthesis of proteins and inhibiting the action of various enzymes.

Chitosan films are biodegradable, bio compatible, flexible, durable, strong, touch and hard to break and have moderate values of water and oxygen permeability, decrease the respiratory rate of food and also inhibit the microbial growth. Chitosan based membranes have been used for protein separations [18].

Thanks to its film-forming properties, chitosan has been reported as a potential material of food packaging, especially as edible films and coatings. For example, in the storage of fruits, vegetables, meat products and sea food products. Unfortunately chitosan film is brittle thus it needs a plasticizer to increase film flexibility. Highly deacetylated chitosan (i.e. > 85%) exhibits low degradation rate in aqueous media. Evidently, the

chitosan based bio degradable polymers are attractive for food industry and will make great progress in the future.

Polyethylene is the simplest hydrocarbon polymer and has the following structure;  $[-CH_2-CH_2-]_n$  It is a very commonly used polymer and was first produced by polymerising the ethylene monomer. There are two types of polyethylene, viz., low density and high density. Low density polyethylene consists of molecules with branches, whereas the high density variety is essentially linear. LDPE melts at 110-125°C and is only around 40% crystalline. The density is around 0.91-0.92g/cc. While practically no solvent dissolves it at room temperature, several solvents can do so at high temperatures. Some of the useful solvents for polyethylene at high temperatures are carbon tetrachloride, toluene, xylene etc.

LDPE films are mainly used for packing and wrapping frozen food, textile products, and so on. It has high tear strength, extreme flexibility, and chemical and moisture resistance. LDPE's inertness to chemicals and resistance to breakage is made use of in „squeeze bottles“ and in many attractive containers. Pipes made of LDPE are used both agricultural, irrigation and domestic water line connection. The non-polar nature of the polymer makes it ideal for providing insulations to electric cables [1].

### **Experimental**

The film grade LDPE (24FS040), 0.923 g/cm<sup>3</sup> density, 6.0 g/ 10 min melt Index and 87.22 C softening point was supplied by Reliance Industries Limited, Mumbai, India. Powdered chitosan was obtained from India Sea Foods, Kochi, Kerala, India, with a minimum deacetylation degree of approximately 80%. All other reagents dicumyl peroxide (DCP) and maleic anhydride (MA) were of analytical grade obtained from Sigma-Aldrich (India).

### **Synthesis of low molecular weight chitosan (LWCS)**

Two grams of chitosan were dissolved in 100 ml 0.1 M HCl and stirred for 30 min. Then, H<sub>2</sub>O<sub>2</sub> was added in one of five concentrations (2.5%, 5%, 10%, or 15%). The mixture was heated and stirred at 60 C for 2 hours and then vacuum filtered. The upper residue was neutralised with distilled water, baked, and weighed. [Huang, K. S., Wu, W. J., Chen, J. B., & Lian, H. S. (2008). Application of low-molecular weight chitosan in durable press finishing.

Carbohydrate Polymers, 73, 254–260].

### Preparation of composite films

The compounds were prepared in a Thermo HAAKE PolyLab System equipped with roller type rotors. The mixing was done at a rotor speed of 60 rpm and at a temperature of 140 C. Initially LDPE was allowed to melt for 3 minutes. Fixed amounts of DCP (0.5 Wt. %), MA (2 Wt. %) and varying amounts of the low molecular weight chitosan (5, 10, 15, 20 and 25 Wt. %) were added in to the LDPE matrix in 2 minutes time intervals for each sample. Mixing was continued for another 4 minutes. The composites obtained from melt mixing were compressed using an electrically heated hydraulic press for 3 minutes at 150 C under a pressure of 200 Kg/cm<sup>2</sup>. After pressing, the samples were allowed to cool at room temperature. The formulations of all the prepared samples are given in Table 1.

**Table 1: Formulation of the composite films**

Sample	LDPE (gm)	LWCS (Wt. %)	DCP (Wt. %)	MA (Wt. %)
nB1	40	-	0.5	2
nB2	40	5	0.5	2
nB3	40	10	0.5	2
nB4	40	15	0.5	2
nB5	40	20	0.5	2
nB6	40	25	0.5	2

### Morphology

The morphology of the composite films was investigated by scanning electron microscopy (SEM). The samples were sputter coated with gold to avoid subsequent

charging before analysis by SEM. Images were taken using a JEOL JSM-820 model SEM and a Field Emission Scanning Electron Microscope, Hitachi SU6600 FESEM.

### **X-ray diffraction**

X-ray diffraction patterns of the films were analyzed using an X-ray diffractometer, Bruker AXS D8 Advance XRD, using Nickel filter with scanning speed 5°/min. The diffracted intensity of Cu K $\alpha$  radiation (0.154nm, 40KV and 30mA) was measured in a 2 $\theta$  range between 5° – 70°.

### **Sorption study**

The sorption properties of composite films were studied at room temperature by immersing each film in demonized water and saline water in glass screw top containers. Circular samples of diameter 1.94 cm were punched out from the composite films by a sharp-edge steel die. The thickness of the samples was measured at several points using a micrometer screw gauge and the average was taken as the initial thickness of the sample. The samples were initially dried overnight in vacuum desiccators and the original weights were taken. These samples were then immersed in distilled de-ionized water and saline water taken in air tight bottles and kept in a thermostatically controlled oven. At regular time interval, films were removed and the surface was dried between filter paper. They were weighed immediately and replaced into the diffusion bottles. The weighing was continued until equilibrium swelling was attained. Since each weighing was carried out within 30 s the error due to the escape of solvent from the sample may be neglected [19]. The procedure was continued until equilibrium swelling was obtained. Similar methodology has been adopted by several researchers [20, 21]. The experiments were conducted in triplicate. The % mol uptake (Q<sub>t</sub>) for the solvents by composite film was plotted against the square root of time and the results were analyzed.

$$Q_t (\text{mol}\%) = \left[ \frac{\left\{ \frac{\text{Mass of solvents orb ed by the polymer}}{\text{Molecul ar mass of the solvent}} \right\}}{\text{Initial mass of the polymer}} \right] \times 100$$

### **Biodegradability studies**

Biodegradability study of the samples was tested by inoculating the films with *Aspergillus niger* (A. niger) on a potato dextrose agar media and incubated at surrounding

temperature (25 C) for 21 days. Samples were cut (2.0 cm × 2.0 cm) and faced on the surface of mineral salts of agar in a Petri dish containing no additional carbon source. Before facing the samples, agar surfaces were cultivated with *A. niger*. After 21 days, the films were examined for evidence of colony growth. The morphology and tensile study of the inoculated composite films were also conducted.

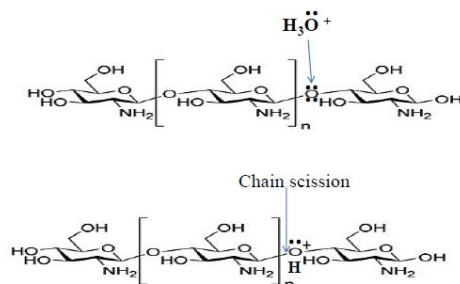
## Results and Discussion

### Morphology

Hydrochloric acid causes scission of the glucosidic linkages, thereby altering the structure and properties of the native chitosan. The amorphous regions of the chitosan flakes are more susceptible to acid hydrolysis than the crystalline regions. Acid hydrolysis has been used to modify renewable polymers such as starch, cellulose and chitosan structure and produce more dispersed composites for many years. In the present study chitosan flakes are hydrolyzed using HCl and resulted low molecular weight chitosan as shown in Fig. 2.

### Mechanism of acid hydrolysis:

During acid hydrolysis, the hydroxonium ion ( $H_3O^+$ ) carries out an electrophilic attack on the oxygen atom of the glycosidic bond. In the next step, the electrons in one of the carbon–oxygen bonds move onto the oxygen atom to generate an unstable, high-energy carbocation intermediate. The carbocation intermediate is a Lewis acid, so it subsequently reacts with water, a Lewis base, leading to regeneration of a hydroxyl group. The schematic steps of chitosan chain scission are given below.



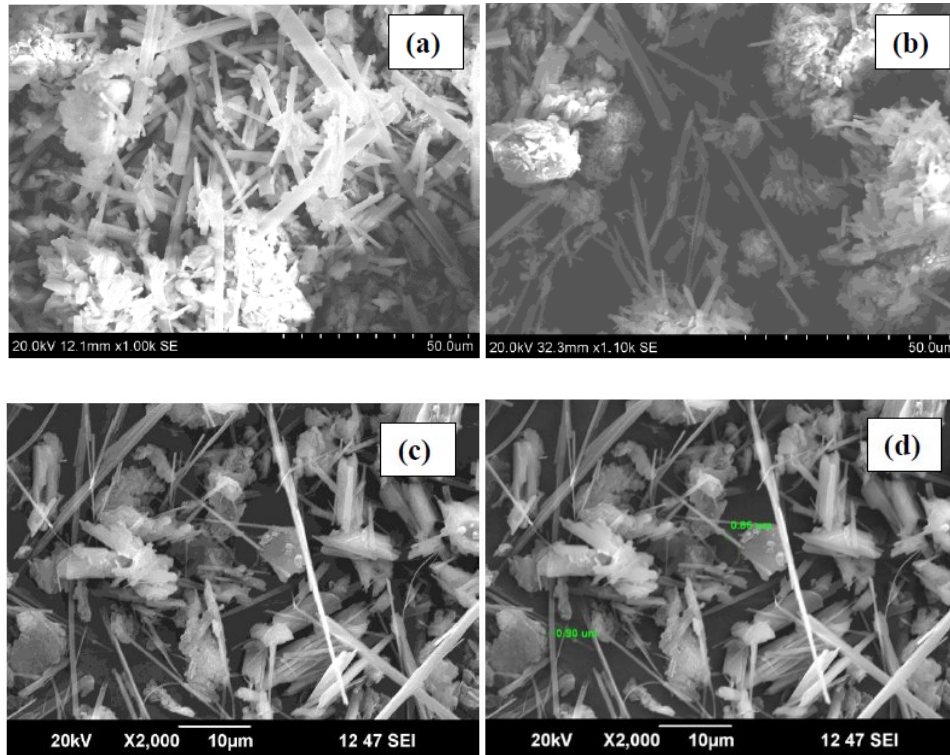


*Figure 1: Chitosan powder before hydrolysis*

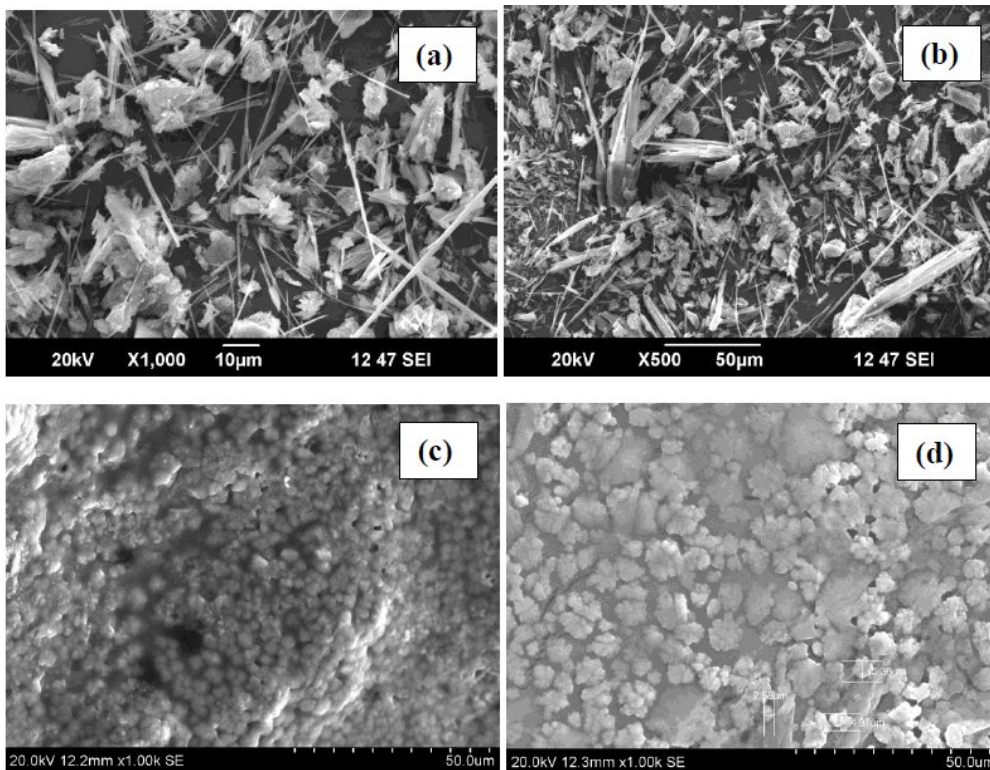


*Figure 2: Low molecular weight chitosan*

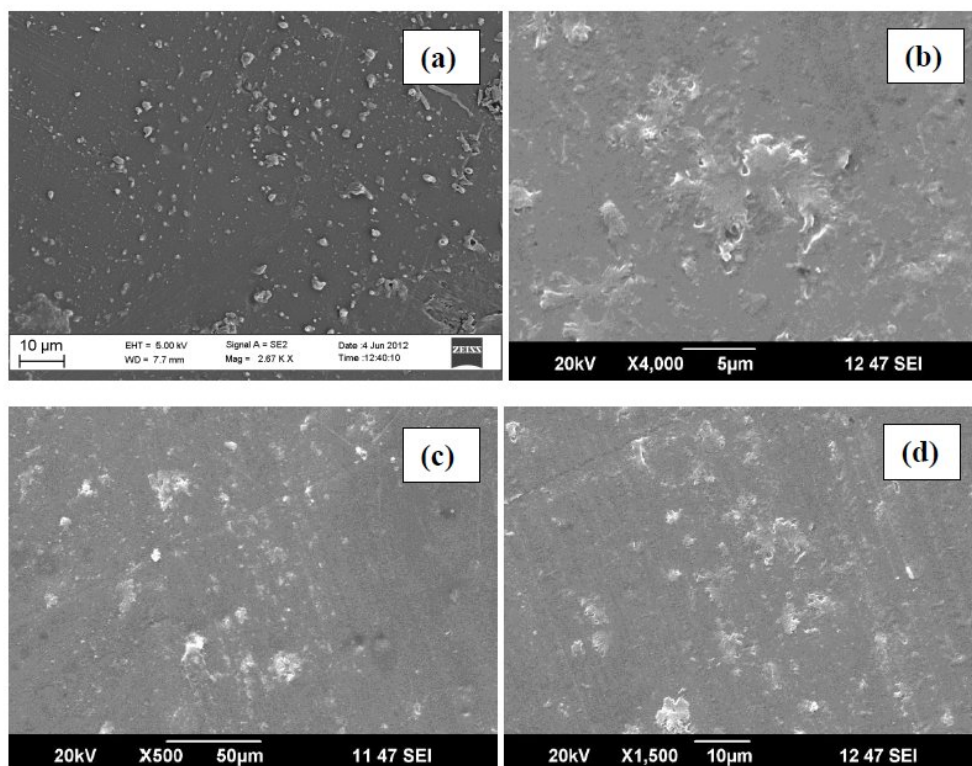


**Figure 3:** LDPE/Low molecular weight chitosan composite films

The scanning electron micrograph images of developed LDPE/LWCS composite film are shown in the Fig. 3. It is clear from the figure that uniform filler dispersion is occurring in the LDPE matrix.

#### ***X-Ray Diffraction Patterns***

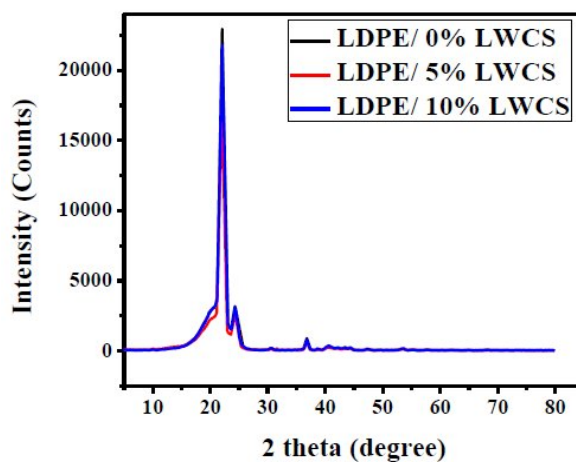


**Figure 4:** XRD pattern of neat LDPE, LDPE/5 wt% low molecular weight chitosan and LDPE/10 wt% low molecular weight chitosan composite films.

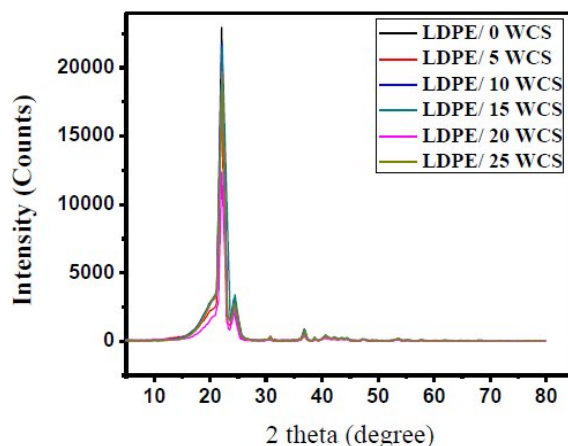


**Figure 5:** XRD pattern of B1 (LDPE), B2 (LDPE/5 wt% chitosan), B3 (LDPE/10 wt% chitosan) and B4 (LDPE/15 wt% chitosan)

Wide angle X-ray diffraction patterns of the LDPE and the LDPE/ Low molecular weight chitosan composite films are shown in Figure ... The typical crystalline peak of LDPE that appeared at  $2\theta \sim 20^\circ$  was found to decrease with the increase in concentration of low molecular weight chitosan in the composite.

Among the low molecular weight chitosan loaded composites, the 5 wt% loaded one, possessed maximum crystalline peak. The formation of maximum dispersion in the 5 wt% chitosan loaded composite film is further evident from the XRD pattern of the composite film.

### Sorption study

#### Water sorption

The mole percentage of water sorbed by developed composite film samples with respect to the low molecular weight chitosan content has been given in Figure 5. It is found that after absorption percentage increases with increase in chitosan content in the sample. This is due to the interaction of water molecules with hydroxyl and amino groups in chitosan [22]. For neat LDPE films a little water uptake can be observed. This is because LDPE is hydrophobic in nature. The water diffusion was strongly affected by chitosan contents as showed by higher percentage of water absorption of nB6. The graph shows a maximum value of % water absorption  $\approx 0.65$ . It is less when compared with starch or cellulose composites [2]. There is a rapid water uptake was observed within the first few days of immersion, but this decreased slowly with time [12]. The decrease in the rate of water uptake with time of immersion could be due to a concentration gradient across the two materials. The absorption of water is related to its rate of diffusion into the

composites. During absorption process, water is penetrated into the films and bonded to the hydroxyl group of chitosan and causes the swelling of chitosan granules. As a result the particles become crowded and the gap becomes smaller and narrowed. Thus water find difficult to diffuse and the rate of water uptake is reduced [2].

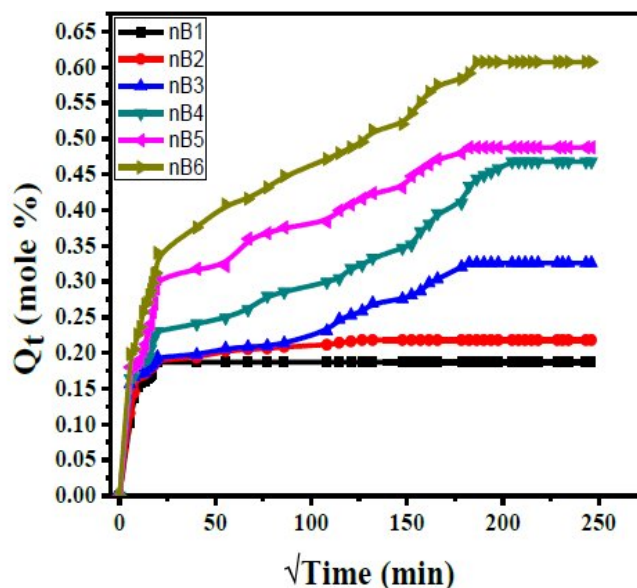


**Figure 6:** The mole percentage of water sorbed by LDPE/LWCS films with respect to the chitosan content.

### Saline water sorption

The figure 7 shows the mole percentage uptake of the LDPE/Low molecular weight chitosan composite films and it follows the same trend as in the case of water sorption graph. The saline water diffusion was strongly affected by chitosan contents as showed by higher percentage of water absorption of vB6. The graph shows a maximum value of % water absorption  $\approx 6$ . The rate of saline water uptake is higher as compare with water because saline water more polar than water. Therefore absorption percentage of saline water increases.

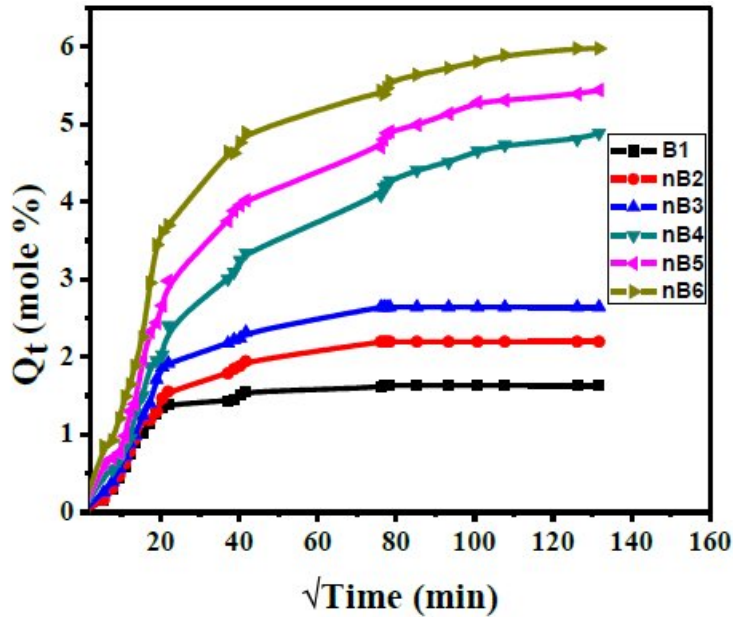


**Figure 7:** The mole percentage of saline water sorbed by LDPE/LWCS films with respect to the chitosan content.

### Biodegradability Study

From the Fig. 8, it shows that there was no fungi growth on the surface of neat LDPE and LDPE/Palm oil films. This is due to microbial resistance behavior which is inherently present in LDPE. LDPE backbone consisting of carbon-carbon (C-C) linkages is not susceptible to microbial attack. In contrast, after 21 days, the fungi growth was clearly visible for various LDPE/LWCS composite films as shown in the figure. Chitosan loading up to 25% shows the apparent of fungi growth. This indicated that the growth of *A. Niger* colony increases as the chitosan content is increased. The chitosan particles present on the surface of the LDPE film is attacked by fungi. This weakens the polymer matrix and increases the surface volume ratio and biodegradability of the film.



**Figure 8:** Evidence of fungi growth (*A.Niger*) on surface of LDPE films with and without low molecular weight chitosan.

### Conclusion

We were able to develop and characterize bio-degradable packaging material and its application in food packaging. We have developed composite materials, based on Linear Density Polyethylene (LDPE) and low molecular weight chitosan and characterized by different techniques. Based on this study we can conclude that low molecular weight chitosan (LWCS) affect the properties of the LDPE/LWCS composite films. In SEM analysis, the SEM picture of chitosan powder before hydrolysis shows a fibrous structure. The amorphous regions of the chitosan flakes are more susceptible to acid hydrolysis than the crystalline regions. During hydrolysis the glycosidic linkage breaks. From the scanning electron micrograph image of developed LDPE/LWCS, it is clear that uniform filler dispersion is occurring in the LDPE matrix. In the Wide angle X-ray diffraction patterns of the LDPE and the LDPE/ Low molecular weight chitosan composite films, the typical crystalline peak of LDPE that appeared at  $2\theta \sim 20^\circ$  was found to decrease with the increase in concentration of low molecular weight chitosan in the composite. Among the low molecular weight chitosan loaded composites, the 5 wt% loaded one, possessed maximum crystalline peak. The formation of maximum dispersion in the 5 wt% chitosan loaded composite film is further evident from the XRD pattern of the composite film. The addition of chitosan reduces the crystallinity of LDPE. The water diffusion was strongly affected by chitosan contents and the % water absorption of chitosan composite films are found less (<1%). The saline water absorption of the LDPE/LWCS composite follows the same trend as in the case of water absorption. The rate of saline water uptake is higher as compare with after because saline water more polar than water. The % water absorption of chitosan composite films are found high (>1%). The addition of chitosan increased the biodegradability of LDPE. The chitosan particles present on the surface of the LDPE film is attacked by fungi. This weakens the polymer matrix and increases the surface volume ratio and biodegradability of the film.

### References

1. V. R. uuuGowariker, N.V.Viswanathan, Jayadev Sreedhar, "Polymer Science" New age international publishers, New Delhi, 1986, Inc. 6-10 P.M. Dr. Wan Aizan Bt Wan Abd Rahman, Roshafima Rasit Ali, Jamarosliza Jamaluddin and

- Ida Yu Mohamad. "Development of low density polyethylene/Sago based bio film via blow film molding technique". 2009. Project faculty of chemical and natural resources engineering University Technology Malaysia.
2. R.N. Tharanathan. "Biodegradable films and composite coatings; Past, present and future." *Trends in Food Science and Technology* 14 (2003) 71-78.
  3. A Charlesby. "Radiation chemistry of polymers" in Farhaaziz and Rodgers, M.A.J *Irradiation of polymers*. VCH Publishers, USA, 1987, Inc. 451 -474.
  4. M. Bhattacharya, R.L. Reis, V. Corrclo and L Boesel. "Materials properties of biodegradable Polymers" in R. Smith *Biodegradable polymers for industrial applications* Wood head publishing limited, England, 2005.
  5. P.B. Shah, S. Bandopadhyay and J.R. Bellare. "Environmentally degradable starch filled low density polyethylene." *Polymer Degradation Stabilization* 47 (1995) 165-173.
  6. F. Khabbas, A.C Albertsson and Karlssor. "Trapping of volatile low molecular weight photoproducts in inert and enhanced degradable LDDE." *Polymer Degradation and stability* 61 (1998) 329 -342.
  7. B. Erlandsson, S. karlsson and A.C. Albertsson. "The mode of action of corn starch and a proxidant system in LDPE: Influence of thermo oxidation and UV irradiating on the molecular weight changes." *Polymer Degradation and stabilization* 55 (1997) 237 -245
  8. O. Akaranta and G.E. Oku. "Erratum to; some properties of Cassava Mesocarp Carbohydrate – Low density polyethylene blends." *Carbohydrate Polymers* 34 (1999) 403 -405.
  9. I.Arvanitoyannis, C.G. Biliaderis, H. Ogawa and N. Kawasaki. "Biodegradable films made from law density polyethylene, Rice starch and potato starch for food packaging application; part 1." *Carbohydrate polymer* 36 (1998) 89 -104.
  10. A Manzur, M. Limon – Gonzalex and E. Favela Torres. "Bio degradation of physic chemically treated LDPE by a consortium of filamentous fungi." *Journal of Applied polymer science* 92 (2004) 265 -271.
  11. I.D. Danjaji. "Degradation studies and moisture uptake of sago starch filled linear low density polyethylene composites." *Polymer Testing* 21 (2002) 75-81.
  12. Y.G. Hooi. "Mechanical, waste absorption weathering properties of polylactic acid/rice starch composites." Master's Thesis, University sains Malaysia Penang, Malaysia, 2005.

13. D.F. Gilmore, S. Antoun, R.W. Lenz and R.C. Fuller. "Degradation of Polyhydroxylalkanoates and polyolefin blends in a municipal waste water treatment facility." *Journal of Environmental Polymer Degradation* 14(1993) 269-274.
14. G.F. Moore and S.M. Saunders. "Advances in biodegradable polymers." *Rapra Review reports* 9: 2 (1995) 3-31.
15. R. Chandra and R. Rutsgi. "Biodegradable polymers." *Progress polymer science* 23 (1999) 1273-1335.
16. A. Pinotti, M.A. Garcia, M.N. Martino and N.E. Zaritzky. "Study on microstructure and physical properties of composite films based on chitosan and methyl cellulose." *Food Hydrocolloids*. 21 (2007) 66 – 72.
17. X. Zenq. E. Ruckenstein. "Cross –linked macroporous chitosan anion – exchange membranes for protein separations." *Journal of Membrane Science* 148 (1998) 195-205.
18. T.M. Aminabhavi, R.S. Munnoli. "An assessment of chemical compatibility of bromobutyl rubber, chlorosulfonated polyethylene and epichlorohydrin membranes in the presence of some hazardous organic liquids." *Journal of Hazardous Matter* 38 (1994) 223.
19. Y.D. Moon, Y.M. Lee "Dynamics of solvent diffusion in an aromatic polyimide." *Journal of Applied Polymer Science* 51 (1994) 945.
20. S.B. Harogoppad, T.M. Aminabhavi. "Diffusion and sorption of organic liquids through polymer membranes.5. Neoprene, styrene-butadiene-rubber, ethylene-propylene diene terpolymer and natural rubber versus hydrocarbons." (C8-C16), *Macromolecules* 24 (1991) 2598.
21. R.A. Talja, H. Hele'n, Y.H. Roos, K. Jouppila. "Effect of various polyols and polyolcontents on physical and mechanical properties of potato starch-based films." *Carbohydrate Polymers* 67 (2007) 288.